UNIVERSITÁ DEGLI STUDI DI PADOVA

FACOLTÁ DI INGEGNERIA

DIPARTIMENTO DI INGEGNERIA MECCANICA, SETTORE MATERIALI

CORSO DI LAUREA MAGISTRALE IN INGEGNERIA DEI MATERIALI

TESI DI LAUREA

Functionalization of carbon nanotubes with quantum dots for photovoltaic applications

Relatore: Dott.ssa GIOVANNA BRUSATIN

Correlatore: Dott.ssa FAYNA MAMMERI

Laureando: Andrea Ballarin
Matr. n. 602763

Anno Accademico 2010 - 2011

"Gli Alieni siamo noi che con la nostra sensibilità, cerchiamo lampi
di poesia tra le pieghe dell'esistenza quotidiana.
Rifiutando l'omologazione, affermiamo con delicatezza la nostra unicità,
facendo della vita un'opera d'arte "
Giovanni Allevi

"L'esperienza è quello che ottieni quando non ottieni quello che desideri"
Randy Pausch

Index

1. Introduction

Photovoltaic energy is a kind of energy that has recently started to be exploited.

Nowadays silicon solar cells cover the biggest slice of the market, but new promising technologies are gaining increasing interest. Organic photovoltaic solar cells (OPVCs) and in particular dye-sensitized solar cells (DSSCs) are based on a different photovoltaic principle whose patent can be assigned to nature (photosynthesis).

These devices, together with their recent developments (hybrid solar cells, quantum dots-sensitized solar cells), in theory allow a significant decrease in costs and materials consumption because they make use of cheap abundant materials disposed in thin-films conformations.

These new technologies offer astonishing potentialities that could lead to devices able to compete with consolidated energy conversion systems. Efficiencies could attain surprisingly high values and environmental benefits should not be neglected.

New devices consist of an electron acceptor, an electron donor and an electrolyte assembled on two electrodes. Each part accomplishes a particular task: the electron donor, that is the semiconductor, is responsible for light harvesting, the electron acceptor for transporting the charge, the electrolyte closes the electrical circuit.

Intense research aims to improve each component of the device.

Particular attention is generally paid on some key factors:

- Exploitation of most of solar light, from UV to IR considering that energy below the semiconductor band gap value is not absorbed and excess energy could be lost as heat: possibility of multi-excitonic generation with QDs or use of semiconductors with different band gaps
- capture of as many photons as possible: some attempts to increase the surface area of the devices have been made
- transfer of photons from the light-harvesting material (dye, QD, etc.) to the electrons carrier (TiO_2 NPs, CNTs) limiting the excitonic recombination
- transfer of electrons from the conductor to the electrode and halls in the opposite direction

Why solar cells?

- this environmentally friendly technology allows to exploit a source completely natural and free (mainly regarding DSSCs where all the components are composed of natural and abundant elements)
- solar cells allow to produce electricity without emitting pollution, producing greenhouse gases and using finite fossil-fuel resources
- solar cells are becoming convenient. In the 1990s their efficiency as well as lifetimes were quite low and their cost really high. Therefore the energy spent to make a cell was greater than that paid back. Nowadays the technology has improved so that the energy payback time is also lower than 1 year. 20 to 30 years are typical lifetimes: this means that modern solar cells are net energy producers, that is they generate significantly more energy over their lifetime than the energy expended in producing them
- With new developments really higher efficiencies are on the horizon
- A great variety of new devices are being studied: they will be cheaper, lighter, more flexible than the existing ones: they will allow to exploit solar energy in different ways, from private to industrial purposes
- Chinese people are investing great energies in the development of this technology; Chinese are 1.3 billion: why shouldn't we do the same?

Beside this, an interest in carbon nanotubes' electrical properties is increasing, as well as in semiconductor quantum dots' their light-harvesting properties; the use of one or both of them to increase solar cells (for example DSSCs) efficiencies has been suggested. CNTs could encourage transfer of charge, one of the weakest points in new hybrid systems.

The aim of this thesis is that of laying the foundations to build a new kind of photoelectrochemical device.

What we would accomplish is a research on interactions between conveniently functionalized CNTs and some particular kinds of QDs. We will devote our attention on the way of joining them to allow the best possible transfer of charge.

First of all we will give an overview on photoelectrochemical cells and after we present an introduction on the features and properties of CNTs and QDs. Then we will describe some recently performed studies. Finally, in the experimental part, we will illustrate our experiments

dealing with the preparation and characterization of CNT-QDs nanohybrids as potential precursors for solar cells.

2. Solar Cells

A solar cell is a device that converts sunlight energy into an electrical current by the photovoltaic effect.

The **photovoltaic effect** involves the creation of a voltage (or a corresponding electric current) in a semiconducting material upon exposure to electro-magnetic radiation. After the absorption of photons some electrons are transferred from different bands (from the valence to conduction band) within the material, resulting in the buildup of a voltage between two electrodes.

There are different types of cells available, some of them exploit the p-n junction principle to create photocurrents (silicon cells, CdTe cells and CIGS), the others follow the nature example (DSSCs, organic and hybrid solar cells).

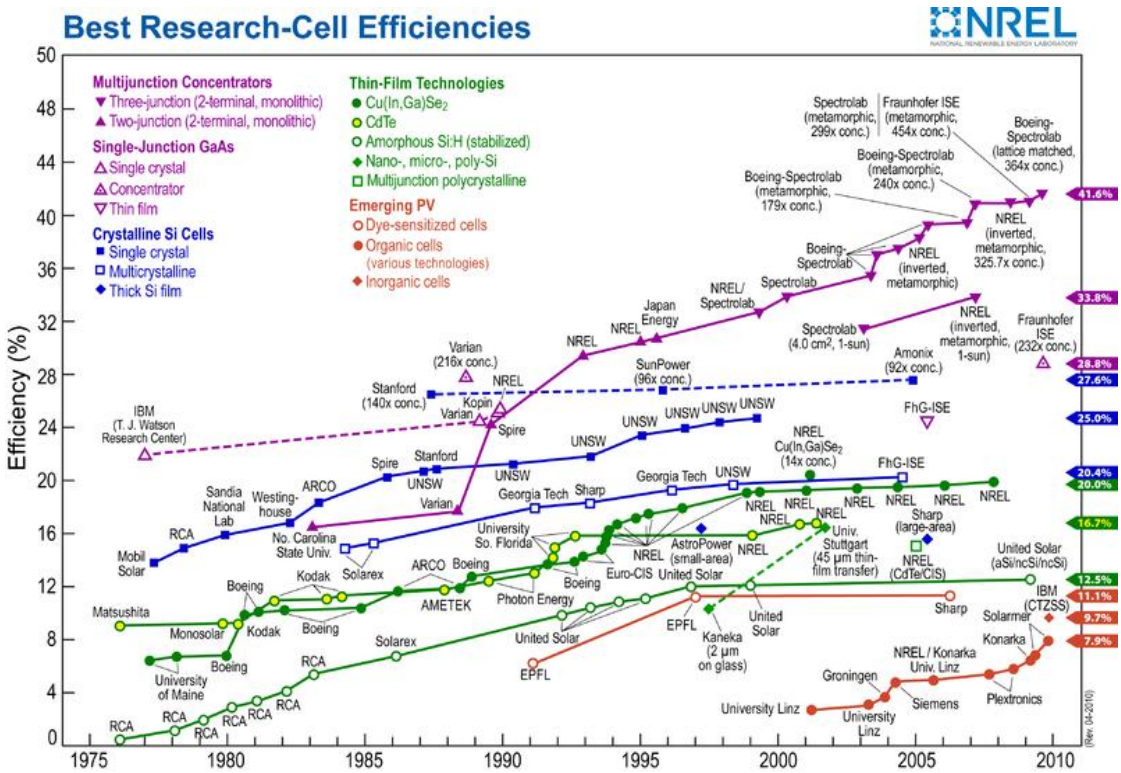

Fig1.: solar cells efficiencies

2.1 Silicon cells

The most employed material for solar cells is *crystalline silicon* (wafer silicon; band gap = 1.1 eV):

- Monocrystalline wafers: photovoltaic cells that reach a 16-17 % efficiency
- Polycrystalline silicon: cheaper cells but with a lower efficiency (15 %)
- Ribbon silicon: waste of material reduced at minimum but still less efficiency (14 %)
- Amorphous silicon: low efficiency (8 %) but much cheaper; the band gap is bigger (1.7 eV)

In these kinds of cells, when a photon is absorbed in the empty zone, an electron-hole pair appears: this immediately separates because of the empty zone differential potential thus creating a photoelectric current that will be adequately exploited.

In regards to semiconductor band-gap, only photons with that amount of energy or higher will give a contribute to produce a current, otherwise they will pass through the semiconductor.

In order to create an electric power electrons and holes must be separated. For this reason a *p-n junction* is used.

2.1.1 P-N junctions

A *p–n junction* is formed by joining p-type and n-type semiconductors together in very close contact. The two regions are created in the same single-crystal semiconductor by doping in order to avoid the presence of a grain boundary. The doping is obtained with the introduction of small amounts of *boron* and *phosphorous* respectively for the p-type and n-type. Each boron atom catches an electron from the valence band (BV) of silicon and it gains a negative charge thus creating a positive hole inside the BV; at the same time a phosphorous atom releases an electron in the conduction band (BC) and results positively charged.

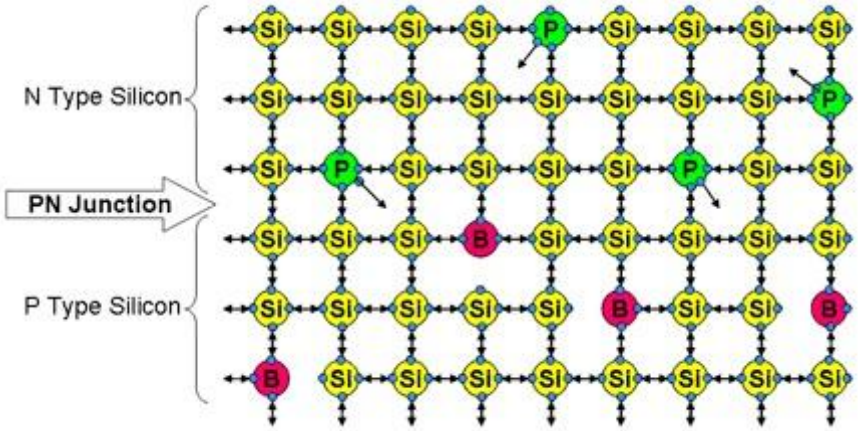

Fig 2: Silicon crystal lattice doped with boron and phosphorus

After joining p-type and n-type semiconductors, electrons near the p–n interface tend to diffuse into the p-region. As electrons diffuse, they leave positively charged ions (donors) in the n-region. Similarly, holes near the p–n interface begin to diffuse into the n-type region leaving fixed ions (acceptors) with negative charge. The regions nearby the p–n interfaces lose their neutrality and become charged, forming the space charge region or depletion region. The electric field created (with direction from n-region to p-region) by the depletion region opposes the diffusion process for both electrons and holes. Without the application of an external voltage, an equilibrium condition is reached in which a potential difference is formed across the junction. This potential difference is called *built-in potential* V_{bi}. Thanks to the created electric field, electrons-holes pairs generated by an incident photon are separated: electrons diffuse towards the n-region, holes do the opposite. Then a resulting photocurrent can circulate in the external circuit.

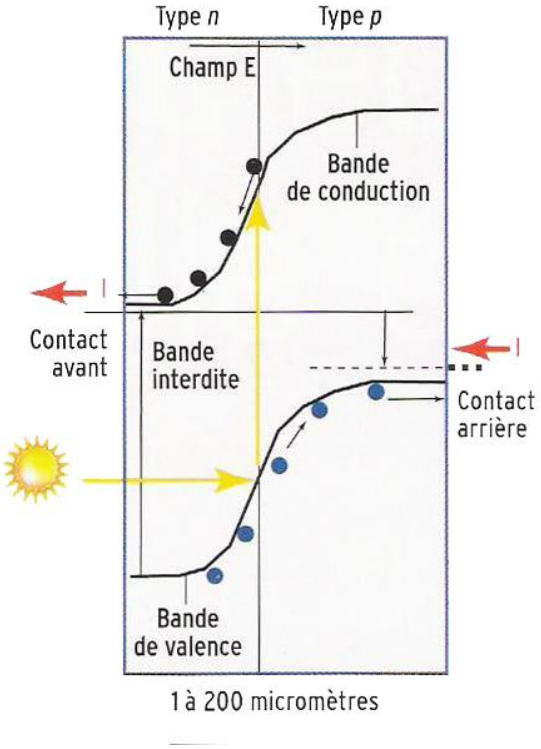

Fig 3: charge separation in a p-n junction

The fundamental parameter for solar cell based on the p-n junction principle is the band-gap extension: the smaller it is the higher is the produced photocurrent, because a bigger amount of electrons own the required energy to cross the gap, but the lower is the available photo-tension as well. The optimum value for the electric power production is placed around an energy gap of 1,4 eV.

Besides the material properties, the created photocurrent depends on the incident-light wavelength, that is the number of electrons per incident absorbed photon collected in the external circuit depends on the wavelength of the photon. Into the most effective zone this value tends to unity, and losses can be ascribed to light reflection rate.

In the case of Silicon, the majority of visible light has enough energy to cross the gap; on the other hand this also means that the higher energy photons have more than the required energy and most of this energy is not transferred to electrons but rather wasted as heat. Besides another issue is that in order to have reasonable photon capture rates the layer has to be fairly thick; but this also increases the chance that a free electron meets up with a hole. These effects produce an upper limit on the efficiency of Silicon solar cells, called Shockley–Queisser limit (after-specified).

However the biggest problem of this kind of cells is cost of Silicon. Different efforts have been made to attempt reducing cost (thin-film approaches, multi-junctions approaches) but costs have dropped only due to increased supply, without any other significant improvement in efficiency.

2.2 Thin-film solar cells

They are made by depositing one or more thin layers (thin film) of photovoltaic material on a substrate.

Many different photovoltaic materials are deposited with various deposition methods on a variety of substrates. Thin-film solar cells are usually categorized according to the photovoltaic material used: amorphous Silicon, CdTe, Copper indium gallium selenide (CIGS), or DSSCs.

Nowadays thin-film solar cells cover the 15 % of the market, the other 85 % belongs to crystalline Silicon panels; the commercial CdTe panels have attained an efficiency of about 11 %.

Although their lower efficiency this kind of cells allow to reduce the amount of light absorbing material and the relative costs. They have also other advantages including flexibility, lighter weights, and ease of integration.

2.3 Grätzel cells (DSSCs)

These cells exploit a principle completely different from Silicon cells: the idea is that of copying nature and to create something similar to *photosynthesis* process.

A Grätzel cell has a sandwich structure: two conducting glass electrodes are separated by a layer of TiO_2, "active material" and the electrolytic solution.

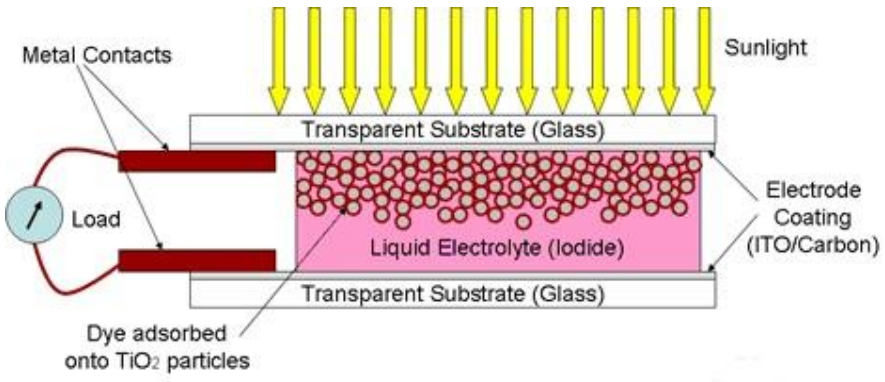

Fig 4: Grätzel solar cell

On the top is a transparent anode made of fluorine-doped tin dioxide (SnO_2:F) deposited on the back of a glass plate. Then a TiO_2 layer is deposited on the back. TiO_2 is a semiconducting material with a large band gap (> 3 eV : it absorbs only UV part of solar light) that is heated to form a porous nanostructure, with a ratio surface/volume as high as possible, where the active material can be covalently bonded. The active material is a dye able to transfer electrons to the conduction band of TiO_2 after absorption of a photon. The separate backing is composed of a thin layer of the iodide electrolyte spread over a conductive sheet, typically Platinum metal. The front and back part are then sealed together to prevent the electrolyte from leaking.

In summary, TiO_2 is the electron acceptor, the organic dye plays the role of an electrochemical pump, while the electrolytic solution supplies the electrons required to close the circuit. This is absolutely the analog of the chlorophyllian photosynthesis, where chlorophyll is the active material, CO_2 is the electron acceptor, H_2O is the donor.

The operation mode is the following: sunlight enters the cell through the transparent top contact, striking the dye on the surface of the TiO_2. Photons with enough energy to be absorbed will create an excited state of the dye, from which an electron can be directly injected into the conduction band of TiO_2. Thus electrons are collected and transferred to the anodic electrode through a chemical diffusion gradient. At the same time holes are carried by the electrolytic solution usually based on Potassium and Iodine (recently a polysulfide has been tested) toward the counter-electrode. In this way the dye gains the electron lost during oxidation : it pulls the electron out of the Iodide (I^-) thus oxidizing it to I_3^-. This reaction is quite quicker than recombination of electron injected into the TiO_2 with the oxidized dye molecule (this recombination reaction would short-circuit the solar cell). The triiodide recovers his missing electron by diffusing to the cell bottom where the counter-electrode furnishes the electrons that have passed through the external circuit and the process can start again.

DSSCs are attractive over silicon solar cells for another characteristic: they can work also in weak illumination conditions.

In fact in Silicon solar cells the electrons gaining energy from the incident photons remain in the same lattice and with a weak incident light the charge carrier has a low mobility and there will be a significant number of recombination of the photoexcited electron with the hole produced by another photoexcitation. Whereas in DSSCs only an electron is injected into TiO_2, not holes. Then an electron-hole recombination with the oxidized dye is energetically possible but not likely compared to the recovery of one electron from the electrolyte. Moreover a direct recombination TiO_2-electrolyte is forbidden by the difference in energetic levels.

Therefore DSSCs can work under cloudy skies and indirect illumination while Silicon solar cells suffer a cut-out condition.

The only big disadvantage of DSSCs is the liquid electrolyte, with thermal stability problems. Actually researchers are making efforts to solve this issue, maybe exploiting a solid electrolyte.

New developments involve new design options. For example alternated semiconductor morphologies have been tested to improve electron transport in these solar cells, while maintaining the high surface area required for dye adsorption: so arrays of nanowires combined with nanoparticles have been thought to provide a direct path to the electrode via the semiconductor conduction band. This could increase the quantum efficiency of DSSCs in the red region of the spectrum.

Very recently DSSCs with a higher effective surface area have been suggested, by wrapping the cells around a quartz optical fiber: photons bounce inside the fiber as they travel, so there are more chances to interact with the solar cell and produce more current.

2.4 QDSCs

This configuration is a variation of DSSCs based on dye-sensitization of nanocrystalline TiO_2 layers. The organic dyes are therefore substituted by the more stable quantum dots. The three main methods of QD adsorption on TiO_2 are in-situ growth of QDs by chemical bath deposition, deposition of pre-synthesized colloidal QDs by direct adsorption, and deposition of pre-synthesized colloidal QDs by linker-assisted adsorption. The first approach involves a nucleation and growth process leading to a high coverage of the effective TiO_2 surface, but rendering rather difficult the control of the size distribution of the deposited QDs. On the other side the attachment of colloidal QDs through molecular wires leads to precise morphological characteristics (shape and size) of the semiconductor nanocrystals.

This kind of cells could allow exceeding the Shockley-Queisser efficiency limit of single-junction solar cells thanks to different mechanisms such as multiple exciton generation. For the moment this devices have a low performance, which is usually hampered by very poor current-potential characteristics, as represented by low fill factors. A low fill factor is due also to the presence of a nearly monoenergetic surface state about 0,4 eV below the TiO_2 conduction band. Coating of QDSCs (for example with ZnS) can partially reduce the recombination of electrons from TiO_2 with the redox couple in the electrolyte leading to higher photocurrents.

2.5 Organic photovoltaic solar cells (OPVs)

Organic solar cells use organic materials in the active layer of the devices. Organic photovoltaic devices are fabricated from thin films of organic semiconductors such as polymers and small-molecule compounds like polyphenylene vinylene and carbon *fullerenes*, typically on the order of 100 nm thick. Although low efficiencies reached so far (6 %), OPVs can be made using a cheap coating process such as spin coating or inkjet printing so they are promising low cost alternatives to silicon solar cells; in addition they have also the advantage of flexibility.

2.6 Hybrid solar cells

A wider use of inorganic PVCs is prevented by the high cost of production and processing of inorganic semiconductors, where high temperatures and deep vacuum are required. Thus organic or hybrid systems allow to decrease costs, exploit different mechanisms of solar power conversion (like photosynthesis) and reduce the amount of expensive materials or rare chemical elements, assuring a certain workability.

There are two disadvantages of organic materials which limit the theoretical producible power: low mobility of charge carriers and weak absorption at energies below 2 eV. These disadvantages can be overcome by means of hybrid materials that combine advantages of both organic and inorganic semiconductors.[32]

An organic material is mixed with a high electron transport material to form the photoactive layer. The two materials are assembled together in a *heterojunction* type photoactive layer. By placing one material into contact with each other, the power conversion efficiency can be greater than a single material.

One of the materials acts as the photon absorber and exciton donor, and the other facilitates exciton dissociation at the junction by charge transfer.

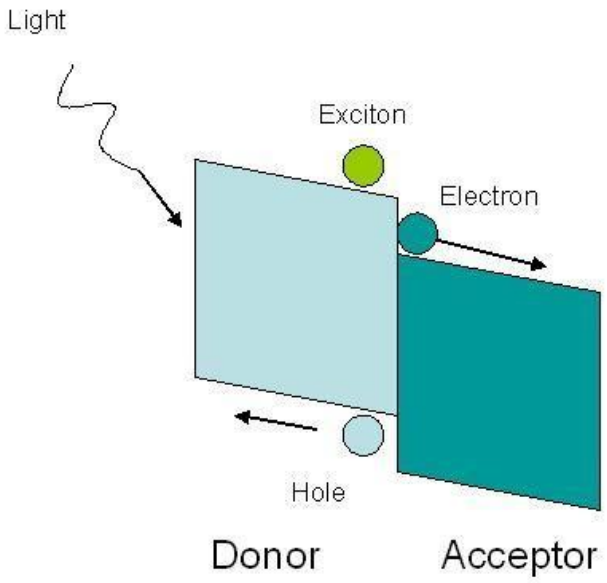

Fig 5: charge separation in hybrid solar cells

The acceptor material needs a suitable energy offset to the binding energy of the exciton to the absorber. An extra energy E_b (bond energy) is required to dissociate excitons, which varies from 0,2 to 1,4 eV for different semiconductors: if an exciton is excited in a donor semiconductor, and the energy gap between the lowest unoccupied molecular orbitals (LUMO) of the donor and acceptor is larger than the exciton bond energy [E_D(LUMO)-E_A(LUMO)> E_b], then there is a high probability that the exciton will dissociate into free charges e^- and h^+. After dissociation, the carriers are transported to the respective electrodes through a percolation network. The open circuit voltage V_{oc} depends on the E_A(LUMO)-E_D(HOMO) difference and satisfies the formula: $e^*V_{oc} \leq E_A(LUMO)-E_D(HOMO)$, where e is the electron charge. Therefore a strong E_D(LUMO)-E_A(LUMO) inequality will reduce the V_{oc}. At the same time, the average distance an exciton can diffuse through a material before annihilation by recombination happens, i.e. diffusion length, in organic films is usually about 10 nm. Consequently only excitons generated within this length close to an acceptor will contribute to the photocurrent.

In normal bi-layer photovoltaic cells only a small fraction (less than 10%) of absorbed photons contributes to photocurrent, so the idea of a bulk heterojunction has been developed: the donor-acceptor junction is extended over the entire working layer so that the exciton excited in any point of the heterojunction bulk can reach the semiconductor junction and dissociate into free charges. In an optimal heterojunction the donor and acceptor phases are characteristically separated by a distance of about the exciton diffusion length. This is a key

challenge together with matching HOMO and LUMO energy levels of acceptor and donor, improving the mobility of electrons (holes) in the acceptor (donor) and ohmic contacts between the acceptor (donor) and the electrodes and in general minimize the contact resistance between each layer in the device to offer higher fill factor and power conversion efficiency.

2.6.1 Types of hybrid solar cells

2.6.1.1 Polymer–nanoparticle composites

Nanoparticles are a class of semiconductor materials whose size in at least one dimension ranges from 1 to 100 nanometers, on the order of exciton wavelengths. This size control creates quantum confinement and allows for the tuning of the optoelectronic properties of QDs, such as band gap and electron affinity. Core-shell quantum dots offer still broader possibilities to control the properties. Nanoparticles also have a large surface area to volume ratio, which presents more area for charge transfer to occur; afterwards they are characterized by a high stability and good electroconducting properties.

The photoactive layer can be created by mixing nanoparticles into a polymer matrix.

For polymers used in this device, the hole mobilities are greater than electron mobilities, so the polymer phase is used to transport holes. The nanoparticle phase is required to provide a pathway for the electrons to reach the electrode, so NPs need to be interconnected to form percolation networks. Aspect ratio, geometry, and volume fraction of the nanoparticles are factors in their efficiency. The structure of the nanoparticles can take a shape of nanocrystals, nanorods and others.

Inorganic semiconductor nanoparticles used in hybrid cells include CdSe (6-20 nm), ZnO, TiO, and PbS. Common polymers used as photo materials have extensive conjugation and also happen to be hydrophobic. The most common polymers used are P3HT (poly (3-hexylthiophene)), and M3H-PPV, a phenylene vinylene derivative.

Fabrication methods include mixing the two in a solution and *spin-coating* onto a substrate, and solvent evaporation (sol-gel). Most of these polymer fabrication methods do not involve high temperature processing.

Power conversion efficiencies of 2.4 % have been reached with PPV-CdSe tetrapods.

Problems include controlling the nanoparticle aggregation as the photolayer forms. The particles need to be dispersed in order to maximize interface area, but need to aggregate to

form networks for electron transport. A possible solution is implementing ordered heterojunctions, where the structure is well controlled. Moreover carrier mobilities have to be increased.

In general inorganic NPs are promising materials for solar cells since they, in principle, make it possible to overcome the Shockley-Queisser efficiency limit. In fact NPs can produce more than one electron-hole pair (for example the generation of up to 7 electron-hole pairs per a single absorbed photon has been reported in PbSe NPs) in response to incident photon (exciton multiplication effect). However the efficient exciton multiplication process is accompanied by no less efficient Auger recombination of excitons, that occurs on a picoseconds scale. Therefore the problem of releasing the multiplied charge carriers from NPs should be solved; this problem is made even more difficult to solve by the fact that NPs are generally stabilized by organic ligands which hinder interparticle electron transport.

2.6.1.2 Use of CNTs

CNTs can be used as either the photo-induced exciton carrier transport medium within a polymer-based photovoltaic layer or as the photoactive (photon-electron conversion) layer. Metallic CNTs are preferred for the former application, semiconducting CNTs for the latter.

For example by incorporating CNTs within the polymer, thanks to their high surface area, dissociation of the exciton pair can be accomplished by the CNT matrix. The separated carriers within the polymer-CNT matrix are transported by the percolation pathways of adjacent CNTs, providing the means for high carrier mobility and efficient charge transfer. Despite this, the open-circuit voltage and the short-circuit current are very low. Metal nanoparticles may be applied to the exterior of CNT to increase the exciton separation efficiency.

Another application involves use of CNTs not only as an add-in material to increase carrier transport, but also as the photoactive layer itself. The semiconducting single walled CNT (SWCNT) has unique structural and electrical properties whose band-gap is inversely proportional to the tube diameter. Hence this single material may show multiple direct bandgaps matching the solar spectrum.

2.7 Solar cells efficiency

Key concepts related to solar technology include *conversion efficiency* (η), *fill factor* (FF), *internal* and *external quantum efficiency* (QE), *short-circuit current* (I_{sc}), and *open-circuit voltage* (V_{oc}).

The open-circuit voltage, V_{oc}, corresponds to the tension measured when there is no electric current flow in the circuit; the short-circuit current, I_{sc}, is the current intensity when the applied voltage is zero. In order to create an electric power the product of tension and current intensity has to be maximized between the open-circuit and short-circuit conditions, choosing the optimal-point.

2.7.1 Solar energy conversion efficiency

It is the percentage of power converted (from absorbed light to electrical energy) and collected when a solar cell is connected to an electrical circuit:

$\eta = \frac{P_m}{E \times A_c}$, where P_m is the maximum power point (V_{mp} x I_{mp}), E is the input light irradiance (correspondent to 1000 W/m^2 with an air mass 1.5 (AM1.5) spectrum, under standard test conditions), and A_c is the surface area of the solar cell (in m^2).

The losses of a solar cell can be split into reflectance losses, thermodynamic efficiency, recombination losses and resistive electrical loss. The overall efficiency is the product of each of these individual losses. Due to the difficulty in directly measuring some parameters often some others are used.

2.7.2 Thermodynamic efficiency

Solar cells are quantum energy conversion devices and so are subjected to a thermodynamic efficiency. In fact sunlight photons with an energy lower than the band gap cannot be absorbed by the semiconductor thus generating an exploitable electron-hole pair which can produce a useful output, but photons energy simply generates heat. The same happens for a consistent part of excess energy above the band gap own by more energetic photons: it is converted to kinetic energy and, through lattice vibrations, called phonons, lost as heat as well.

The use of multi-gap solar cells could partially solve this problem allowing to improve the efficiency achieved for single portions of the spectrum thus improving the overall thermodynamic efficiency.

This possibility could be also offered by *multi-exciton generation* (MEG) in cells based on quantum dots.

2.7.3 Quantum efficiency

It considers the number of charge carriers collected by the solar cell to the number of incident photons that is the probability that a photon generates an electron/hole pair and a real transfer of electrons takes place.

QE therefore relates to the response of the solar cells to the different wavelengths of the incident light. If all the photons of a particular frequency are absorbed the QE at that wavelength is one. The QE for photons with energy below the bandgap is zero.

The QE is fairly constant across the entire spectrum of wavelengths above the energy correspondent to the band gap. However it is reduced because of the effects of recombination that inhibit charge displacement into an external circuit; in addition surface characteristics can affect carriers generated near it so the blue portion of the QE is diminished since the high-energy (blue) light is preferentially absorbed very close to the surface; in the same way lower-energy light is absorbed in the bulk of the solar cell and the short diffusion length can prevent it and affect the collection probability, hence reducing the QE in the green portion of the spectrum.

So the QE can be defined as the collection probability integrated over the device thickness and normalized to the number of incident photons.

Quantum efficiency is also referred to IPCE = Incident-Photon-to-electron Conversion Efficiency. Two types of QE of a solar cell are often considered: external quantum efficiency (EQE) and internal quantum efficiency (IQE).

IQE concerns the number of photons that are absorbed versus the number of charge carriers (electrons and holes) produced. This can be improved by reducing recombination. EQE takes into account the amount of light that is transmitted or reflected and is therefore a lower value than internal QE. The use of anti-reflective coatings can improve external QE.

Often EQE is measured as the $\frac{current/_{charge\ of\ 1\ e^-}}{total\ power\ of\ photons/_{energy\ of\ 1\ photon}}$.

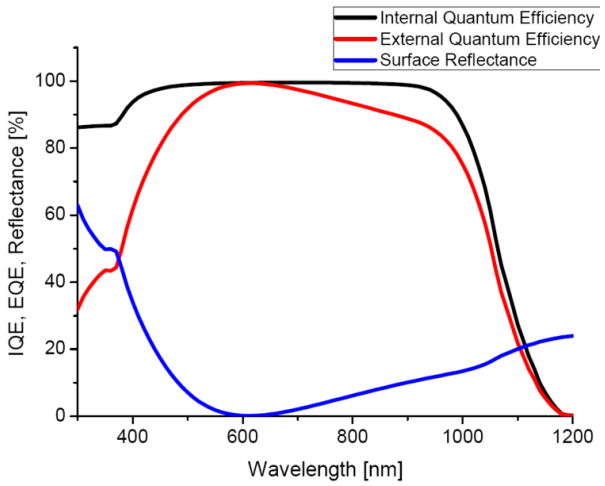

Fig 6: Quantum efficiency

2.7.4 Fill Factor

It is defined as the actual maximum obtainable power, $P_m = V_{mp} \times J_{mp}$, to the theoretical power $P_{th} = (J_{sc} \times V_{oc})$.

Fill factor is a calculation based on the maximum achievable voltage (V_{oc}) and current (I_{sc}) versus the power produced at the maximum power point (P_m). V_{mp} is the actual voltage achieved by a solar cell at maximum power. I_{mp} is the actual current a solar cell can produce at maximum power. The maximum power theoretically possible, P_{th}, is $V_{oc} \times I_{sc}$. The maximum power actually possible, P_m, is $V_{mp} \times I_{mp}$. Dividing P_m by P_{th} provides the fill factor of the device, which is always less than 100% because P_m is always less than P_{th}.

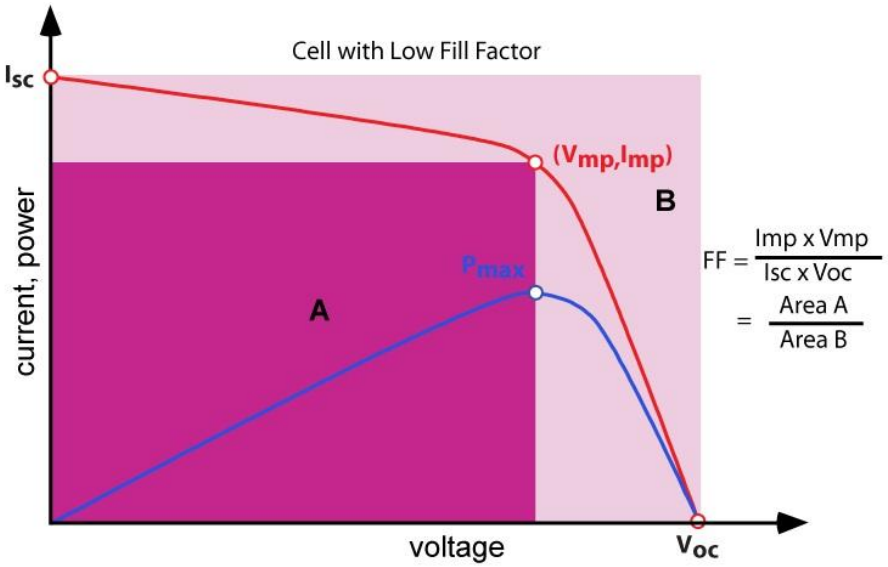

Fig 7: solar cell with low fill factor

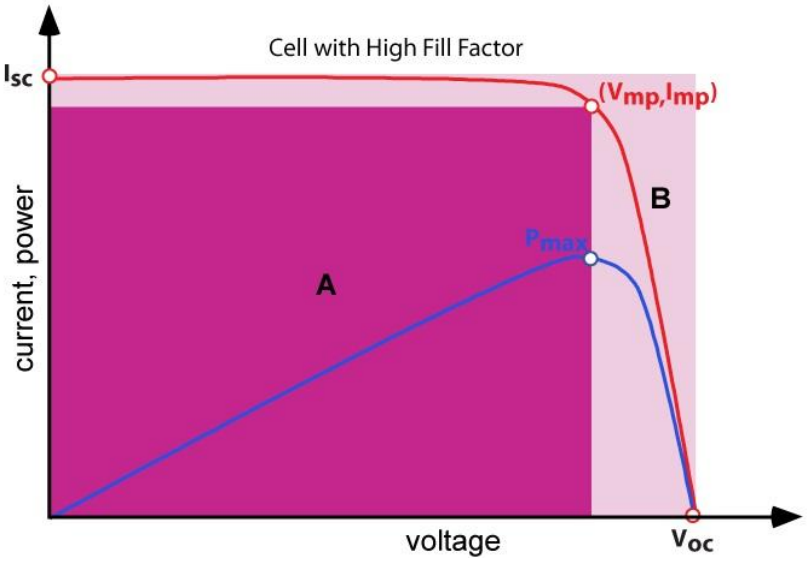

Fig. 8: solar cells with high fill factor

2.7.5 Shockley–Queisser limit

The Shockley–Queisser limit refers to the maximum theoretical efficiency of a solar cell using a *p-n junction* to collect power. It is calculated by examining the amount of electrical energy that is extracted per photon of incoming sunlight. It is principally due to three contributions:

- *Blackbody radiation*: any material above absolute zero temperature will emit radiation that cannot be captured by the cell, and represents about 7% of the available incoming energy
- *Recombination*: when an electron is ejected through photoexcitation, the atom it was formerly bound to is left with a net positive charge. Under normal conditions, the atom will attempt to remove an electron from a surrounding atom in order to neutralize itself, a process known as recombination; that atom will then attempt to remove an electron from another atom, and so forth, thus creating a net positive charge (holes) motion. Like electrons, holes move around the material, but their mobility is often lower: this means that during the finite time while the electron is moving forward towards the p-n junction, it may meet a slowly moving hole left behind by a previous photoexcitation; when this occurs, the electron recombines at that atom, and the energy is lost (normally through the emission of a photon of that energy). Recombination places an upper limit on the *rate* of production; past a certain rate there are so many holes in motion that new electrons will never make it to the p-n

junction. In silicon this reduces the theoretical performance under normal operating conditions by another 10%

- *Spectrum losses*: since the act of moving an electron from the valence band to the conduction band requires energy, only photons with more than that amount of energy will produce a photoelectron. In the case of silicon, of the 1000 W/m² in AM1.5 sunlight, about half of that has less than 1.1 eV of energy (energy gap), and will not produce power: that means there is a theoretical conversion efficiency of about 50% or less. Moreover any energy above and beyond the bandgap energy is lost; while blue light has roughly twice the energy of red light, that energy is not captured by devices with a single p-n junction: the electron is ejected with higher energy, but it loses this extra energy as it travels toward the p-n junction, this energy being turned into heat in the crystal.

Considering the blackbody and recombination effects alone, a solar cell has a peak theoretical efficiency of 68%. Thus the spectrum losses represent the vast majority of lost power. Considering all three effects, a single-junction cell made of silicon will have a theoretical peak performance of about 33.7%, or about 337 W/m² in AM1.5.

It is worth noting that the limit makes several fundamental assumptions: that the cell contains a single p-n junction, that the junction is tuned to visible light, and that any extra energy in the photons is lost. None of these assumptions is necessarily true, and a number of different approaches have been used to significantly surpass the basic limit. In fact the Shockley–Queisser limit only applies to cells with a single p-n junction; cells with multiple layers can outperform this limit. In the extreme, with an infinite number of layers, the corresponding limit is 86%.

2.7.6 Efficiency of DSSCs by comparison with Silicon solar cells

If we consider quantum efficiency, DSSCs are extremely efficient. There is both a high probability that an incident photon could be absorbed, due to the structure thickness, and converted into an electron. So the quantum efficiency is about 90 %, like traditional cells.

The maximum voltage generated is simply the difference between the Fermi level of TiO_2 and the redox potential of the electrolyte : about 0.7 V. This value is slightly bigger than Silicon solar cells (0.6 V). The heavier difference between these two kinds of cells is then the current value (I_{sc}). In fact, in spite of the great ability of the dye in photons-electrons conversion, only electrons with enough energy to overcome the band gap will be able to contribute to the final current. This gap is bigger than Silicon cells: this means that less electrons of sunlight are

available. Besides the electrolyte limits the speed at which dyes regain their electrons being so available again for photoexcitation. In conclusion the current (I_{sc}) produced by a DSSC reaches 20 mA/cm^2 against 35 mA/cm^2 of Silicon solar cells. Combined with a fill factor of 70 %, the efficiency we can attain with DSSCs is 11 % against 12-15 % of low-cost Silicon cells.

3. Carbon nanotubes

Carbon nanotubes (CNTs) formation has been noticed by different scientists since 1950s after the invention of TEM which allowed direct visualization of nanostructures. Nevertheless the discovery is attributed to Sumio Iijima of NEC in 1991, the first scientist who suggested a production method (arc discharge).

CNTs are allotropes of Carbon with a cylindrical structure. They consist of graphitic sheets which have been rolled up into a cylindrical shape.

- They possess a ratio length-to-diameter up to 28,000,000:1 that is significantly larger than any other known material (usually they have a length of some micrometers and diameters from 1 to hundreds of nm) ; this confer some extremely anisotropic properties.
- They form bundles which are entangled together in solid state by Van der Waals forces giving rise to a complex network

These nanotubes have novel properties that make them potentially useful in a lot of fields such as electronics, photovoltaic applications, optics, medicine, they can be used in biosensors, as fillers in polymer matrixes and many others; in fact they exhibit extraordinary strength and unique electrical properties and are efficient thermal conductors too.

CNTs belong to the fullerene structural family, which also include the spherical buckyballs.

CNTs are based on graphitic sheets, so the chemical bonding is composed only by sp^2 bonds, similar to the graphite ones. The bonding structure, which is stronger than the sp^3 bonds found in diamonds, and is not affected by the weak Van der Waals forces present among the graphitic planes, provides the molecules with their unique strength.

3.1 Types of carbon nanotubes and related structures

CNTs are divided in different categories according to the related structure.

The principal subcategories distinguish between:

- SWCNTs (or SWNTs): single-walled carbon nanotubes
- MWCNTs (or MWNTs): multi-walled carbon nanotubes

Most of SWCNTs have a diameter close to 1 nanometer and lengths that vary from nanometers to some centimeters. Their structure can be thought as wrapping a one-atom-thick layer of graphite into a seamless cylinder. The cylinder can be rolled up in different ways, represented by a couple of indices (n,m), called the chiral vector.

After having designed two base vectors a_1 and a_2 (lattice vectors), each of them connecting equivalent points in the CNT's structure and forming a 60° angle between them, the chiral vector OA = C_h=na_1+ma_2 is defined together with the chiral angle θ with the zig-zag axis.

All possible structures of SWCNTs can be formed from chiral angles lying in the range 0° < θ < 30°, just enrolling the nanotube by overlapping the extremities O and A of the chiral vector.

So tubes having *n* = *m* (θ = 0°) are called "*armchair*" and those with *m* = 0 (θ = 30°) "*zigzag*". All the others are "*chiral*" nanotubes.

The nanotube diameter *d* is related to *m* and *n* as

$$d = \frac{a}{\pi}\sqrt{(n^2 + nm + m^2)}.$$

In this equation, *a* is the magnitude of either unit vector a_1 or a_2.

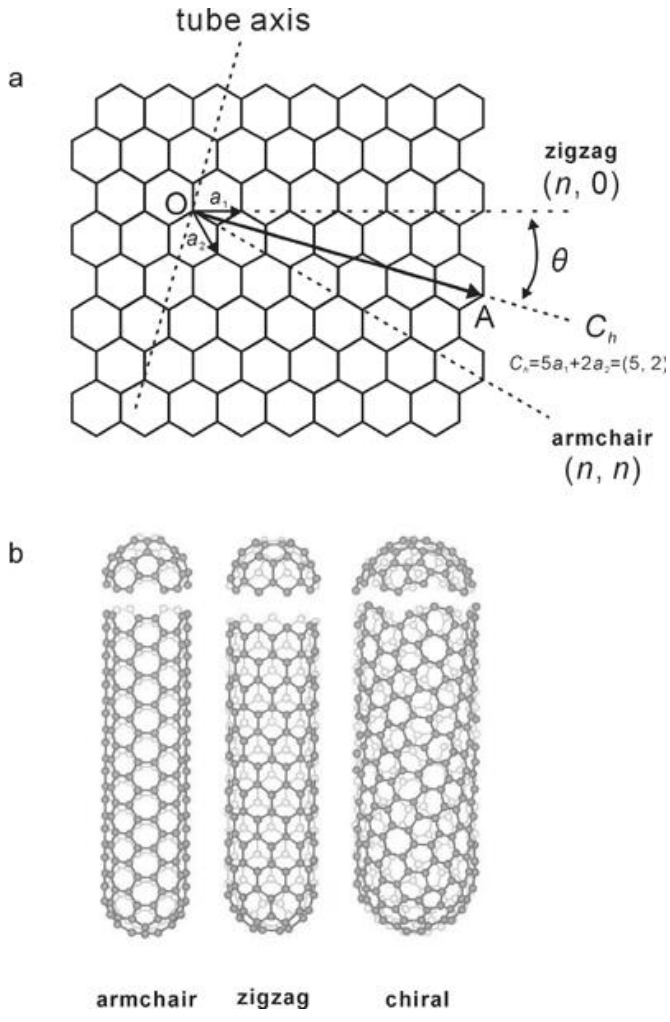

Fig. 9: CNT structure

SWCNTs are an important variety of nanotubes because they exhibit electric properties that are not shared by the MWCNTs: they are the main candidates chiefly in electric applications where their conducting ability can be exploited.

MWCNTs instead consist of multiple walled layers: concentric tubes of graphite. The interlayer distance is close to the distance between graphene layers in graphite, approximately 3.4 A.

Particularly interesting are DWCNTs (double-walled carbon nanotubes) which have morphologies and properties similar to SWCNTs but an improved resistance to chemicals: in fact covalent functionalization, required to add new properties to CNTs, will break some C=C double bonds, leaving holes in the nanotube, thus modifying both its mechanical and electrical properties; in the case of DWCNTs only the outer wall is modified.

There are then other structures such as Torus (carbon nanotubes bent into a doughnut shape, with predicted extraordinary magnetic properties), Nanobuds (CNTs combined with fullerenes), CSCNTs (cup-stacked carbon nanotubes, with a semiconducting behavior).

Thanks to potentiality of characterization techniques like TEM (transmission electron microscopy) and AFM (atomic force microscopy) and new chemical strategies an almost infinite number of Carbon nanostructures are available.

3.2 Synthesis

Different techniques have been employed to produce CNTs and some new ones are developing to let the commercialization of these materials:

- Arc discharge: carbon nanotubes were observed (together with fullerenes) in the carbon soot of graphite electrodes during an arc discharge. The yield of this method is up to 30 % and it produces both SWCNTs and MWCNTs with few structural defects and length up to 50 nm.
- Laser ablation: a pulsed laser vaporizes a graphite target in a high-temperature reactor while an inert gas is bled into the chamber; the yield reaches the 70 % and produces primarily SWCNTs with diameters controlled by the reaction temperature. However it is more expensive.
- Chemical vapor deposition (CVD): a blend of a carbon-containing gas and process gas is used. Organic vapors decompose and let carbon nanotubes (in a forest-like array) grow at the sites of a metal catalytic substrate, heated to 700 °C ; of the various methods for a CNTs industrial-scale production, CVD is the most promising owing to its price/unit ratio and because of the collecting opportunities. CVD growth of MWCNTs is nowadays used by several companies to produce materials on the ton scale.

3.3 Properties

Strength

CNTs are the strongest and stiffest materials yet discovered if we consider their strength and elastic modulus. They are estimated to be 100 times stronger than steel and 6 times lighter. This strength results from the covalent sp^2 bonds between the individual C atoms. (A test showed that a MWCNT reaches a tensile strength of 63 Gpa and a Young Modulus of 1000 GPa). Considering that CNTs have a low density (1.3-1.4 g/cm^3) it's clearly possible to obtain an incredibly high specific strength. A plastic deformation of CNTs starts at strains of approximately 5 %.

Electrical properties

Because of the CNTs nanoscale dimension together with symmetry and unique electronic structure of graphene, the structure of a nanotube strongly affects its electrical properties. Electrons flow only along the tube axis ("one dimensional transport") and their propagation involves lots of quantum effects.

For a (n,m) SWCNT,

- if n = m, the nanotube is metallic
- if n-m = 3*x , with x =1,2,… the nanotube is semiconducting with a very small band gap
- otherwise, the nanotube is a moderate semiconductor (gap is function of the tube's diameter)

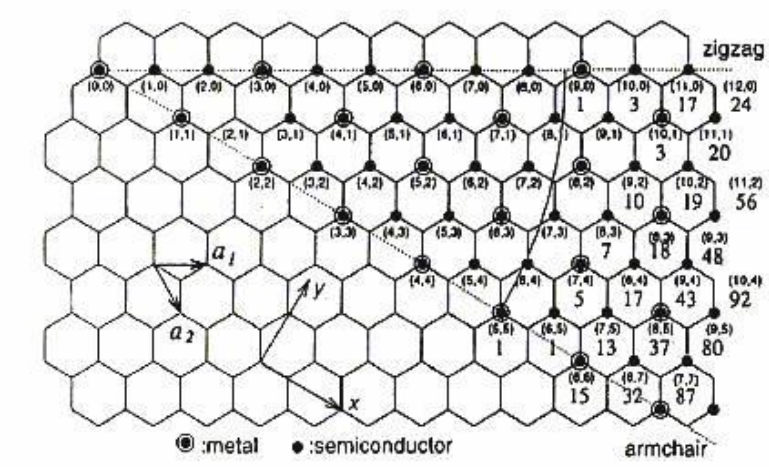

Fig. 10: metallic and semiconducting CNTs

In theory, metallic CNTs can carry an electrical current density of $4*10^9$ A/cm^2, that is 1000 times greater than copper.

The situation in MWCNTs is more complicated as they are made of different concentric tubes and properties are the result of contribution of the individual shells.

MWCNTs with interconnected inner shells show superconductivity with a relatively high transition temperature T_c = 12 K.

Thermal properties

All nanotubes are very good thermal conductors along the tube (10 times that of copper), but good insulators laterally to the tube axis. The temperature stability of CNTs is estimated to be up to 2800 °C in vacuum and about 750 °C in air.

Optical properties

CNTs have some particular optical properties which make them interesting for photovoltaic applications. CNTs quality is quite easily detectable by means of some quick and reliable characterization techniques such as optical absorption, photoluminescence and Raman spectroscopies. Thanks to these, non-tubular carbon content, structure (chirality) of the produced nanotubes, and structural defects can be monitored. From the latter features arise optical, mechanical and electrical properties.

CNTs are different each other. A wide variety of nanotubes is possible, with different diameters and so different curvatures, different lengths etc. , resulting in different tunable CNTs properties.

Optical properties of CNTs derive from electronic transitions between some certain one-dimensional density of states (DOS). A bulk material has a continuous DOS, instead for structures that are not 3-dimensional DOS is not a continuous function of energy; in particular for one-dimensional materials it descends gradually and then increases in a discontinuous spike. The sharp peaks found in one-dimensional materials are called Van Hove singularities.

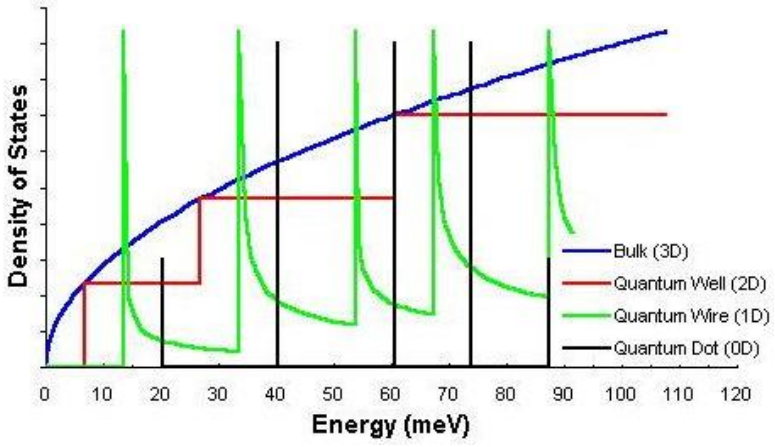

Fig. 11: density of states in bulk semiconductors and quantum structures

Van Hove singularities are responsible for the following remarkable properties of CNTs:

- Optical transitions occur between the $v_1 - c_1$, $v_2 - c_2$, etc., states of semiconducting or metallic nanotubes and are traditionally labeled as S_{11}, S_{22}, M_{11}, etc., or more generally as E_{11}, E_{22}, etc. Crossover transitions $c_1 - v_2$, $c_2 - v_1$, etc. are dipole-forbidden and thus are extremely weak, but it's possible to detect them.
- The energies between the Van Hove singularities depend on the nanotube structure. By varying this, the optoelectronic properties can be tuned.
- Optical transitions are rather sharp (~10 meV) and strong. Consequently, it is relatively easy to selective excite nanotubes having certain (n, m) indexes, as well as to detect optical signals from individual nanotubes.

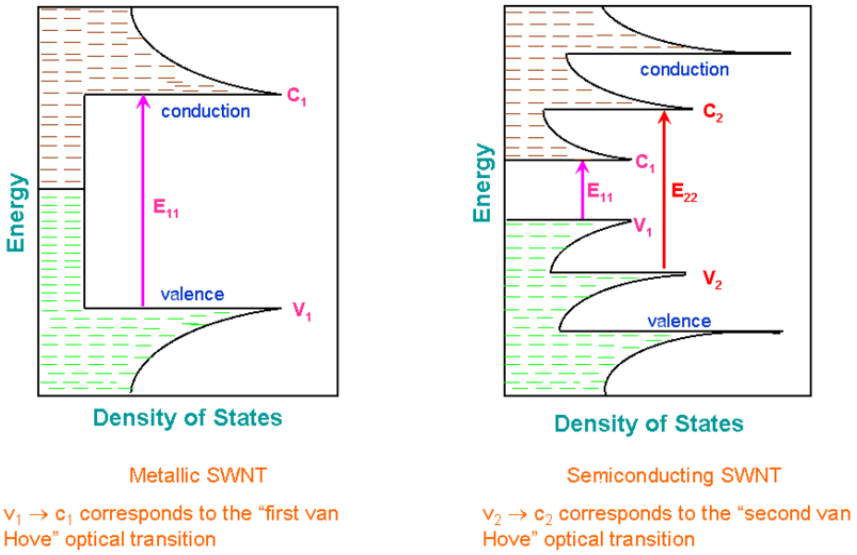

Fig. 12.: Energy levels in metallic and semiconducting CNTs

By means of an experimental graph named "Kataura plot" it is possible to predict the band structure of certain (n,m) CNTs. A Kataura plot relates the nanotube diameter and its bandgap energies.

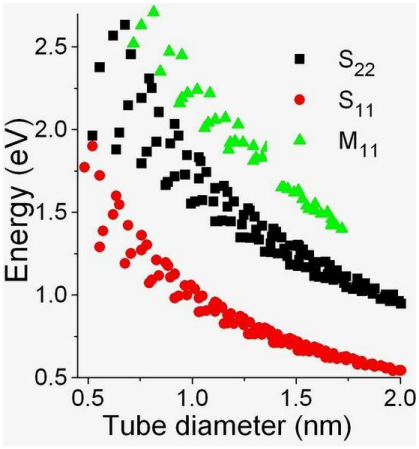

Fig. 13: Kataura plot: band-gap energies related to CNT diameters

Optical absorption spectra of CNTs are different from those of conventional 3D-materials. They present some sharp peaks (electronic transitions from the v_2 to c_2 (energy E_{22}) or v_1 to c_1 (E_{11}) levels, etc.) instead of an absorption threshold followed by an absorption increase. The transitions are relatively sharp, so they can be used to recognize different CNTs types.

Interactions between nanotubes, such as bundling, broaden optical lines. However bundling affects much more photoluminescence characterizations than optical absorption and Raman scattering.

Carbon nanotubes (in vertically aligned arrays of SWCNTs) are almost “ideal black bodies” in a wide spectral range having an absorbance of about 0.98 – 0.99. This arises from the fact that these arrays are composed of CNTs different each others with a wide variety of band-gaps. Moreover light might be trapped in these forests due to multiple reflections.

Luminescence

Photoluminescence is a powerful tool for CNTs characterization. The mechanism of PL is this: when a photon is absorbed a S_{22} transition takes place and we have the formation of an exciton (an electron-hole pair). The pair tends to rapidly relax (within 100 ps): from c_2 to c_1 state for the electron and from v_2 to v_1 for the hole. Then they recombine through a $c_1 - v_1$ transition resulting in light emission. This excitonic luminescence is not observed in metallic-CNTs: light photons can be absorbed and electrons thus can be excited to upper energy levels but the hole is immediately filled by another electron out of the many available (in fact in metallic-CNTs Van Hove singularities overlap in a continuous DOS).

Interaction between nanotubes or between nanotube and another material (substrate) quenches PL. For this reason, no PL is observed in multi-wall carbon nanotubes.

3.4 Defects

CNTs possess some defects that affect the material properties, as with any material. Examples of defects are:

- atomic vacancies: high levels can lower the tensile strength by up to 85%
- Stone Wales defects, which create a pentagon and heptagon pair by rearrangement of the bond.

Because of their very small structure, tensile strength of CNTs is dependent on the weakest segments present on the tube.

Crystallographic defects also affect the electrical properties of the nanotubes: a defect in some conducting CNTs can cause the surrounding region to become semiconducting and brings magnetic properties; generally the conductivity of the CNT is lowered. Moreover they reduce the tube's thermal properties leading to phonon scattering.

3.5 CNTs FUNCTIONALIZATION – selective chemistry of SWCNTs

As for fullerenes, where the reactivity is proportional to their curvature, CNTs reactivity depends on their curved morphology: the outer surface reactivity increases with increase in curvature. The sp^2 bonds of the graphene rolled layer show a certain degree of pyramidalization (a distortion of the molecular shape) and misalignment of π-orbitals: it means that the C=C bonds are not planar. The pyramidalization angle θ_p is a function of curvature thus of the diameter of CNTs: with increasing n, the diameter increases too, so θ_p decreases and thereby the reactivity. Some examples: for planar graphene $\theta_p = 0°$, for a (5,5) - SWCNT $\theta_p = 6°$, and for fullerenes $\theta_p = 11.6°$.

Reactivity is also highly sensitive to chiral wrapping (n,m) which determines its electronic structure.

CNTs are metallic or semiconducting based upon delocalized electrons occupying a 1D density of states; however every covalent bond on SWCNT sidewall causes localization of these electrons. Close to localized electrons SWCNT can no longer be described using a band model that assumes delocalized electrons moving in a periodic potential.

The biggest problem of CNTs is their lack of solubility and difficult manipulation in any solvent: as-produced CNTs are insoluble in all organic solvents and aqueous solutions (the hydrophobic surface disfavors the absorption of hydrophilic particles). They can be dispersed in some solvents by sonication but they immediately precipitate when this process is interrupted. On the other hand CNTs can interact with different classes of compounds, so their reactivity has to be exploited for their integration into inorganic, organic and biological systems.

Functionalization of CNTs can be summed up in some different approaches [38],[39]:

- defect site functionalization
- non-covalent interactions
- sidewall covalent functionalization
- endohedral inclusion

Defects functionalization

CNTs are usually purified by means of very strong oxidizing conditions, with a mixture of sulfuric and nitric acid with a 3 to 1 ratio: so an oxidation of the tubes occurs giving also rise to shorter nanotubes with opened ends. However the main result is the production of -COOH groups in the region of the oxidative damage (sidewall and opened ends). This treatment affords a wide variety of functionalized nanotubes. Generation of acyl chloride followed by simple esterification or amidation reactions offers the possibility to attach many organic fragments and synthesize a great variety of CNTs derivatives. We can see some examples found in literature:

- SWCNTs have been functionalized with octadodecylamine to get the corresponding SWCNT@ODA-amide. If hydrocarbon chains are inserted, the solubility of the ODA-CNTs in organic solvents will increase.
- SWCNTs have been decorated with fragments of N-anilinopyrazolino-[60]fullerene: this increases the mechanical properties of the CNT and tune the electronic and optical properties of the fullerene derivative making them interesting for optoelectronic applications
- With the same purpose SWCNTs@COOH have been functionalized with tetrathiafulvalene (TTF, that is a strong electrons donor)to evaluate the possible use of CNTs in solar energy conversion applications. Photo-physical analysis by time resolved spectroscopy revealed the presence of radical species ($TTF^{\cdot+}$ and $SWCNT^{\cdot-}$) indicating the presence of an efficient photoinduced electron transfer, a critical point for photovoltaic devices.

Non-covalent functionalization

Non-covalent interactions provide a way to functionalize CNTs without causing any damage to their electronic structure. It deals with a non-covalent adsorption of molecules thanks to Van der Waals forces or to π- π stacking.

A recent research work has suggested a π- π pyrene-SWCNT interaction. The scientists prepared a [60]fullerene-bisadduct bearing a pyrene unit, that was capable of solubilizing the CNT thanks to non-covalent interactions between pyrene and the sidewall of the SWCNTs; this was the first supramolecular hybrid of [60]fullerene and SWCNTs yet realized. By following the same strategy a variety of organic addends, including photo- and electro-active moieties have been supramolecularly connected to CNTs.

Covalent functionalization

As already mentioned, the curved morphology of CNTs plays an important role in their reactivity. The pyramidalization degree of sp^2 bonds makes the CNTs convex surface susceptible to addition reactions.

The insertion of a covalent bond destroys the CNT band structure, that consequently becomes an insulator, at least in the proximity of the sp^3 bond created.

Among the kinds of covalent functionalization we can mention:

- **Sidewall halogenations**: As an example we can mention fluorination, a process which improves solubility and processability. It is reversible: the fluorine moieties can be removed by treatment in hydrazine. Fluorination is useful because further substitution can be accomplished. Reaction with Grignard or organolithium reagents gives life to CNTs soluble in THF; instead nucleophilic substitutions with diamine or diols produce compounds soluble in water and diluted acids
- **Hydrogenation**: It consists of a protons bombardment or a reduction of CNTs with metallic Lithium
- **Cycloaddition**: it's an addition reaction of carbene, nitrenes or azides to pristine CNTs. An example of cycloaddition spawns CNTs bearing pendant amino groups (SWCNT@NH2), that are particularly suitable to attach for example to electron donors like ferrocene whose photophysical analysis reveals the existence of a photoinduced electron transfer process and an effective generation of charges, evidencing the great potential of these compounds in photovoltaic applications. A base-catalyzed cycloaddition of the osmium tetroxide (among the most powerful oxidants for alkenes) occurs at low temperature, forming osmate esters that generate diols, if hydrated. The reaction is highly selective to the metallic tubes (chemoselective)
- **Radical or nucleophilic addition**: it has particularly developed after the discovery of *diazonium salts* (compounds based on an aromatic ring with a highly reactive diazonium group that make the compound instable). It provides a great probability of

reaction of radicals on the walls of CNTs. Two types of coupling reactions can take place: the reductive coupling of aryl diazonium salts, and the oxidative coupling of aromatic amines, the former creating a C-C bond, the latter a C-N bond. The reaction with diazonium salts can be in-situ via electrochemistry or it can be a two-steps reaction. Diazonium reaction doesn't modify the CNT structure so maybe it keeps its mechanical properties

- **Grafting of polymers** : covalent reaction of CNTs with polymers is important because the long polymer chains help to dissolve the tubes into a wide range of solvents even at a low degree of functionalization. We remember two strategies for attachment of polymers:
    - **Grafting to**: synthesis and end-group transformation of a polymer and then attachment to CNTs
    - **Grafting from**: polymers precursors are brought to the surface of CNTs and a subsequent propagation of polymerization occurs in the presence of monomeric species. It is an in-situ radical polymerization process: CNT surface double bonds are opened by initiators molecules and the CNT surface plays the role of grafting agent

  For example, assemblies of PSS-grafted CNT with positively charged porphyrins were prepared via electrostatic interactions. Incorporation of CNT-porphyrin hybrids onto indium tin oxide (ITO) electrodes led to solar energy conversion devices. This systems displayed monochromatic photoconversion efficiencies up to 8.5 %. Instead anion polymerization was exploited for covalent grafting of polystyrene chains and in-situ ultrasonic induced emulsion polymerization to get MWCNT@PMMA. A different approach called ATRP (atom transfer radical polymerization) let to attach some initiators to the graphitic network to obtain various acrylates.

Endohedral inclusion

Pure elements (Au, Ag), small molecules (metallic halides, metal oxides) or fullerenes can be inserted into the cavities of CNTs.

Others functionalizations

After a first functionalization of CNTs it's possible to go on with more complex treatments exploiting the reactivity of these functions.

For example a *Sol-Gel approach* was used to cover CNTs with different oxides (SiO_2, ZnO, TiO_2 etc.). Most of sol-gel processes are performed on CNTs oxidized via acid treatment: in fact for example an amidation of the –COOH is a simple task.

3.6 CNTs characterization techniques

Different techniques can be used to characterize the structure and the surface of CNTs. None of them is exhaustive and give a complete description of the sample. Some standards are required for a more reliable interpretation.

Raman spectroscopy

Raman spectroscopy is used to study vibrational, rotational, and other low-frequency modes in a system. It relies on inelastic scattering from a laser source which interacts with phonons in the material. In practice laser light collides with the material molecules and interacts with their electronic clouds and bonds. The photon excites the molecules from the ground state to an upper energy state and transfers some energy (inelastic scattering). When the molecule relaxes it emits a photon and returns to a different rotational or vibrational state. The difference in energy between the original state and this new state leads to a shift in the emitted photon's frequency that is a change in the molecular polarization (or amount of deformation of the electronic cloud). The pattern of shifted frequencies with respect to the vibrational coordinate is determined. The shift in energies gives information about the phonon modes in the system.

Raman spectroscopy is probably the most popular technique of carbon nanotube characterization, especially SWCNTs. The principal characteristic peaks in the spectrum are identified as:

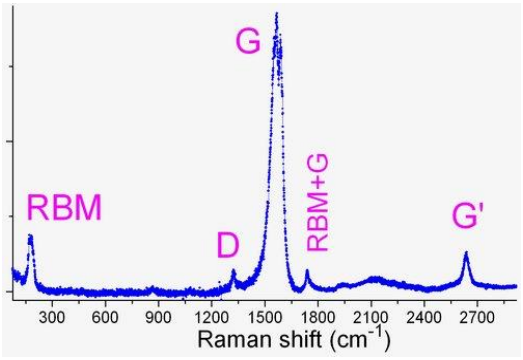

Fig. 14: typical Raman spectrum

- *Radial breathing mode (RBM)*, which correspond to a radial contraction/expansion of the nanotube. Therefore the associated frequency depends on the CNT diameter
- *Bundling modem,* that is a special form of RBM probably originating from collective vibration in a bundle of SWCNTs
- *G*("graphite") *mode*, which corresponds to planar vibrations of carbon atoms and is present in most graphite-like materials. G band in SWCNT is shifted to lower frequencies compared to graphite and is split into several peaks. It can be used to estimate the tube diameter and whether the tube is metallic or semiconducting
- D mode, that is present in all graphite-like carbons and originates from structural defects. Therefore, the ratio of the *G*/*D* modes is used to quantify the structural quality of carbon nanotubes.
- *G' mode*, which is the second overtone of the defect-induced D mode. While D mode is forbidden in the ideal nanotube and requires a structural defect to appear, G' mode does not require defects. Its spectral position depends on SWCNT diameter, so it can be exploited to roughly estimate it. G' mode is a doublet in DWCNTs.

In summary, Raman spectroscopy provides information about CNTs diameter, electronic structure, purity, crystallinity, chirality and allow the distinction between metallic and semiconducting SWCNTs.

Electron microscopy

Scanning electron microscopy (SEM) and transmission electron microscopy (TEM) are based on the direct observation of the samples. They provide a quantitative analysis, for what concerns CNT length, diameter, bundle sizes, catalyst particle sizes, and a qualitative determination which considers surface coatings, impurity structures, relative concentrations.

Photoluminescence

The coordinated energies of the v_2-c_2 and v_1-c_1 transitions are mapped to the diameter and helical properties of individual SWNTs with specific *n*,*m* coordinates. The ovals in the map define (S_{22}, S_{11}) pairs, which uniquely identify (*n*, *m*) index of a tube. The data are conventionally used for the identification.

Thermal gravimetric analysis (TGA)

It is a controlled oxidation process that gives quantitative data on the weight fractions of carbon and metal catalyst in the sample, and the temperatures of bulk oxidation events.

4. Quantum Dots

4.1 Generalities

Semiconductor nanocrystals are tiny crystalline particles, with typical dimensions in the range of 1-100 nm, that exhibit size-dependent optical and electronic properties principally due to their small dimensions and the high ratio surface/volume: it's well known that superficial atoms possess different characteristics from inner atoms and this fact has a non negligible impact.

These particles bridge the gap between small molecules and large crystals thus enabling the exploitation of discrete electronic transitions (characteristic of isolated atoms and molecules) as well as useful properties of crystalline materials.

In *bulk semiconductors* electrons are distributed in a range of levels very close each other so that to be considered a continuum: it deals with two energy bands, the valence and conduction band, separated from a *band gap*, which is composed of various energy levels, precluded to electrons. The band gap is constant and characteristic of a specific material.

In classic semiconductors the great majority of electrons are in the valence band, that is in practice completely filled thus electrons can be considered motionless. To jump into the conduction band electrons have to gain enough energy (for example from heat or light photons) to cross the gap, but most of electrons at room temperature have not it. When an electron is raised into the conduction band it can move as well as the positively charged hole that it leaves into the valence band, to yield a current if an electric field is applied. Their lowest energy state is an electrostatically bound electron-hole pair, known as the "exciton". Electrons can't stay forever at the higher conduction band energy level and tend to come back into the valence band, releasing electromagnetic energy at the wavelength correspondent to the energy lost: the most common transition (radiative recombination) occurs between the lowest energy level of the conduction band (LUMO) and the highest level of the valence band (HOMO) ,i.e the band gap: as the band gap is constant for a certain semiconductor, the transition has a fixed emission frequency.

We can extend the same considerations for microscopic semiconductors (QDs). However there is a substantial difference. Excitons have an average physical separation between electron and hole, referred to as the *Exciton Bohr Radius*. This distance is different for each material. In bulk, the dimensions of the semiconductor are much larger than the Exciton Bohr Radius,

allowing the exciton to extend to its natural limit. Otherwise if the semiconductor NP is so tiny that its size approaches the material's Exciton Bohr Radius, the charge carriers become spatially confined, which raises their energy; energy levels can no longer be considered as continuous but rather they must be treated as discrete, meaning that some appreciable finite separations come up: we refer to that as to a "*quantum confinement*" regime; under these conditions, the semiconductor material ceases to resemble bulk, and instead can be called "*quantum dot*".

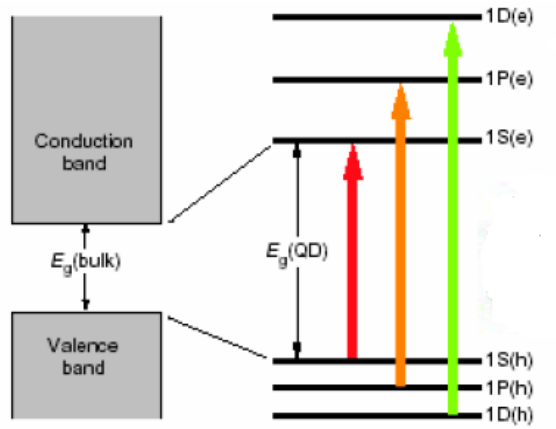

Fig. 15: discrete energy levels in quantum dots

For NPs littler than 10 nm electronic excitations feel the effect of particle borders and respond to dimensions changes by modifying their spectra. This affects the absorbance and emission of semiconductor.

Consequently to discrete energy levels, the addition of only few atoms to QDs (changing superficial geometry) involves a change in the band gap extension: it will be always bigger than bulk semiconductor resulting in a shift towards lower wavelengths and bigger energies in the emitted radiation (blue shift). In QDs the emissivity can be monitored: the size of the band gap is controlled simply by adjusting the size of the dot.

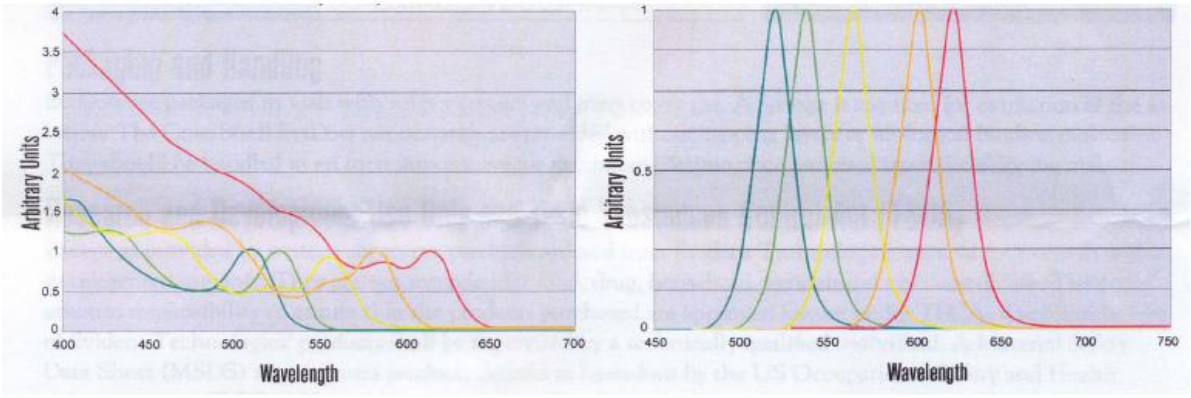

Fig. 16 : Absorption and emission spectra of QDs of different dimensions

Generally the littler the QD dimensions the bigger the band gap.

For what concerns *emission spectra*, it's interesting to evaluate their variability as a consequence of both the superficial conditions and the number of unsaturated bonds.

Above all emission life-time and emission quantum yield (QY) are affected: quantum efficiency of radiative recombination can approach unity at room temperature, in the visible and near-IR regions of the spectrum. This high efficiency is largely due to strong overlap between the electron and hole wave functions in the confined structure, whereas the exciton in bulk semiconductors is not confined in space and can rapidly dissociate increasing the probability of non-radiative relaxation associated with crystalline defects. In fact superficial defects and charge carriers traps can furnish some energy levels, inside the band gap, that can modify the emission spectrum. However most semiconductor nanocrystals are not used in vacuum but are usually suspended in solution and coated with organic ligands. Thereby the dangling bonds on the surface are passivated by bonding with atoms or molecules. For example, molecules such as TOPO (trioctylphosphine oxide) and HDA (hexadecylamine) adsorb to the nanocrystal surface through dative ligand-metal bonds between the basic moiety on the ligand and metal atoms on the nanocrystal surface. If the surface is passivated so that to eliminate the non-radiative superficial recombination, high luminescence yields are obtained. Another advantageous passivation method is used for light-emitting applications: a different kind of semiconductor is deposited on the surface of the first semiconducting nanocrystal thus setting up a core-shell QD.

4.1.1 Carrier multiplication

When a QD is excited with an energy at least twice its band gap, the electron that has been raised into the conduction band can collide with another electron and release its excess kinetic energy thus achieving another electron-hole pair: the result is a *biexciton* and an internal quantum efficiency greater than 100 %. The multi-exciton generation (MEG) may yield improved efficiencies in *photovoltaic devices*.

These Auger processes are most observed in nanocrystals rather than in bulk semiconductors because of the suppression of the phonon-assisted decay rate and the large energy separations between electronic energy levels. Although the Auger processes are so fast to leave few time for radiative recombination, biexciton and triexciton fluorescence has been observed at room temperature with high quantum efficiency and long lifetimes in CdSe/ZnS QDs. The challenge is to exploit at best this extra charge carriers by maximizing their stabilization before they decay via Auger processes, to convert them into an external electric current.

So far MEG has been demonstrated in synthesized quantum dots including PbS, PbSe, PbTe, CdS, CdSe, InAs, InP and Si.

4.1.2 Band gap engineering

Unlike bulk semiconductors, nanocrystals have a lot of parameters such as size, shape, composition (for example by impurity doping) and lattice straining that can modulate their electronic band gaps.[47] Quantum confinement can shift the gap giving a continuous tunability.[46]

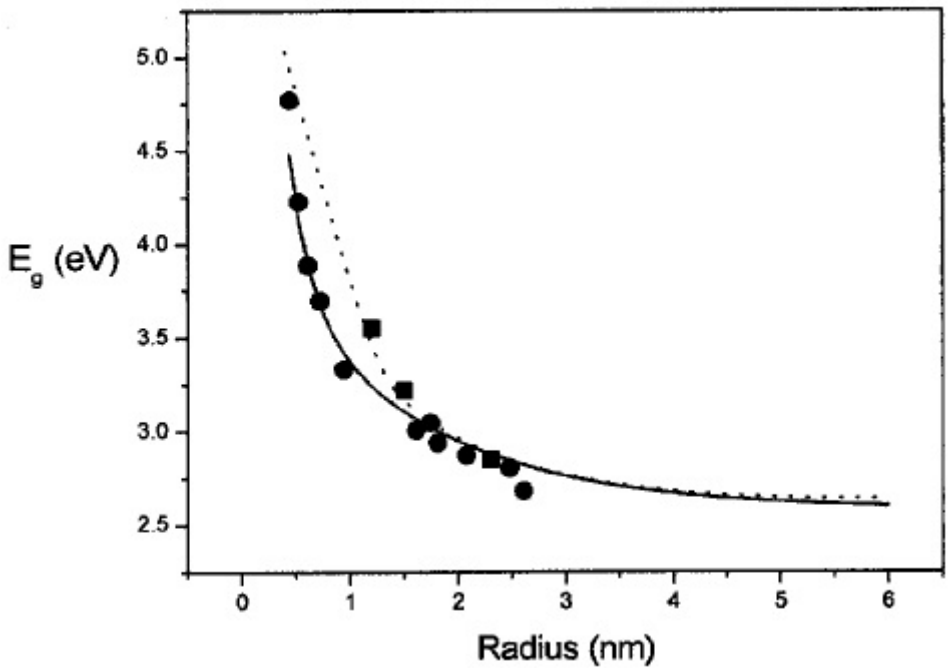

Fig. 17: Experimental and calculated effective band-gap energies for CdS semiconductor Qds as functions of the QD radius.

Recently have been developed some *core-shell* semiconductor NPs in which the conduction and valence bands of the core and shell material are staggered, resulting in the segregation of the electron and the hole between the core and the shell materials. For example (CdTe)CdSe particles form a *Type-II structure* where the electron is kept in the shell and hole in the core, and carrier recombination can occur across the interface at a lower energy (higher wavelength) than the band gaps of either of the constituent semiconductor materials. The reduced spatial overlap between the electron and hole also results in a significant increase in excited state lifetimes.

With Type-II materials it is possible to control which charge carrier is accessible to the surface for charge transfer applications. Therefore they can be exploited for *photovoltaic devices*, especially with the development of anisotropic materials in which the directional segregation of charges can enhance directional charge transport.

In our work we will use a Type-I core-shells: they are based on a CdS core (the semiconductor responsible for light capture) and a higher band gap ZnS shell. This is a structure where both carriers are localized within the same material (the core in this case), thereby they have to tunnel through some additional potential barrier to extend into the surrounding matrix. Then the optical and electrical properties reflect the confinement of carriers in all three dimensions. The ability to localize electron-hole pair in type-I structures is beneficial for applications in

which high PL and chemical stability is required (we will have exactly the above mentioned problems).

4.2 Synthesis methods

Synthesis of semiconducting QDs made of two different elements (usually belonging to II-VI groups or III-V) involve the reaction between two solutions which contain the respective elements that are going to constitute the crystal lattice of the desired semiconductor.

Among nanometric semiconductors, CdS NCs have attracted much attention due to their size-dependent photoluminescence (PL) tunable across the Visible spectrum, and to the advances in their preparation method that make them suitable for *solar energy applications*.

We are pretty interested in calchogenic elements semiconductors and chiefly CdS and ZnS quantum dots.

By means of nanocrystals growth within nanocavities it is difficult to get monodispersity. Otherwise NPs dimensions can be controlled by affecting kinetic parameters, thus hindering nucleation and growth by varying reaction conditions and monodispersity is achieved.

Numerous colloidal (solution) chemistry methods have been developed for the preparation of nanocrystals. The solution chemistry synthesis utilizes organic stabilizers to cap surface atoms of nanoparticles in order to control the growth process; the kind of stabilizer is of great importance since it affects the chemical and the physical properties of the NCs. We can distinguish between two principal routes:

- organic routes
- aqueous ways: recently developed; these are more reproducible, low-cost and environmentally friendly than organic routes and the “as-produced” samples are more water-soluble.

We concentrate our attention on the organic routes. The most known methods are:

- Use of organometallic precursors in coordinating solvents
- Use of non-organometallic precursors in non-coordinating solvents

The difference between these two approaches resides in the possibility for monomers reactivity in non-coordinating solvents to be controlled by varying the concentration of ligands in the solvent.

Whatever the method is, the QDs surface plays an essential role. It is composed of unsatured bonds that is empty orbitals of calcogenic (Se, S, etc.) and metallic (Cd, Zn, etc.) elements, passivated by organic ligands. The nature of the ligands sets the solubility properties, which are in fact dependent on the chemical environment present around the surface. The functional

group of the ligand choice is accomplished with regards to the nucleation and growth conditions required. The conditions of solubility can be controlled by means of two different methods: the direct exchange of ligands which bind more or less strongly to the surface, or the use of a *shell-micelle* which doesn't attach the particle surface and doesn't depend on functional groups.

4.2.1 Polyol synthesis of nanoscale MS particles (M = Zn, Cd)

To perform our synthesis we have chosen the polyol process. It involves a metal precursor that is heated in a high-boiling alcohol (b.p > 200 °C). In the case of noble metals cations are reduced by the alcohol to form particles of the metallic element; in contrast, while adding a defined amount of water, non-noble metals precipitate to yield nanoscale oxide particles. Owing to the high temperature during the synthesis, normally well-crystallized materials are realized. As a further advantage, the polyol medium efficiently complexes the surface of the particles; consequently, the particle growth is limited and an agglomeration of particles is prevented.

The particle diameter depends on experimental conditions: concentration of precursors, temperature, heating time as well as on the solubility of the NPs obtained. The size distribution is closely related to the average particle diameter: the larger the particle diameter, the broader the particle size distribution.

5. Carbon nanotubes and QDs in photovoltaics

Because of the interesting electrical properties of CNTs lots of efforts have been made to use them in photovoltaic applications as charge (electrons) carriers.

Otherwise QDs have shown extraordinary light-harvesting abilities. They have been used in solar cells in composites with polymers with quantum yields less than 2 %. This percentage is relatively low in comparison to *inorganic solar cells*. This disadvantage is mainly due to the difficulties in transferring the charge carriers away from QDs in the device.

Use of CNTs can be a solution: they can "electronically communicate" with NPs. CNTs decorated by QDs could act as nanowires that promote direct charge transport and efficient charge transfer to QDs, thus creating efficient solar cells.

Our experience will revolve around these concepts.

5.1 Solar cells based on NPs

In solar cells based on NPs the photoexcitation of the QDs results in the formation of an electron-hole pair in the conduction band and the valence band respectively. The ejection of the conduction-band electrons to the electrode, with concomitant scavenging of the valence-band holes by a solution-solubilized electron-donor, results in the formation of an anodic photocurrent.[48] Alternatively, the trapping of the conduction-band electrons by an electron-acceptor, solubilized in the electrolyte solution, and the subsequent transfer of electrons from the electrode to the valence-band holes yield a cathodic photocurrent. The electron-hole recombination in the NPs is, however, a rapid process that competes with the electron-ejection process, to the electrode or to the acceptor trap, and this results in a low light-to-electrical energy conversion efficiency. Thereby many efforts have been done to improve the efficiencies of solar cells by delaying the electron-hole recombination. Among these we can consider the use of composite semiconductor nanoparticle structures, such as $CdSe/TiO_2$, CdS/SnO_2 [20],[33], or core-shell semiconductor NPs as means to enhance charge separation, and still the incorporation of semiconductor NPs in organic semiconductor polymer matrices. Finally we concentrate on the methods that involve the creation of an hybrid structure between semiconductor NPs and functionalized carbon nanotubes.

Before talking about our functionalization strategies we report some studies on the use of CNTs and QDs for opto-electronic devices.

5.2 CNTs in OPVs

Organic photovoltaic cells operate in a different way compared to P-N junction devices. They don't capitalize on electric field of a P-N junction to separate the electrons and holes created when photons are absorbed. When a photon is converted into an electron-hole pair, typically in the donor material, the charges tend to remain bound in the form of an exciton, and are separated when the exciton diffuses to the donor-acceptor interface. The short exciton diffusion lengths of most polymer systems tend to limit the efficiency of such devices.

Combining the physical and chemical characteristics of conjugated polymers with the high conductivity along the tube axis of CNTs is an interesting idea to improve efficiency of OPV devices.

5.3 CNTs in DSSCs

In DSSCs TiO_2 nanoparticles have been widely used as a working electrode because they provide a high efficiency, more than any other metal oxide semiconductor investigated. Despite the success of this cells the effort to further enhance efficiency has not produced any major result. The transport of electrons across the particle network has been detected as a key problem in achieving higher photoconversion efficiency. Because of many grain boundaries on the electrons random path the probability of their recombination with oxidized sensitizers, before they are efficiently collected at the electrode surface, is increased. This results in inconvenient enlarging of oxide electrode surface area.

Therefore *semiconducting CNTs* electron-accepting ability could be used to direct the flow of photogenerated electrons and assist in charge injection and extraction. To assist the electron transport to the collecting electrode surface in a DSSC, CNTs can be used as anchor light harvesting semiconductor particles.[33] On the other hand the organization of photoactive donor-acceptor assemblies on the electrode surface has already shown to offer significant enhancement in the photoconversion efficiency of solar cells.[35]

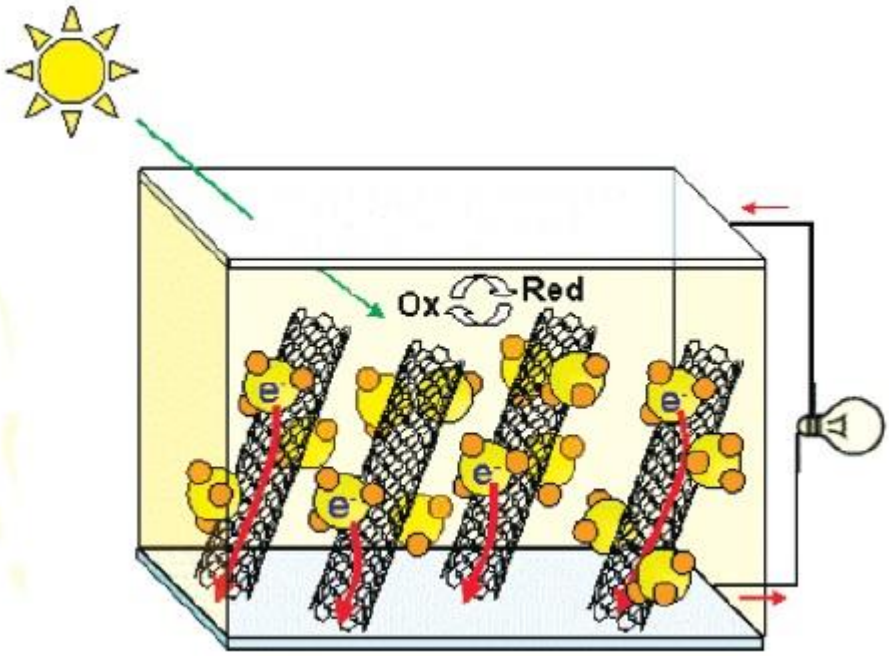

Fig. 18: photovoltaic device based on CNT-TiO_2 hybrids [33]

The analysis performed on CNT/DSSCs has highlighted no significant influence in the charge injection rate by the presence of SWCNTs in the film. However the photoinjected electrons in TiO_2 survive roughly 50 % longer when embedded within the SWCNT network. The equilibration of electrons between SWCNT and TiO_2 results in the transfer of a fraction of electrons into SWCNT, thus stabilizing the photogenerated electrons and reducing the rate of exciton recombination. Moreover, suppressing the back electron transfer and improving the electron transport within the nanostructured TiO_2 film are regarded as the two most important factors controlling the overall IPCE of the cell: in fact photoconversion efficiencies are generally enhanced.

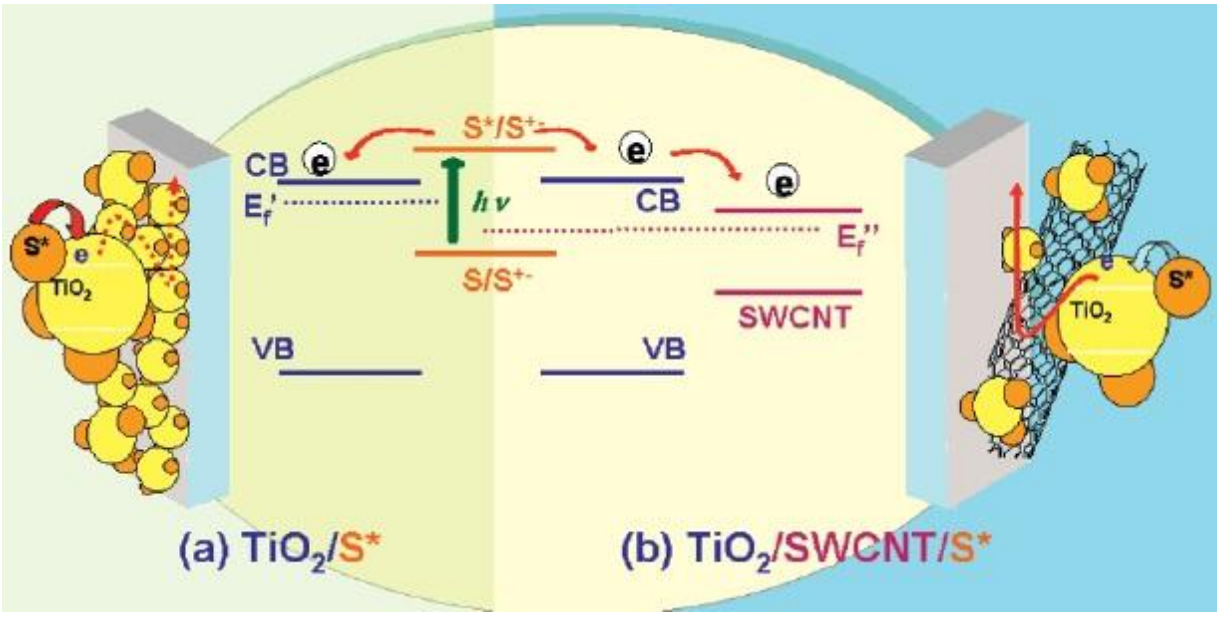

Fig. 19: influence of CNTs in DSSCs [33]

Furthermore, some researches indicate that introducing CNTs decreases the TiO_2 crystalline grain and particle size: thus TiO_2 semiconductor may possess a larger surface area and have a greater number of contact points among the particles, CNTs and the substrate. These results are beneficial for the improvement of the cell performance.

In few words, CNTs facilitate charge separation and promote electron transport to the electrode surface, thus generating higher photocurrent at the expense of the open-circuit voltage. Unfortunately any improvement in photocurrent is nullified by the increase in photovoltage. But this is the result of a multiple separated deposition of semiconducting CNTs followed by a TiO_2 film onto an electrode.

Other essays have been done with a CNT dispersion of MWCNTs in TiO_2 through a modified *acid-catalyzed sol-gel procedure* from alkoxide precursors that prevents the aggregation of MWCNTs.[34] Here the CNT loading is quite low (0,1-0,5 % in weight) and the overall behavior of the cell depends on it. It was observed that the efficiency value was enhanced effectively with the increase of MWCNT loading (until a certain percentage) owing to higher IPCE values, photocurrents and this time also higher open-circuit voltages. However with a higher MWCNT loading the I_{sc} values exhibit a considerable decrease as the MWCNT content increases. This may be due to the light harvesting competition between the dye-sensitizer and the MWNTs (it's always the case of the presence of semiconducting CNTs).

5.4 Combination of CNTs and conductive polymers

Use of *polyanilines*, *polypyrroles* and *polythiophenes* has been investigated to combine conductive electroactive polymers and CNTs into composites with unprecedented mechanical and electrical properties. Different preparation methods are currently in use to get the best interaction between the two materials. For example composites prepared by *in-situ* polymerization of aniline in the presence of MWCNTs enhance electronic properties, attributed to interactions between the Pan-quinoid unit and the MWCNT surface: during polymerization CNTs are thought to guide the growth of aniline acting as molecular templates, facilitating efficient π-π interactions between Pan and CNT. It can be expected that composites based on "metallic polyaniline" and individual CNTs should be able to push conductivity values toward and possibly beyond 104 S/cm depending on the quality of CNTs, the state of CNTs *debundling* and interactions between Pan and CNTs.

5.5 Decorating CNTs with metal or semiconductor NPs

Due to their large chemically active surface and stability at high temperatures CNTs have been used as a support material for linkage of metal and semiconductor NPs. Several ways have been investigated to immobilize NPs on the CNTs surface:

- formation and stabilization (reduction and deposition, in-situ) of metal NPs directly on CNTs surface
- connection of chemically modified NPs to CNTs or to modified CNTs using *covalent linking* through organic fragments or *weaker bonds* (the linker simply sticks to the CNT surface through weak intermolecular interactions such as $\pi-\pi$ stacking, hydrophobic or electrostatic attractions).

The most important issue for the development of these hybrid materials for technological applications is related to discovery of powerful synthetic strategies to create materials with reproducible properties and performances. Each approach possesses some advantages and drawbacks. It is the potential application that determines which one is preferable each time.

- The *direct reduction-deposition method* is simple and effective, it allows to deposit a large amount of NPs; on the contrary it is difficult to control NPs characteristics such as size, shape and composition
- *Chemical linking processes* are more complicated and often based on a multistep reaction (formation of NP, chemical modification of both components and their connection); moreover the number of NPs linked to CNT depend on the number of –COOH or other functional groups present on the nanotube thus it is limited; otherwise

NPs, which are formed separately previously, can be selected by size or shape and the connection can be reversible.

Generally approaches relied on covalent methods require breaking of C=C bond and the reaction of the resulting –COOH group to give products via *nucleophilic acyl substitution*: this alters the SWCNTs structural and electronic properties by disrupting the sp^2 hybridized bonding and the 2p-2p π conjugation. Instead non-covalent strategies which use π–orbital interactions mitigate this concern.

For our purpose we concentrate on chemical linking of preformed NPs. Here we present some examples:

- oxidation of SWCNTs and subsequent reaction with aliphatic amines, to give amides leads to soluble functionalized nanotubes; then Au NPs are connected to oxidized SWCNTs using *aminothiols* or *bifunctional thiols* which act as linkers for Au colloids; the same strategy is also used for functionalization with *thioether* groups.
- acetone molecules absorbed on CNTs are seen to interact hydrophobically with Au nanoclusters covered with a monolayer of *octanethiols*. Besides if NPs are covered by a mixed-monolayer of decanethiol and mercaptoundecanoic acid they can be efficiently linked to oxidized CNTs: we have a double interaction both hydrophobic between the alkyl chains and the CNT surface and hydrogen-bond between COOH groups of CNTs and those present on the NPs surface; this leads to very stable composite materials (for example, thermal treatment at 300 °C to remove the capping shells of the Au NPs induces aggregation of the NPs that stick strongly to CNT surface, and sonication in hydrophobic solvents fails to disassemble the composite material).
- recently a predictive model for interactions (charge transfer, Van der Waals, covalent..) between TOAB-stabilized Au NPs and covalently modified MWCNTs with *alkyl* and *alkylthiol* chains has been reported to predict the coverage of CNTs by Au NPs for a range of different experimental conditions. For example, arising from both experiments and theory, it has been seen that as length of the alkyl chains at the surface of the MWCNTs increases the coverage decreases. The understanding of the parameters that control MWCNTs-NPs assembly are the basis for design and control of more complex hybrid materials.
- pyrene molecules, bearing a long aliphatic chain terminated by a thiol group can connect CNTs to Au NPs via *π-stacking* of the *pyrene* moiety to the CNT surface. Spectroscopic experiments on the composite material show that the pyrene fluorescence is completely quenched: this implies a charge transfer character between

CNTs and Au NPs mediated by the linker. This kind of electron transfer process has also been observed to occur on SWCNT-Zn *porphyrin* hybrid materials. The approach has been extended to other linkers with similar structures such as *1-pyrenemethylamine*, *N-(1-naphthyl)ethylenediamine* and *phenethylamine* demonstrating the generality of this strategy.

- *electrostatic interactions* have also been used to anchor metal NPs to CNTs. For example oxidized CNTs have been treated with a ionic polyelectrolyte which serves as an anchor for charged metal NPs. By choosing different kinds of polyelectrolytes (cationic or anionic) the surface of the CNT can be positively (negatively) charged in order to accept negatively (positively) charged NPs.
- CdSe has been connected to CNTs. QDs are stabilized with a mixed-monolayer of *trioctylphosphine oxide* and *2-aminoethanethiol*. The amino-functionalized QDs react with the carboxylic groups of the oxidized SWCNTs, forming amine bonds. A significant charge transfer is observed.
- heterojunctions between MWCNTs and *thiol*-stabilized ZnS-capped CdSe QDs have been created. The same strategy was used to attach CdS QDs to CNTs and this allows to reach an efficiency up to 70 %, higher with shorter CNTs. The result suggests that the length of CNT plays a major role in the formation of photocurrents and probably the defects in the CNTs affect the extent of charge separation that follows the photoexcitation of the CdS NPs.
- A LBL (*layer-by-layer*) self-assembly technique has been exploited for the deposition of CdTe nanocrystals onto CNTs yielding linear colloidal CNT@CdTe composites with a high degree of coverage. The photoluminescence quenching of the QDs can be controlled through the growth of a silica-shell spacer between the CNT surface and the deposited QDs: the SiO_2 layer minimizes the photoluminescence quenching and preserves the quantum confinement effects.
- a *1-pyrenebutyric acid N-succinimide* ester (PBASE) molecule has been used for the non-covalent functionalization of SWCNTs (both metallic and semiconducting), then attached to *4-aminothiophenol* functionalized NPs. The effectiveness of the $\pi-\pi$ interaction between PBASE and CNT is highlighted by absortion spectra analysis; in fact in the SWCNT@PBASE spectrum we can notice a red-shift for the second SWCNT semiconducting transition (E_{22}) and first metallic transition (E_{11}): these red-shifts imply $\pi-\pi$ interactions which promote delocalization of π electrons in the

SWCNT thereby lowering the absortion energy associated with the interband electronic transitions. These results are consistent with shifts observed in Raman spectroscopy analysis: peaks frequency slightly changes in SWCNT@CdSe (congruent with red-shifts) but none of the major Raman modes are disrupted by the non-covalent interaction with PBASE or attachment of CdSe QDs.

5.6 Our strategies

The focus of our work will be the creation of MWCNTs@QDs composites using CdS and CdS/ZnS core-shells as semiconductors and exploiting their sulfur-affinity to embed them into CNTs by means of different functional groups. Among these linkers we aim to test a *mercaptosilane*, *mercaptobenzene* and a *carbamate* compound.

Therefore here we will show the characteristics of these ligands and their use in applications we can take advantage of.

5.6.1 Ligands characteristics

Phosphines, amines and *thiols* are groups able to strongly adhere to the surface of the QDs. *Thiols* exhibit the strongest affinity thus being the most used, but they can be easily photo-oxidized on the surface of the QDs, which can cause aggregation of the QDs. *Carbodithioate* ligands are much more stable against photo-oxidation and thus would be a better choice for protecting the QDs, however their flexibility is limited. *Dithiocarbamates* instead are highly photostable as well as easy to synthesize.

Therefore to embed QDs in CNTs a double strategy can be followed by means of dithiol-functions: CNTs can be functionalized and later the affinity of cations of NPs for Sulfur can be exploited; otherwise QDs can be directly functionalized with ligands with a double function which allows them to interact both with NPs and aqueous/organic solvents. Generally most of the organic synthesis lead to QDs coated with hydrophobic molecules. Two main strategies exist for converting hydrophobic QDs into hydrophilic ones: the former involves the use of some amphiphilic micelles hosting internally QDs, the latter consist of exchanging of the original organic layer with hydrophilic ligands.

The advantages of a process using dithiocarbamate moieties, for example, are the easy reaction setup: it consists in simply mixing the amines with carbon disulfide (CS_2) in the presence of a base. Depending on the intrinsic nature of the substituents borne by the amino group, different properties are conferred to the compound, such as solubility in various solvents (if the amine has a carboxylic group we obtain solubility in water etc.).

Examples

- *Dithiocarbamates* have been used to decorate PbSe nanocrystals with fullerenes. This compound C[60]-PbSe shows potential applications in solar energy conversion. Dithiocarbamate is suitable for the ligand exchange reaction of nanoparticles due to its strong coordination ability to metal ions. However a drawback has to be taken into account: such kind of ligand is stable only in its salt form (basic conditions), so its solubility in common organic solvents is quite low. To solve this problem a small-molecular-weight co-ligand with a long ethylene glycol chain has been used, to ensure solubility of the C[60]-PbSe in both polar and non-polar solvents.
- MWCNTs have been functionalized with *mercaptobenzene* moieties and gold nanoparticles have been self-assembled onto their surface. It has been demonstrated that *aryl-diazonium salts* react efficiently with individual CNTs via sidewall covalent modification, and *thiol* derivatives interact strongly with noble nanoparticles. Mercaptobenzene has an aryl nature: delocalization of electrons in benzene ring facilitates *electron tunneling* and hence reduces electrical resistance between Au and MWCNTs.

6. Absorption and photoluminescence spectroscopy

As mentioned in the fourth chapter bulk semiconductors have a fixed band gap and a continuous conduction band, so the absorption spectrum presents a sharp increase in correspondence of the energy gap and a quite constant absorption for higher energies.

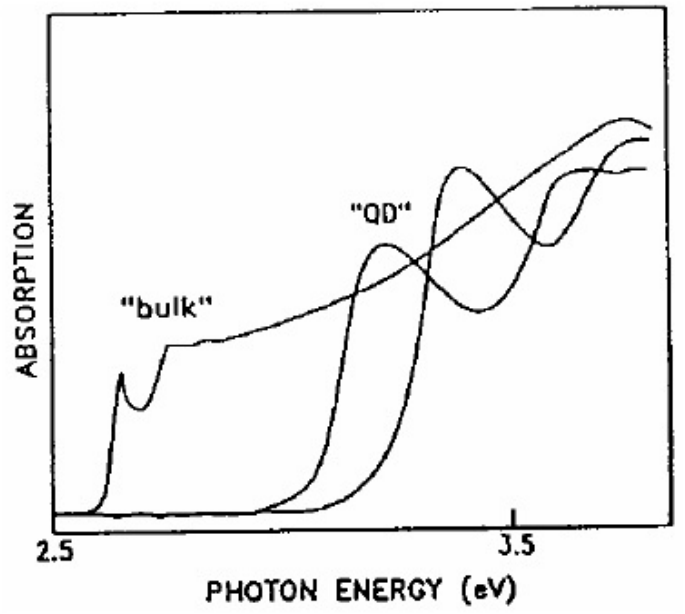

Fig. 20: absorption spectra of bulk semiconductors and quantum dots

Instead for quantum dots the spectrum involves the presence of a first peak (the 1s(e)-1s transition) and a non-constantly increasing absorption at shorter wavelengths, sometimes showing other more or less definite peaks or shoulders in correspondence of higher levels transitions (1p(e)-1p, etc.).

6.1 Absorption and photoluminescence of CNTs

Absorption and photoluminescence properties of CNTs depend on various conditions: first of all we have to remark that most of knowledge about the properties of CNTs concerns single-wall carbon nanotubes and really poor literature is found about multi-walled CNTs; besides the semiconducting or metallic nature of CNTs has to be taken into account: normally different manufacturing processes give different size and helical distributions of SWNTs composition (typically up to 50 SWNT species are believed to be contained in HiPCO (high-pressure carbon monoxide method) samples); afterwards a main role is played by the dispersion conditions of

the nanotubes in respective solutions (mono-dispersion or CNTs bundles). Eventually the diameter of SWNTs influences the optic characteristics because of the modulation of the band-gap.[44]

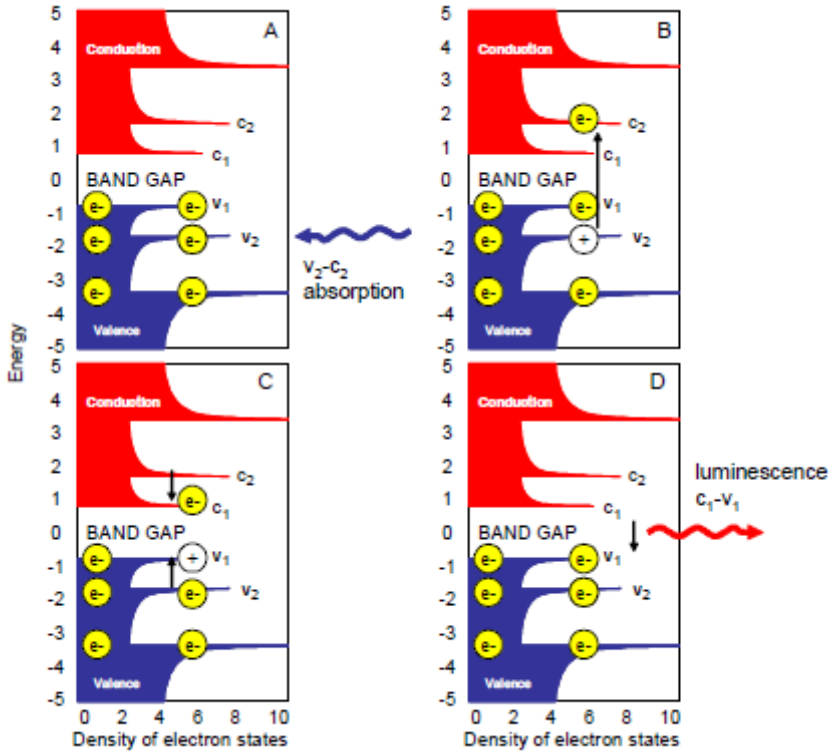

Fig. 21: Representation of the photoluminescence absorption and emission sequence in semiconducting SWNTs

Absorption spectra of SWNTs bundles contain three broad absorption regions corresponding to the first and the second allowed transitions for semiconducting SWNTs, and the first allowed transitions for metallic SWNTs, respectively.[45] However, these spectra do not exhibit any features identified with a particular nanotube structure, since strong electronic coupling mixes the energy states from the different SWNTs in the bundle. This strong intertube coupling, combined with the large inhomogeneity in nanotube structures present in an ensemble, completely obscures any fine structure in the absorption spectra.

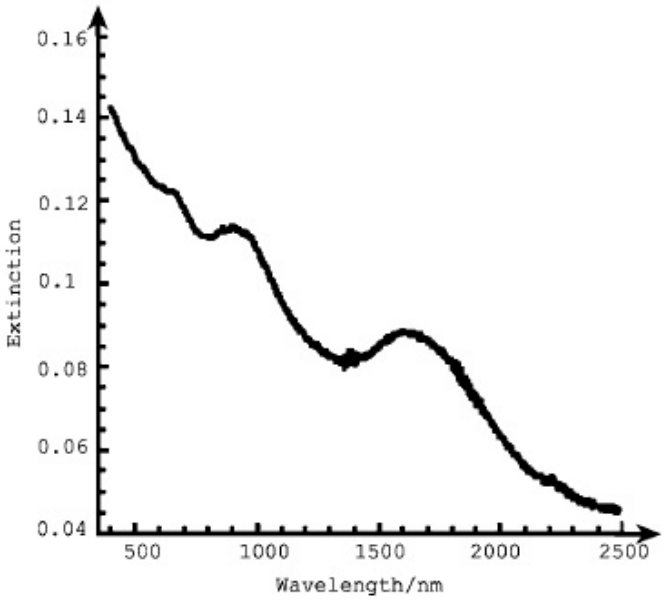

Fig. 22: Absorption spectrum of SWNTs. The peaks at 1700 and 950 nm are due to semiconducting NTs, the peak at 650 nm to metallic NTs.

Isolation of individual nanotubes is critical for decoupling the optical response of one nanotube from another. Absorption spectra of an ensemble of isolated SWNTs show many more highly resolved features than the corresponding absorption spectrum from nanotube bundles. These distinct features correspond to dipole-allowed optical transitions from SWNTs with different (n,m) values and/or from higher interband transitions for a nanotube with a given (n,m) value.

6.2 Luminescence principle

We call luminescence the emission of an electromagnetic radiation which is not of thermal origin. It is a process in which an atom/molecule absorbs photons (e.m radiation) and is consequently excited to a higher energy state. Following this, electrons go to populate more energetic levels, leaving some correspondent holes in the valence band they have abandoned. Electronic transitions occur in 10^{-15} s, that is an instantaneous time compared with the time scale of nuclear motion (Franck-Condon principle).

The electrons with a higher energy are unstable and tend to come back to the less energetic state, thus recombinating with the hole. Disexcitation can occur in different ways:

- Radiative pathways: fluorescence and phosphorescence
- Non-radiative pathways: vibrational relaxation, energy transfer to other molecules or to the solvent

For what concerns radiative pathways, it can happen that:

- a photon with $\lambda_{emiss} = \lambda_{excit}$ is emitted (resonance transition)
- different photons with $\lambda_{emiss} > \lambda_{excit}$ are emitted, so passing through intermediate levels (S_1) (Stokes shift)
- following collision with other atoms, the excited atom can be taken to an energy level where disexcitation is unlikely (T1): atoms can spend a lot of time in this state, before other collisions lead them to the lower energy state (Phosphorescence).

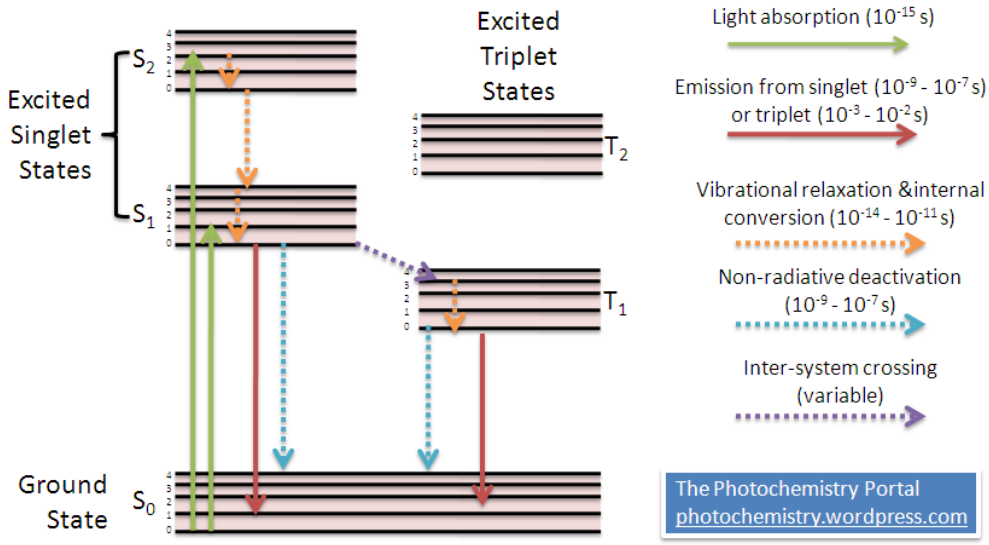

Fig. 23: Energetic levels in a molecule of fluorophore

During an electronic transition a change from one vibrational energy level to another will be more likely to happen if the two vibrational wave functions overlap more significantly (fig. 24). We concentrate our attention on photoluminescence of semiconductors, particularly of small dimensions, i.e. quantum dots. Quantum dots are semiconductor clusters of few hundreds of atoms characterized by a gap between the HOMO and LUMO energy levels, as previously mentioned. According to the Morse potential, at each electronic state are associated some vibrational (and rotational) excited states. At room temperature energy is not enough to let electrons populate excited energy states (S_1, S_2 etc.); thus we must make use of electromagnetic radiation rather than heat to induce fluorescence.

In photoluminescence analysis a monochromatic radiation is used (wavelength sufficiently low to cross the gap). The fluorophore is usually excited to some higher vibrational levels of either S_1 or S_2. With few exceptions, the excess energy is rapidly dissipated, in fact molecules quickly relax to the lowest vibrational level (Kasha's rule) of S_1 (internal conversion, which lasts 10^{-12} s

or even less) and from there can decay to the lowest electronic state via photon emission (Fig.23).

Since fluorescence lifetimes are longer (10^{-8} s) internal conversion occurs before emission takes place. Hence fluorescence emission generally results from a thermally equilibrated excited state, that is, the lowest energy vibrational state of S_1. Return to the ground state typically occurs to a higher excited vibrational ground state level, which then quickly (10^{-12} s) reaches thermal equilibrium.

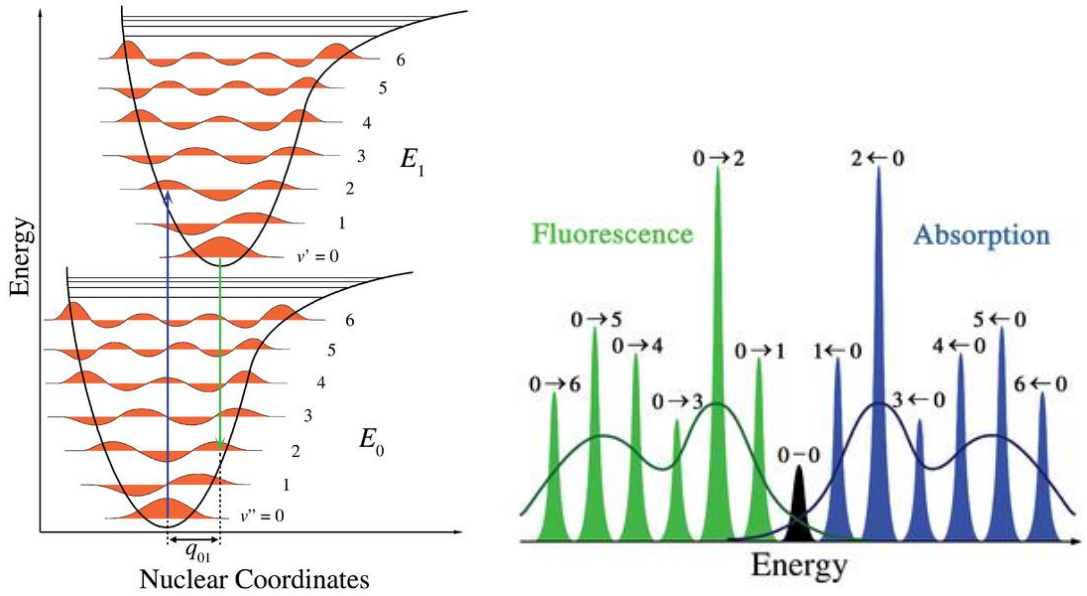

Fig. 24: Franck-Condon principle energy diagram (left), and schematic representation of the corresponding absorption and fluorescence spectra (right)

An interesting consequence of emission to higher vibrational ground states is that the emission spectrum is typically a mirror image of the absorption spectrum of the S_0-S_1 transition. This similarity occurs because electronic excitation does not alter the nuclear geometry (the spacing of the vibrational energy levels of the excited states is similar to that of the ground state). So emission spectra are typically independent of the excitation wavelength.

Typical PL spectra of quantum dots show a peak correspondent to the emission from the LUMO level (excited state) to a vibrational state of the HOMO (ground state), then resulting in a little red-shifted peak respect to the absorption one (fig.25).

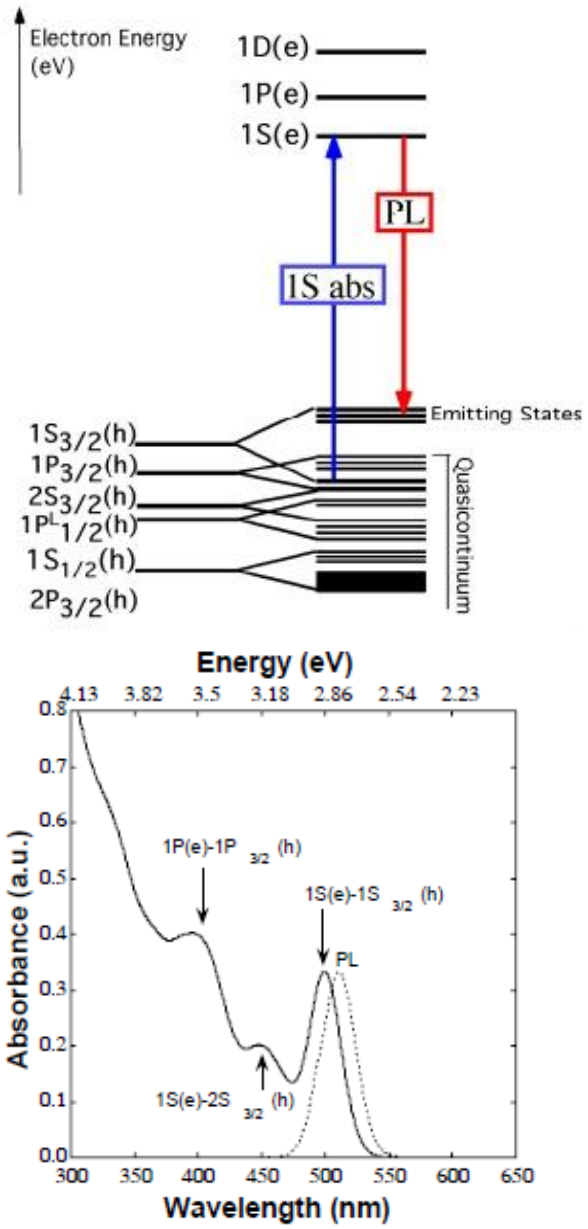

Fig. 25: PL peak shift respect to absorption spectrum

Due to the presence of some defects , thus to some energy states available inside the band gap, radiative transitions involving higher wavelength photons emission are possible; for the same reason an assessment of their concentration can be obtained.

Fluorescence lifetime and quantum yield are the most important characteristics of a fluorophore.

Quantum yield (QY) is the number of emitted photons relative to the number of absorbed photons. Substances with the largest QY, approaching unity such as rhodamines, display the brightest emissions. Non-radiative decays affect both the excited state lifetime and the QY; the

more frequent include: dynamic collisional quenching, near-field dipole-dipole interaction (fluorescence resonance energy transfer, FRET), internal conversion and intersystem crossing.

Fluorescence quantum yield is measured by comparison with a standard with known QY. It doesn't depend on the excitation wavelength.

Fluorescence *lifetime* of the excited state refers to the average time the molecule spends in the excited state prior to return to the ground state. It typically follows first-order kinetics:

$$[S1] = [S1]_0 \, e^{-\Gamma t}$$

where *S1* is the concentration of excited state molecules at time *t*, $S1_0$ is the initial concentration and *Γ* is the decay rate or the inverse of the fluorescence lifetime. If different radiative (Γ_{rad}) and non-radiative (Γ_{nrad}) processes contribute to depopulate the excited state, the total decay (Γ_{tot}) will be the sum of the two terms: $\Gamma_{tot} = \Gamma_{rad} + \Gamma_{nrad}$

Generally fluorescence lifetimes range from 0,5 to 20 ns.

6.2.1 Luminophores

Among the most known luminophores we can remind the organic dyes with unsatured bonds (benzene and derivatives), inorganic crystalline substances (ZnO, ZnSe, CdS, CdTe, GaAs, InP ..), doped silicates and oxides, inorganic liquid or amorphous substances (UO_2, Neodymium glass,..).

The majority of organic fluorophores are not photostable and display photobleaching with high illumination intensities. There are different types of luminophores that are mostly inorganic or display unusually long lifetimes (semiconducting NPs, lanthanides and transition metal-ligand complexes (MLCs)).

Quantum dots allow to obtain a wide range of emission wavelengths by simply changing the size or chemical composition of the NPs: it has been extended to 4 μm using PbSe particles (PbSe QDs with emission λ near 2 μm display QY as high as 25 %).

Chemical and photochemical stability are improved by coating the QD core with a material with a higher band gap (core-shell quantum dots), which confines the excited state to the center of the particle, thus preventing interaction with the surface.

QDs display several favorable spectral features. The emission spectra of homogeneously sized QDs are about twofold more narrow than typical fluorophores. QDs don't display the long wavelength tail common to all fluorophores.

QDs also have large extinction coefficients (ε) that on a molar basis can be up to tenfold larger than rhodamine.

6.2.2 Fluorescence of CNTs

SWNTs are poor emitters: the fluorescence QY of SWNTs is on the order of about 10^{-4}. Metallic SWNTs with continuous valence and conductance bands display little or no PL.

Early optical studies could only determine an average overall behavior that obscures crucial electronic characteristics of the individual nanotubes. For example, since spectra from SWNTs with different (n,m) values will overlap, it is difficult to make definite conclusions regarding important emission features such as the spectral line width or details of the band shape, or to observe evidence of coupling to vibrations.

Interaction between nanotubes or between nanotube and another material (substrate) quenches PL. For this reason, no PL is observed in MWNTs.

For the same reason bundled SWNTs do not fluoresce since any metallic tube present in the bundle provides an efficient non-radiative pathway for photoexcited electrons.

The situation could be different whether CNTs are functionalized with some aromatic/conjugated compounds with $\pi-$orbitals which absorb light. For example for MWNTs with in-situ polymerized thiophene (PTh) there is an intense emission at about 430 nm which can be attributed to the emission of polythiophene. [(17)]

6.2.3 Quenching

The intensity of fluorescence can be decreased by a wide variety of processes. Such intensity reduction is the result of some disexcitation processes due to charge or energy transfer from excited states. These processes are known as *Quenching*.

It can be dynamic or static. So if we talk about luminophores in solution it's possible that some particular molecules called *quenchers* diffuse, collide and interact with fluorophores disexcitating them (implying a transfer of charge/energy): the presence of the quencher adds another deactivation pathway in competition with luminescence (*dynamic quenching*). Otherwise if the luminophore is somehow associated with the quencher prior to light absorption another kind of transfer can take place: *static quenching*. The reduction in emission intensity will be affected by the extent to which the quencher associates to the luminophore and the number of quenchers present.

As shown in recent works by many authors, CNTs can well play the role of effective quenchers. When QDs are grafted to functionalized CNTs, an efficient transfer of charge generally occurs.

There are some possible explanations for the PL-band quenching [(11)]: electron transfer, hole transfer or both into the MWNTs, or resonant energy transfer [(14)],[(18)].

PL spectra of QDs generally show a strong emission peak in correspondence of band-edge electron hole recombination along with some peaks at higher wavelength which can appear following trap emission. This signal is partially quenched in the simple mixture of CNT and QDs and totally quenched in the nanohybrids. Thus the reduction of the main peak can be assigned to the charge/energy transfer from CNTs to QDs. In CNT-QDs systems electron-hole recombination competes with an electron injection mechanism, and this competition depends on the distance between the CNTs and QDs. So for the CNT/QDs mixtures just part of the electrons is transferred to the CNTs, while the remainder of them produces a reduced emission through radiative relaxation. In contrast when the QDs are well linked to the CNTs by means of some functionalities, the emission is totally quenched, because electron injection from the QDs to the CNTs dominates. [17]

Moreover red-shifts in the peak position can be seen for CNT@QDs nanohybrids respect to the lonely QDs [19], suggesting that strong electronic interaction of QDs with CNT occurs after photoexcitation of the hybrid material.

On the other hand MWNT can have a weak absorption band located near the emission peak of QDs [12], so that energy transfer from QDs to MWNT might also contribute to the quenching mechanism, thus decreasing the electron transfer efficiency.

6.2.4 CNTs/QDs distance

Some studies about distance issue have been accomplished. For example different capping agents with various chain lengths have been used to wrap QDs subsequently attached to CNTs (the separation between the QDs and the CNTs is adjusted by the lengths of alkyl chains of the capping agents). [15] The PL spectra show that the intensity of the QD emission peaks in the QD@CNT hybrid is strongly dominated by the shell thickness, that is the PL brightness increases with the chain length of the capping agent (mercapto-carboxylic acid in this studied case) on the QDs. It has been seen that as the average distance between the QDs and CNTs increases within 10 Å ranges, the photoluminescence properties of the nanohybrids change from total quenching to nearly no quenching. These studies consider charge transfer through alkyl chains, so maybe thanks to electro-tunneling. Perhaps it is different with conductive and/or aromatic interlinkers.

6.2.5 CNT direct linking

The properties of a monolayer of CdS NPs assembled on a Au electrode by covalent coupling have been compared to that of a CdS/CNT system and the results show that, despite the same

surface coverage of NPs, both the photocurrent generated by the systems that lacks the CNT connectors and the photon-to-electron quantum efficiency are substantially lower. This means that CNTs which bridge the CdS NPs to the electrode play a major role in the enhanced generation of photocurrents. [27]

6.2.6 CNT length

We know that the longer time intervals of acidic digestion yields shorter tubes. Then CNTs of different lengths (different digestion times) have been used to assemble CNT/CdS NPs-functionalized electrodes. The photocurrent obtained reveal that it is enhanced as the digestion time of the CNTs is increases (shorter linking CNTs). The quantum efficiencies increase as the digestion time increases (shorter CNTs) as well [31]. Some hypothesis can support this behavior. The conductive CNTs provide efficient paths for the transport to the electrode of the trapped conduction-band electrons originated in the NPs, and the charge-transport rates in CNTs should be almost length-independent. But we have to consider that the oxidative acidic digestion of the CNTs not only shortens the CNTs but it also introduces defects into the sidewalls. So according to a back-scattering model, as the electron reaches a defect site, it is back-scattered to find an alternative conjugated path to be transported along the CNT. As the number of defects in the CNT increases with its length, charge transport along the CNT could be dominated by its length. As the CNTs become longer, more defects exist in the connecting wires and thus the back-scattering process retards the conductance of the trapped electrons to the electrode; so they can recombine with the valence-band holes to result in lower quantum yields for the photon-to-electron conversion process.[27]

6.2.7 Energetic levels position

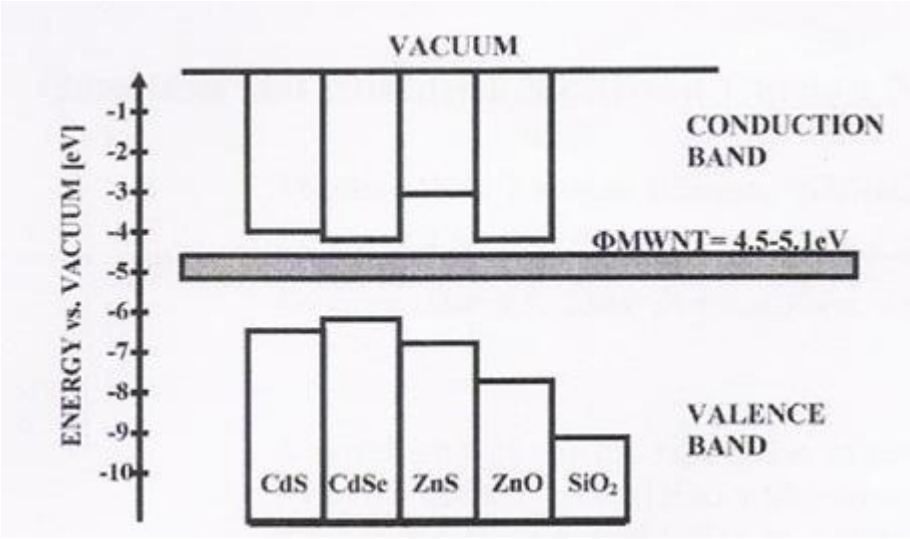

Fig. 26: Schematic energetic band position for MWNT and some semiconductors

The non-radiative decay path occurs because the difference in electron affinity between the QDs and the CNTs is sufficient to allow electron transfer from the QDs to the CNTs.

The conduction energy level of CNTs (about -4,5/-5 eV against vacuum) resides normally inside the band gap of the quantum dots, so that to scavenge electrons from the conduction band of the last ones, preventing exciton recombination thus decreasing (or cancelling) luminescence intensity.

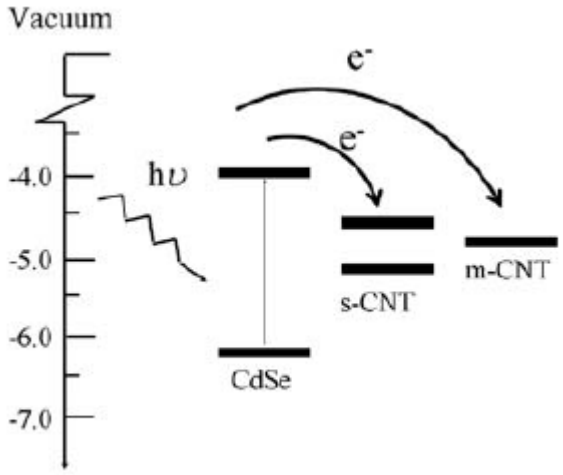

Fig. 27: Energy level diagram and possible charge-transfer process for the conjugate complex between CdSe QDs and semiconducting NTs (s-CNT) or metallic NTs (m-CNT)

The conduction and valence band levels for both QDs and SWNTs depend on their diameter. [14] For instance, since the effective mass of a hole (1,19 m_e, where m_e is the electron mass) in CdSe is much larger than the effective mass of an electron (0,11 m_e), the valence energy in CdSe QDs does not change, while the conduction energy changes noticeably.

In MWNTs the presence of numerous concentric graphene cylinders provides different acceptor levels [19].

The absolute and relative position of the Fermi levels of the components of the photovoltaic device are fundamental for the solar cell efficiency.

The Fermi level equilibration between the sensitizer and the CNTs often drives the open circuit voltage lower than the one obtained with the sensitizer and TiO_2 films (that is the case of DSSCs). [20] Thus despite the success in the fast capture of electrons from the QD to the CNT, the lower energy difference (and hence the open circuit potential) limits the overall photoelectrochemical performance of these solar cells. Further modifications of CNTs with semiconducting composites and/or functional groups are necessary to drive the Fermi level to more negative potentials.

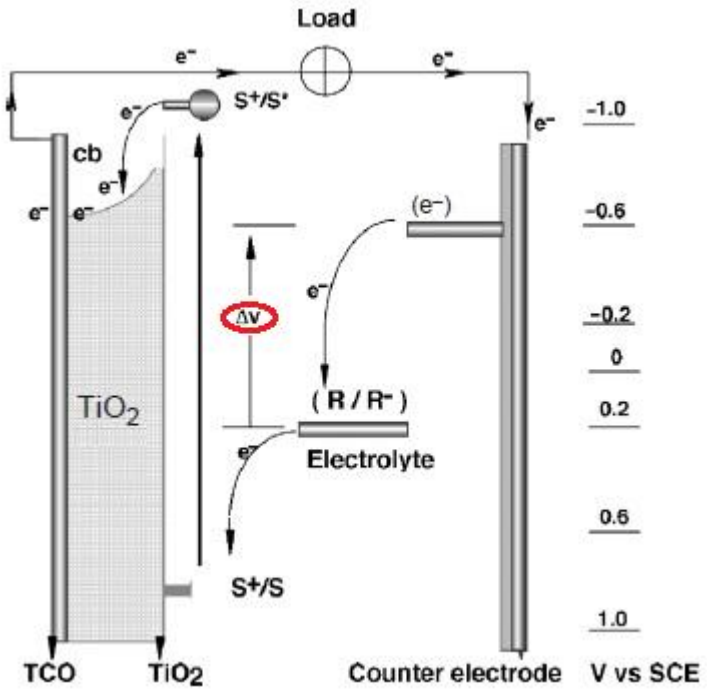

Fig. 28: DSSCs scheme with indication of the "Open circuit voltage" (V_{oc}): grossly it can be determined by the energy difference between the Fermi level of the solid under illumination and the Nernst potential of the redox couple in the electrolyte (difference between the conduction band of TiO_2 and the redox couple for DSSCs; difference between the CNT Fermi energy level and the redox couple for these kind of photovoltaic devices)

The efficiency of charge transfer is determined not only by the energy difference between donor (QD) and acceptor (CNT), but also by the exciton binding energy of the QDs. [14] The donor-acceptor energy difference should be greater than the exciton binding energy of the QD. That is relatively large in a quantum-confined system (over 0,1 eV for CdSe QDs).

6.2.8 Core-shells

We have to pay attention to the case of core-shell QDs attached to CNTs.

For example when CdSe/CdS core-shell particles (Type-I structures) are attached to MWNTs, the PL is completely quenched. Instead the PL of CdSe/ZnS core-shells (type-I) decreases slightly upon association with SWNTs. [14]

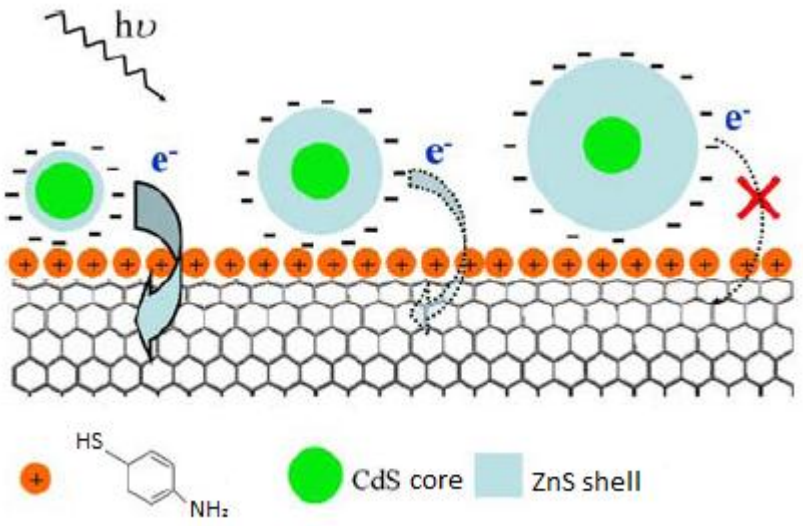

Fig. 29: Photo-induced charge-transfer between core-shell QDs and CNT@diazo-SH. The transfer is controlled by the shell thickness

In fact it has been observed that if the shell coating is not sufficiently thick charge carriers may leak from the core. Therefore CdS NPs, which have a smaller band gap (respect to ZnS) and a smaller conduction band offset with CdSe (about 0,32 eV) are more susceptible to PL quenching. On the contrary ZnS has a larger band gap and may confine the exciton more efficiently.

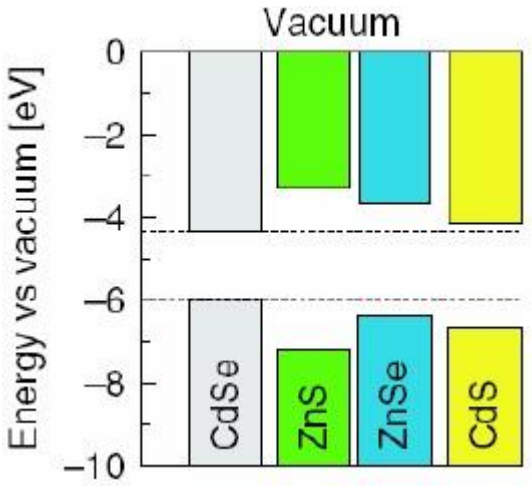

Fig. 30: enegy levels positions against vacuum of some semiconductors

Another proof has been taken from the study of MWNTs coated with silica. The large band gap and thickness of the SiO_2 rules out both charge transfer and electron tunneling as possible quenching mechanisms. [(11), (20)]

6.2.9 Time-resolved spectroscopy

To probe the ultrafast electron transfer in the sub-nanosecond time scale, some researchers have employed *Femtosecond transient absorption spectroscopy*.[(20)] The analysis points out that the charge injection between excited QD and CNT is an ultrafast process, and it can be modulated by controlling the particle size. An increase in the electron transfer rate constant is observed while decreasing the particle diameter from 4,5 to 3 nm. The higher energy conduction band in the smaller size quantum dots play a role in maximizing the electron transfer rate to the CNTs.

In order to further prove and support electronic communication between CdS and CNT, the photoinduced dynamics of the nanohybrid excited state were investigated by *Time-resolved spectroscopy* techniques. [(19)]

Fluorescence lifetimes of the excited CdS in nanohybrids have been evaluated to be more than 10 times shorter than the lifetime of capped QDs, thus supporting the efficient emission quenching of CdS by the nanotubes in the nanohybrids, as observed in the fluorescence-intensity quenching in the steady-state spectra and the appreciable red-shift of the fluorescence peak.

Time resolved spectroscopy has highlighted a quick recovery for the bleaching (most of which is completed within 200 ps) in CNT@CdS hybrid systems [(21)]; instead the CdS alone shows long-term recovery and extends beyond 1500 ps. This indicates that an additional deactivation

pathway exists for the electrons in the quantum dot conduction band and this is likely another proof of the transfer of charge carriers to the CNT.

6.2.10 Identity of carriers

The identity of the primary carrier in the QD/CNT device can be determined by measuring various electrical signals of the QD-CNT assemblies. [14]

Generally the SWNTs are hole-transport materials [13]; electron transfer from the quantum dots to the nanotubes under illumination results in electron-hole recombination within the nanotubes and thus a reduction of carrier concentration and also a decrease of the photocurrent. In contrast to the SWNTs it's very likely that functionalization (with oleylamine in the cited experiment) induce n-doping of the SWNT, hence making the electron a major carrier in the hybrid system (a photocurrent build-up can be seen from analysis).

7. Experimental objectives

We aim to prepare nanohybrids made from CNTs and QDs.

Various functionalizations of CNTs will be presented in this part:

- grafting of thiol functions through mercaptosilane (on oxidized CNTs) or diazonium salts (on pristine CNTs)
- grafting of amine functions through an electroyte (poly-allylamine)
- grafting of dithiol functions: as no commercial product was available, the synthesis of two molecules is here presented.

CdS quantum dots will be synthesized via a polyol method and characterized.

The properties of all the compounds will be investigated especially through TEM and XPS analysis.

Particular emphasis will be put on photoluminescence properties of the nanohybrids.

7.1 Synthesis of a dithiocarbamate

A lot of different synthesis which aim to get some dithiocarbamate salts have been attempted. Most of reactions that involve the simple addition of an amine to Carbon disulfide (CS_2) are conducted under harsh conditions (use of strong basic conditions, high reaction temperatures and long reaction times) in order to obtain high yields.

It has been said that most of reactions involve the use of secondary alkyl-amines, which are more nucleophilic than primary ones. In general primary and secondary amines can react with electrophilic carbon systems to form C-N bonds. These bonds are strong and thus the products of these nucleophilic additions are stable. Besides in aryl-amines the effect of an aromatic ring delocalizes the ion pair of electrons on nitrogen into the ring, resulting in decreases basicity and reactivity.

We have decided to try two routes, the former less reliable (very few literature [(22), (23), (24)]), the latter more successful. [(25), (26)]

The first aims at making phenylenediamine react with carbon disulfide trying to extract the by-product functionalized only on one side to exploit the diazonium mechanism to further functionalize carbon nanotubes.

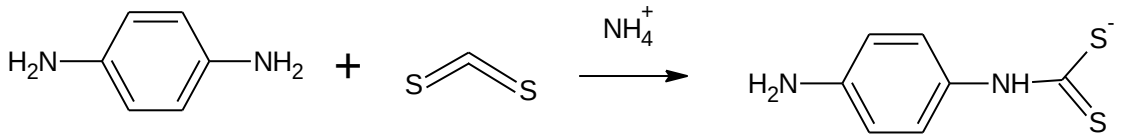

Fig. 31: synthesis of a dithiocarbamate from a phenylenediamine

7.1.1 Experimental route

300 mg of 1,4-phenylenediamine are dispersed in 10 ml of ammonia (38 % in water); 1,1 equivalent (0,2 ml) of carbon disulfide is added and the solution stirred overnight at 50 °C ($Tb(CS_2)$ = 46 °C).

The solution is of a frothy pale yellow. TLC identifies the presence of at least four compounds in our mixture. We expect that the compound that migrates the less (one-side reacted phenylenediamine is supposed to be more polar than the two-sides reacted product) corresponds to our desired compound which we try to draw out. First of all we would eliminate water from the mixture (so that to perform some NMR analysis), but because of our product polarity we cannot just draw it out without extracting part of the product too. We want to try to transfer our product into chloroform (not soluble in water and polar enough to catch the desired product). Just after mixing, the mixture becomes an emulsion, thus we use a great deal of NaCl to enable precipitatation. Then we extract the phase with chloroform and add $MgSO_4$ to absorb the remaining water. TLC analysis seem to confirm the presence of only one product, so the solution is filtered and dried. The obtained product weighs 41 mg net. (perhaps part of it has remained in the aqueous phase: maybe it is quite acid, giving rise to a zwitterion, so it is difficult to separate it).

NMR and mass spectrometry are used without success to identify the product: NMR spectra are too confused and from mass spectrometry we don't find any compound with the desired molecular weight (moreover if our product is a salt, it cannot even volatilize and thus cannot be analyzed).

Consequently synthesis conditions have been changed a little: 2 equivalent of CS_2 is used and the temperature set at 40 °C. Then the product is solubilized in acetone, left overnight to precipitate and finally filtered. Unfortunately from further NMR and IR analysis we cannot demonstrate the presence of our hypothesized product (from IR we don't perceive the presence of NH and NH_2 bonds in the spectrum).

We would need some bibliographic data to ameliorate the synthesis.

The second attempt involves the synthesis of a dithiocarbamate starting from an aminosiloxane (thus a primary amine) according to some recent literature. [25]

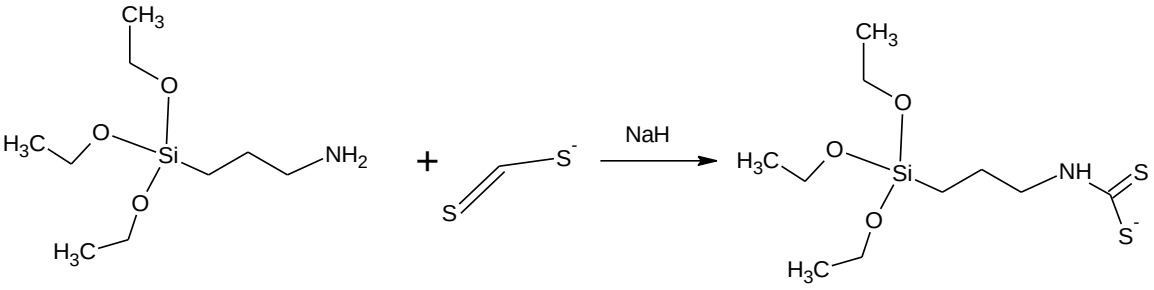

Fig. 32: synthesis of a dithiocarbamate from an organosilane

We know that the reaction is sensitive to the amount of both the reagents and solvent. The protocol is the following:

to a suspension of degreased NaH (12 mmol) in dry THF (20 ml) cooled to 0 °C are added dropwise via syringe 3-aminopropyltriethoxysilane (APTES) (10mmol) and carbon disulfide (CS_2) in a molar ratio of 1:1,5. After being stirred under vacuum at 0 °C for 0,5 hours, the reaction is refluxed at 65 °C for 2 hours under vigorous stirring. After cooling the volatiles are removed under reduced pressure. The crude yellow solid obtained is purified by washing with dry diethyl ether (Et_2O) and filtered. The product seems to be partially soluble in Et_2O, in fact from NMR analysis we get the same results from the compounds which pass and doesn't pass through the filter. So washing with Et_2O seems useless. NMR results are still confused, and IR analysis reveal that maybe the product is a little polymerized.

For further attempts concerning this synthesis maybe we have to change the solvent to wash the obtained solid, and use degreased NaH which is more reactive, or KH or LiH as an alternative (the last ones are stronger bases). Moreover we must remind to prevent the contact with air throughout the synthesis procedure because water can give some hydrolysis reactions.

8. CNT functionalization

8.1 MWNTs oxidation

In literature different ways to oxidize CNTs are presented, using solutions of nitric acid (HNO_3), sulfuric acid (H_2SO_4) and hydrogen peroxide (H_2O_2) in different proportions.[40] We choose a solution of concentrated acids as H_2SO_4:HNO_3 in a 3:1 ratio.

As far as the experiment is concerned:

200 mg of MWNTs is introduced into a 50 ml Erlenmeyer flask followed by 8 ml of HNO_3 (69 %) and 24 ml of H_2SO_4 (95 %). The solution is then vigorously shaken for 1 minute and sonicated for 5 minutes. This operation is repeated twice. Later on the flask is left in the ultrasonic bath with heating for 3 hours.

The solution is thus soon poured in another flask and about 500 ml of distillated water are added. Afterwards it is filtrated by means of a Buchner funnel and a nitrocellulose filter with the diameter of the pores of 200 nm (the last one has been chosen in place of a 650 nm – nylon membrane to keep the majority of CNTs); then some washing cycles with water let take away the acid. In the end the CNTs are dried under vacuum for at least 2 hours. We call the sample: MWNT@COOH.

It's important to filtrate just after oxidation as well as wash oxidized CNTs to prevent further attach by acids: in fact CNTs in contact with acids cut continuously in more and more little tubes.

Oxidation under slightly different conditions has been performed to compare the oxidation degree. According to another protocol we have accomplished oxidation by means of an equimolar solution (8M) of nitric and sulfuric acid.

So 200 mg of MWNTs is introduced into a 50 ml Erlenmeyer flask followed by 20,5 ml of HNO_3 (8M) and 18 ml of H_2SO_4 (8M). Then the procedure is the same as before.

8.1.1 Synthesis with Aminobenzoic acid (diazo-COOH)

50 mg of MWNTs and 233 mg (1,7 mmol) of 4-aminobenzoic acid is added to a 50 ml flask equipped with a stir bar. The mixture is then deoxygenated for 5 minutes. 10 ml of isoamylnitrite is then added via an argon-purged syringe and the solution is thus heated at 60 °C for 3 hours.

The product is then purified by filtration, washed with acetone, redispersed in DCM (dichloromethane) and sonicated for 5 minutes; thus the filtration/washing/redispersion cycle is repeated for 3 other times.

The functionalized nanotubes (MWNT@diazo-COOH) are then dried under vacuum for 2 hours.

8.1.2 Results

TEM analysis

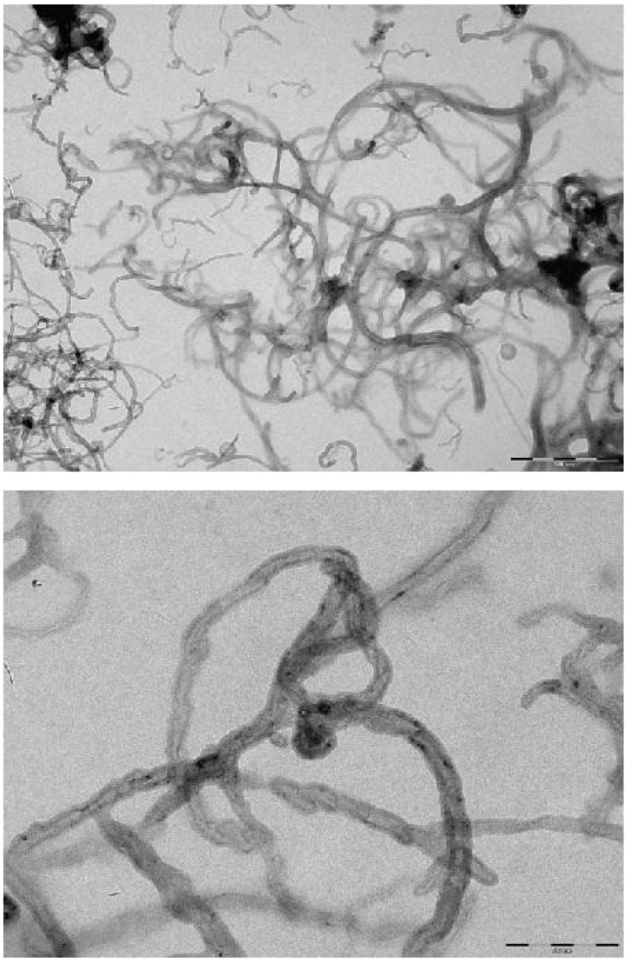

Fig. 33: NTC@COOH (up and down): CNTs oxidized in a sulfuric acid - nitric acid (3:1) solution

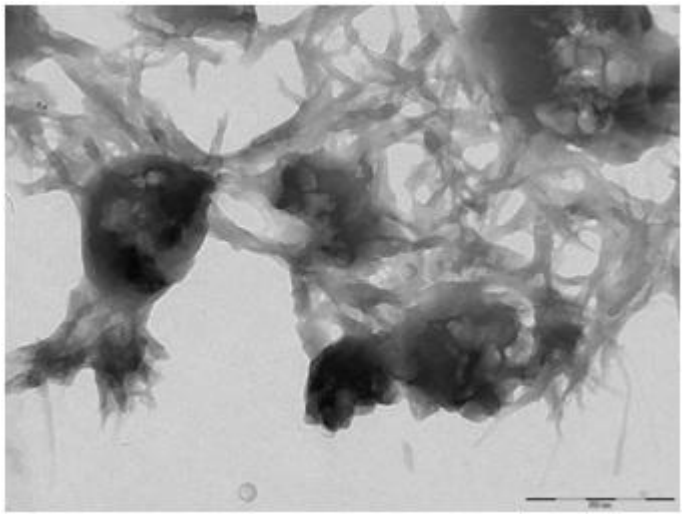

Fig. 34: CNT@Diazo-COOH : CNTs oxidized with aminobenzoic acid

From TEM analysis we can perceive as result of harsh acid conditions the presence of long and short CNTs which are by the way well functionalized. For CNTs that have reacted with amino-benzoic acid the functionalization seems deeper and the CNTs covered with thicker layers.

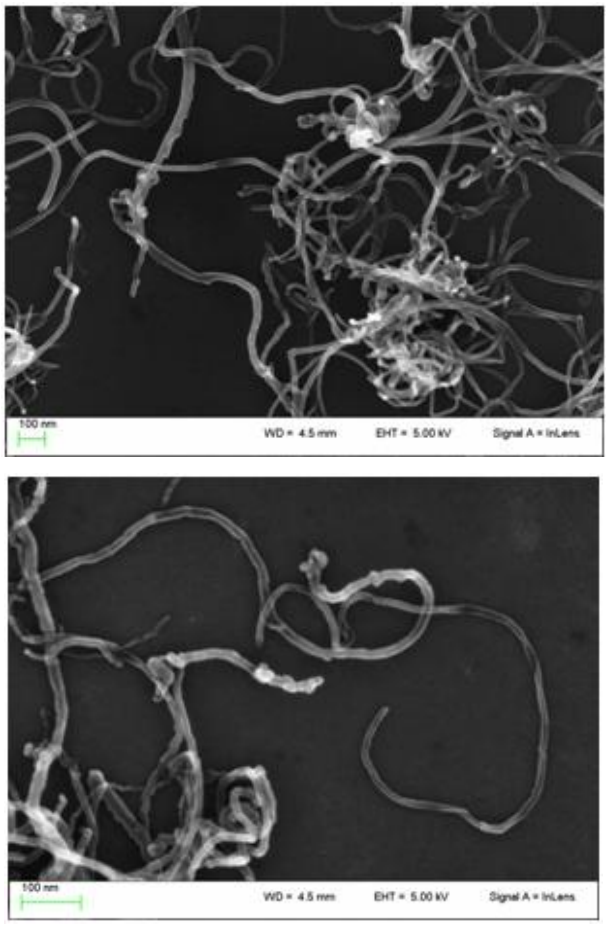

Fig. 35: pristine CNTs (up) and CNTs oxidized (down) with a sulfuric acid – nitric acid solution (1:1)

From these SEM images we can notice that there are only slight differences between pristine MWNTs and oxidized MWNTs. We can underline the presence of some shorter CNTs and less smooth walls.

SEM images of MWNTs oxidized by means of stronger acid conditions could reveal a higher degree of functionalization according to the bigger amount of oxygen displayed on XPS analysis.

XPS analysis

Pristine MWNT:

Name	Start BE	Peak BE	End BE	Height Counts	FWHM eV	Area (P) CPS.eV	Area (N)	At. %
C1s	294,1	285,1	283	13654,7	1,1	20826,9	0,2	98,3
O1s	538,4	533,5	529,4	87,6	2,5	255,1	0	1,7 ± 0,2

Oxidized MWNT (1:1):

Name	Start BE	Peak BE	End BE	Height Counts	FWHM eV	Area (P) CPS.eV	Area (N)	At. %
C1s	293,1	284,4	282,7	118561,2	1,06	175275,5	1,5	94,7
O1s	536,5	532,3	528,3	8056,1	3,23	26959,8	0,1	5,3 ± 0,5

Oxidized MWNT (3:1):

Name	Start BE	Peak BE	End BE	Height Counts	FWHM eV	Area (P) CPS.eV	Area (N)	At. %
C1s	296,6	285,0	282,6	185583,7	1,1	345784,8	3,0	85,76
O1s	540,4	533,1	528,3	46230,4	3,1	151979,4	0,5	13,65 ± 1,4
N1s	411,4	402,5	398,2	1048,6	2,5	4181,4	0,0	0,59 ± 0,1

MWNT@Diazo-COOH:

Name	Start BE	Peak BE	End BE	Height Counts	FWHM eV	Area (P) CPS.eV	Area (N)	At. %
C1s	295,2	284,6	282,0	151050,5	1,1	245469,8	2,1	89,2
O1s	543,9	533,2	528,3	13490,7	3,4	62195,7	0,2	8,2 ± 0,8
N1s	410,5	400,7	396,7	3764,4	2,4	12603,0	0,1	2,6 ± 0,3

From XPS analysis we can glean some information about the atomic percentage of oxygen and nitrogen on MWNTs. We can notice that pristine MWNTs are already oxidized: almost 2 % of oxygen is present onto CNT surface. This quantity bumps up after an oxidation treatment using an equimolar solution of nitric and sulfuric acid but it's only with an acid solution in the ratio H_2SO_4:HNO_3= 3:1 that a significant oxidation takes place: that lets us understand that we can vary the oxidation conditions by playing on the ratio of acids used, taking into account that harder conditions yield shorter and more damaged CNTs.

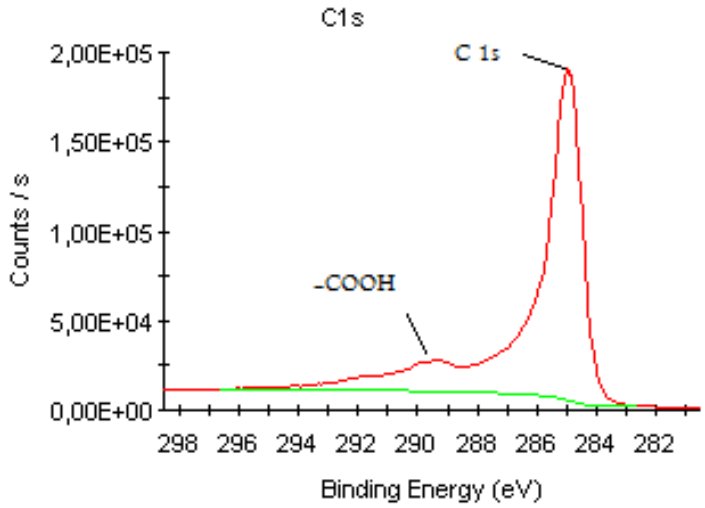

Fig. 36: XPS Carbon high resolution spectrum of CNT oxidized (3:1); the peak at about 289 eV correspond to the group COOH

As far as nitrogen on the unmodified CNTs spectra is concerned, only a weak signal at around 400 eV is observed: it is assigned to the atmospheric nitrogen. In oxidized CNT (under harsh conditions) we have a slight increase in this element.

A remarkable increment in nitrogen percentage can be seen on MWNTs modified by diazonium salts methods: this is probably due to the presence of N=N bonds among aminobenzoic molecules which produces a multilayer structure onto CNTs surfaces.

8.2 Functionalization with a mercaptosilane

8.2.1 Synthesis

10 mg of MWNT@COOH obtained from the MWNTs oxidation process is dispersed into 40 ml of distilled toluene in a polypropylene tube and sonicated for 1 hour at room Temperature. Then 2 ml of MPTS (3-mercaptopropyl-trimethoxysilane) is added and the solution further sonicated for 4 hours at about 60 °C.

Subsequently the CNTs are centrifuged at 23.000 rpm for 20 minutes and undergone 4 washing cycles with ethanol absolute. In the end the majority of supernatant is taken away with a pipette and then with the aid of an argon atmosphere and the CNTs are dried under vacuum for 2 hours.

We call this sample MWNT@MPTS.

In this experiment we have used distilled toluene to prevent hydrolysis mechanisms that could lead the mercaptosilane to react on itself.

Moreover the MPTS has been afterward substituted by the less reactive MPTES (3-mercaptopropyltriethoxysilane) also to enable a better comparison with another molecule that we have tried to synthesize (a triethoxysilane-dithiocarbamate); the resulting product is called MWNT@MPTES.

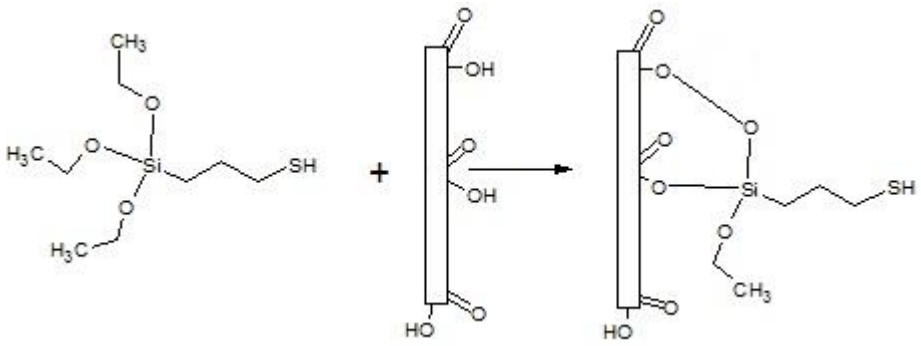

Fig. 37: CNT functionalization with MPTES

8.2.2 Results

In some experiments we have varied the organosilane quantity and temperature to find out the best conditions. We can see that with about 0,2 equivalent of MPTS the CNT functionalization reaches its maximum.

Here we present the sulfur and silicon atomic percentages derived from XPS spectra owing to different quantities of MPTS; CNT amount is always the same (10 mg):

MPTS (ml)	S (atomic surface %)	Si (atomic surface %)
0,5 (0,05 eq)	1,1 ± 0,1	2,1 ± 0,2
1 (0,1 eq)	4,5 ± 0,5	6,8 ± 0,7
2 (0,2 eq)	4,6 ± 0,5	7,1 ± 0,7

Each mercaptosilane molecule contains one atom of Sulfur and one of Silicon so these elements should be present in the same quantities: however from XPS spectra we notice a ratio of 1,5 between the two elements, and it is difficult to explain why it happens.

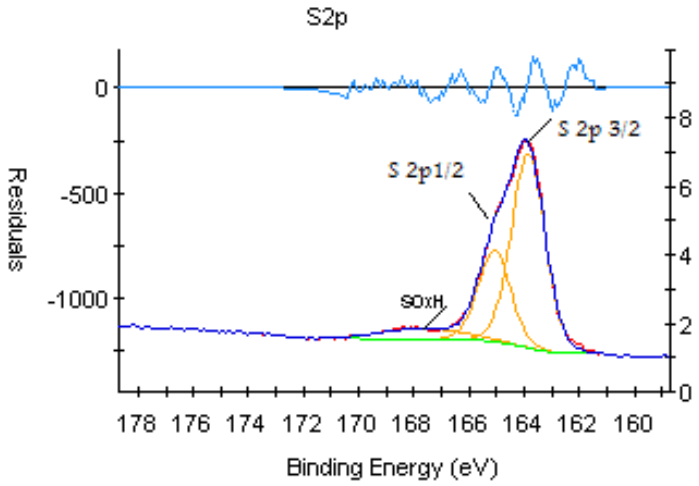

Fig. 38: XPS Sulfur high resolution spectrum of (MPTS-0,2 eq)

From Sulfur high resolution spectrum (fig.38) we can see a large peak that could correspond to different bonds: apart from the main peak at about 164 eV (with the characteristic doublet correspondent to the orbitals S-$2p_{1/2}$ and S-$2p_{3/2}$) that should match the –SH or maybe a S-S bond, there is a percentage of oxidized sulfur at about 168 eV (-SO_xH bond).

So we can hypothesize that both the reduced sulfur oxidizes to –SO_xH and it is eliminated through bond scission. On the other hand it could correspond to the S-C bond present in the molecules.

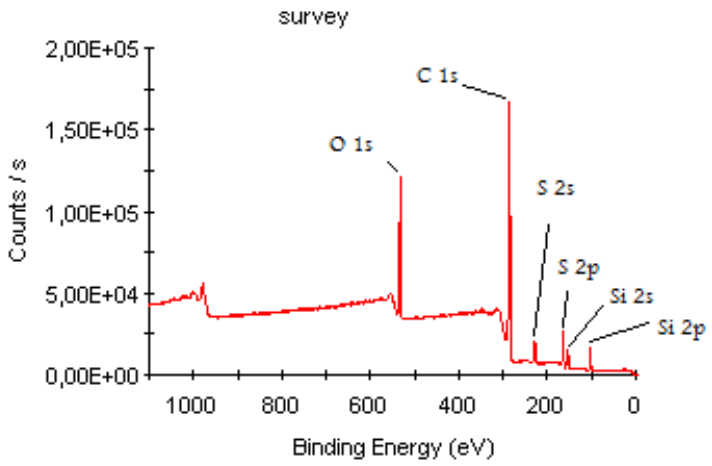

Fig. 39: XPS spectrum of (MPTES-2ml)

We can also underline the difference encountered using MPTES: sulfur spectra (fig. 40) don't show the peak correspondent to -SO_xH and S percentage is closer to Si one:

MPTES (ml)	S (atomic surface %)	Si (atomic surface %)
2 (0,2 eq)	6,1 ± 0,6	7,2 ± 0,7

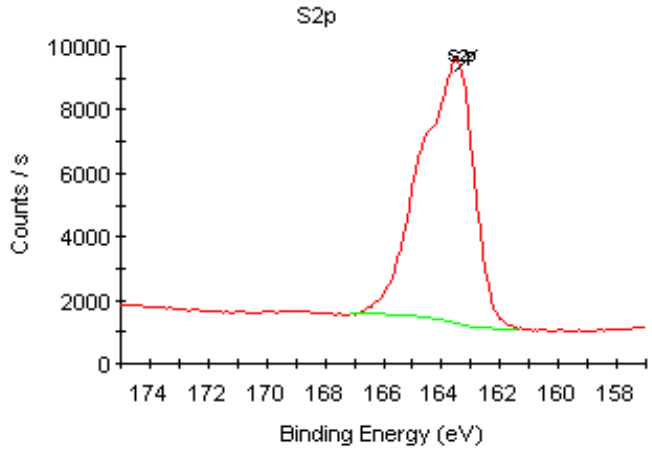

Fig.: 40 XPS Sulfur high resolution spectrum of (MPTES-0,2 eq)

However we would establish whether MPTS and MPTES react themselves producing a certain amount of polymerization but neither with XPS nor with IR analysis we can evaluate this (with IR the quantity of MPTS is too less compared to toluene to allow a clear peaks analysis).

TEM analysis

This photos made by TEM reveal to us that CNTs are well surrounded by MPTS molecules and perhaps its concentration is bigger in correspondence of the CNTs ends, where there should be the biggest quantity of COOH groups to which MPTS molecules can bind.

The MPTS layers thickness is quite small (this is vital for charge transfer issues, see chapter 6) and no significant interactions are present among the CNTs: for CNTs modified by means of diazonium salts it will be quite different.

Later on we will further discuss this.

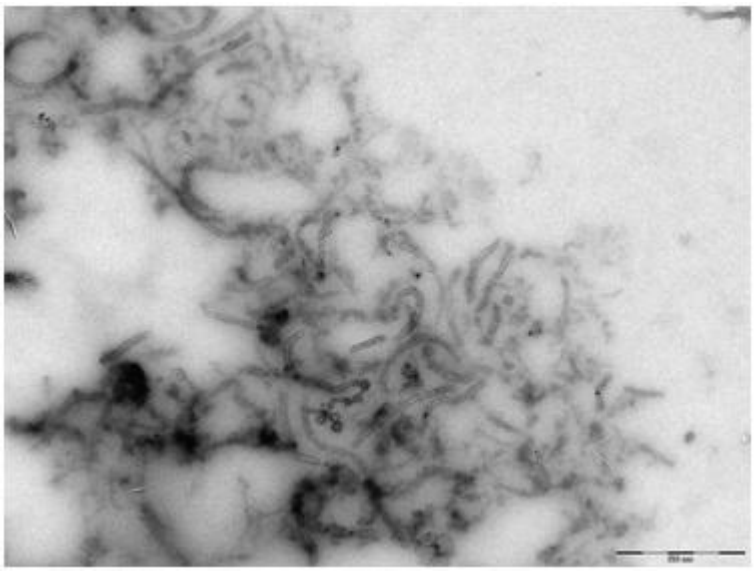

Fig. 41: CNT@mercaptosilane: oxidized CNTs functionalized with a mercaptosilane

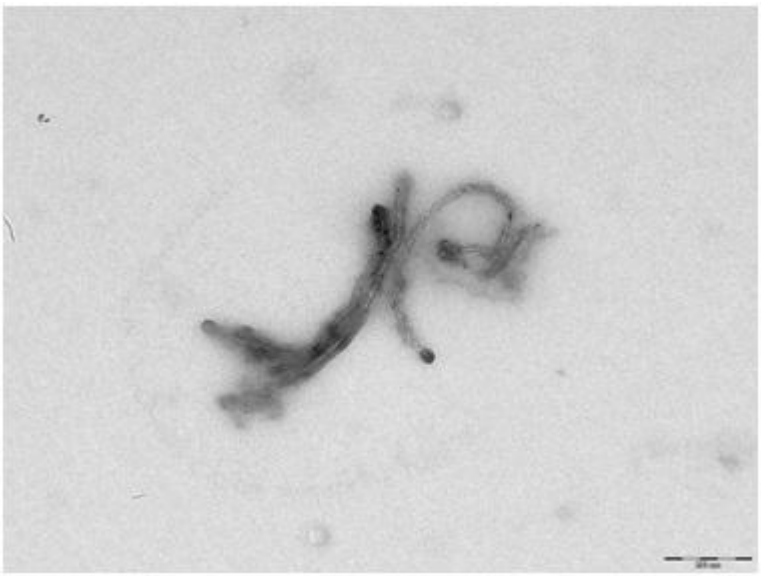

Fig. 42: CNT@mercaptosilane: oxidized CNTs functionalized with a mercaptosilane

8.3 Coating of CNTs with PAH (Poly-allylamine hydrochloride)

A polyelectrolyte (PAH) has been used to coat the surface of pristine and oxidized CNTs.[43] A polyelectrolyte is a polymer whose units contain an electrolyte; this group dissociates in an aqueous solution leaving a charge on the polymer itself. In our case the group NH_2 becomes NH_3^+ giving life to a cationic polyelectrolyte.

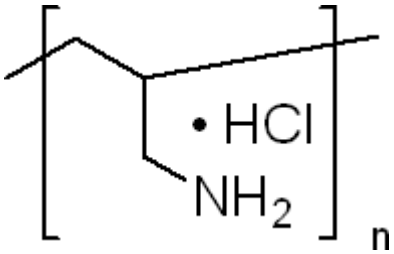

Our aim consists in enrobing the nanotube with this polymer to see if the coating involves all the CNT or chiefly the sites where a –COOH group is present.

Afterwards we would try to graft some NPs thanks to the presence and possible interaction with the NH_2 group.

8.3.1 Synthesis

Inside a volumetric flask we dissolve 1 g of PAH into 100 ml of distilled water; the solution is poured into another tube together with 15 mg of pristine MWNTs.

We put the tube into an ultrasound bath for 3 hours. The tube is stirred overnight at 80 °C and sonicated again for 2 hours. Afterwards we put the compound through five centrifugation cycles at 22000 rpm for 25 minutes and redispersion in water. Finally the powder is dried under vacuum for 6 hours.

8.3.2 Results

From XPS analysis we can get some basic information.

Pristine MWNTs are only weakly oxidized so interaction between PAH and the CNTs are principally of electrostatic nature: the polymer is physically absorbed onto CNT surface and it's the protonated amine (NH_3^+) which interacts with CNT π-orbitals. Nitrogen amount is weak (1,16 %); from deconvolution analysis (fig. 43) we can see that it is present under two forms: basing on area ratios we can assign the 0,3 % to the protonated amine (NH_3^+) and the 0,9 % to NH_2.

The value for NH_3^+ is really close to the chlorine atomic percentage (0,3 %): in fact Cl^- plays the role of counter ion.

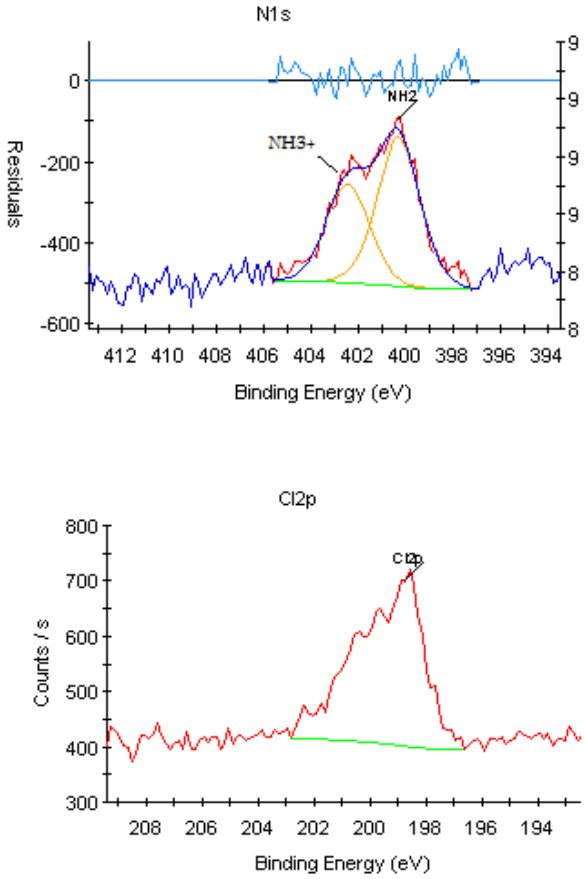

Fig. 43: XPS high resolution spectra of Nitrogen and Chlorum of (MWNT@Pah)

With MWNT@COOH nitrogen and chlorine percentages bump up respectively to 4,5 % and 0,7 %.

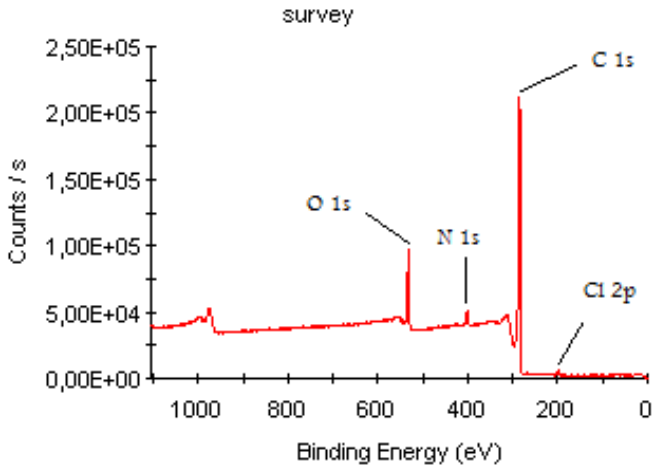

Fig. 44: XPS spectrum of (MWNT@COOH@Pah)

From the deconvolution of nitrogen spectrum (fig.45) we can evaluate approximately the ratio of NH_3^+/NH_2: the protonated amine rate is about the 76 %.

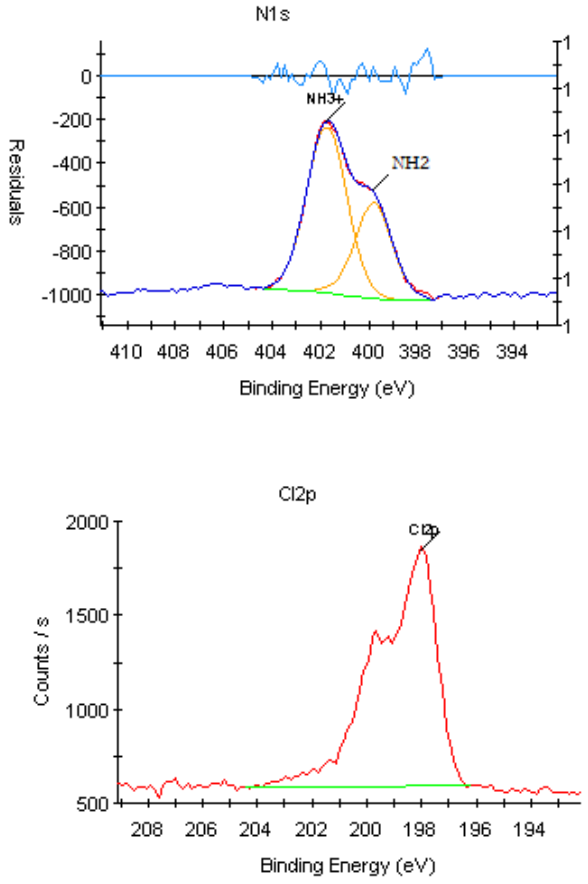

Fig. 45: XPS spectra of Nitrogen and Chlorine of (MWNT@COOH@Pah)

The protonated amine is however in excess respect to chlorine ions (3,46 % against 0,67 %). This could mean that there are two possible counter ions for the NH_3^+ : the Cl^- and the COO^- ions of the oxidized CNTs.

Unlike with pristine CNTs, with oxidized CNTs we can have different types of interactions: electrostatic, as for pristine CNTs, and the possibility of a ionic bond between COO^- and NH_3^+ and a covalent reaction between COOH groups and the amine NH_2.

This unclear results will be confirmed by TEM analysis where CNTs will appear not to be well functionalized. However we could hypothesize the failure of the synthesis just by considering the difficulties occurred during the centrifugation cycles.

New XPS measurements are in progress.

8.4 In-situ generation of diazonium salts for grafting to the surface of CNTs

The functionalization of MWNTs with diazonium salts allows to functionalize better the entire surface of the CNT (the external surface) and to alter less its structure.[41],[42]

The process of forming diazonium compounds is called diazotization. The most important method for the preparation of diazonium salts is treatment of aromatic amines such as aniline with nitrous acid. Usually the nitrous acid is generated in-situ from sodium nitrite and mineral acid. In aqueous solution diazonium salts are unstable at temperatures above +5 °C; the $-N^{+}\equiv N$ group tends to be lost as N_2. One can isolate diazonium compounds as tetrafluoroborate salts, which are stable at room temperature. Often, diazonium compounds are not isolated and once prepared, used immediately in further reactions. In our experiments we follow this second route, starting the in-situ reaction between aryl-amines and isoamyl nitrite.

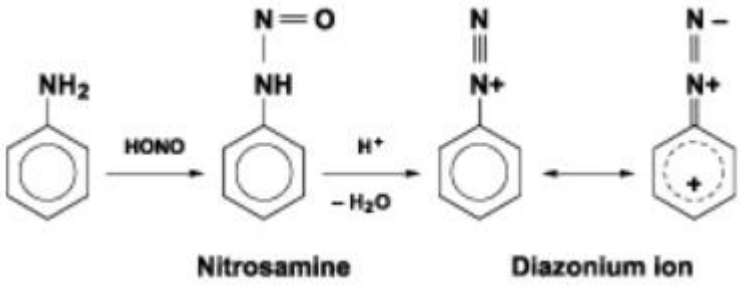

Fig. 46: in-situ synthesis of diazonium compounds

The in-situ produced aryl radicals are close to the surface, in the diffusion layer , so they can react with the surface (CNTs in this case , metals or semiconductors in others) and form a stable covalent aryl bond (C-C or different). [28], [29]

This bond forms with extremely high affinity for electrons with energies near (within a certain ΔE) the Fermi level, E_f of the nanotube: metallic-CNTs have a high electron density near E_f and this results in their high reactivity over semiconducting ones. The reaction mechanism implies a charge transfer from the CNT surface to the reactant, stabilizing the transition state. The creation of this “defect” increases the selectivity and makes the metallic-CNTs still more reactive over semiconducting ones because of the disrupted bond symmetry.

The reaction is composed of two steps. First the diazonium reagents quickly adsorb non-covalently to a CNT surface empty site, forming a charge transfer complex. During the slower second step the reactant forms a covalent bond with the CNT.

These two steps are normally recognizable thanks to *Raman spectroscopy*: after the first stage we can notice a decrease in the tangential vibrational mode (G-peak) of the spectrum; in the end the G-peak is restored and the D-band increases.

The aryl radical-substrate is not the only reaction that can occur. Since the radicals produced during this process are highly reactive, they can also interact with the aryl groups already attached to the surface, resulting in multilayer films (generally oligomers of 5,6 units are obtained with the possible presence of N=N, C-O and other unexpected bonds). [30]

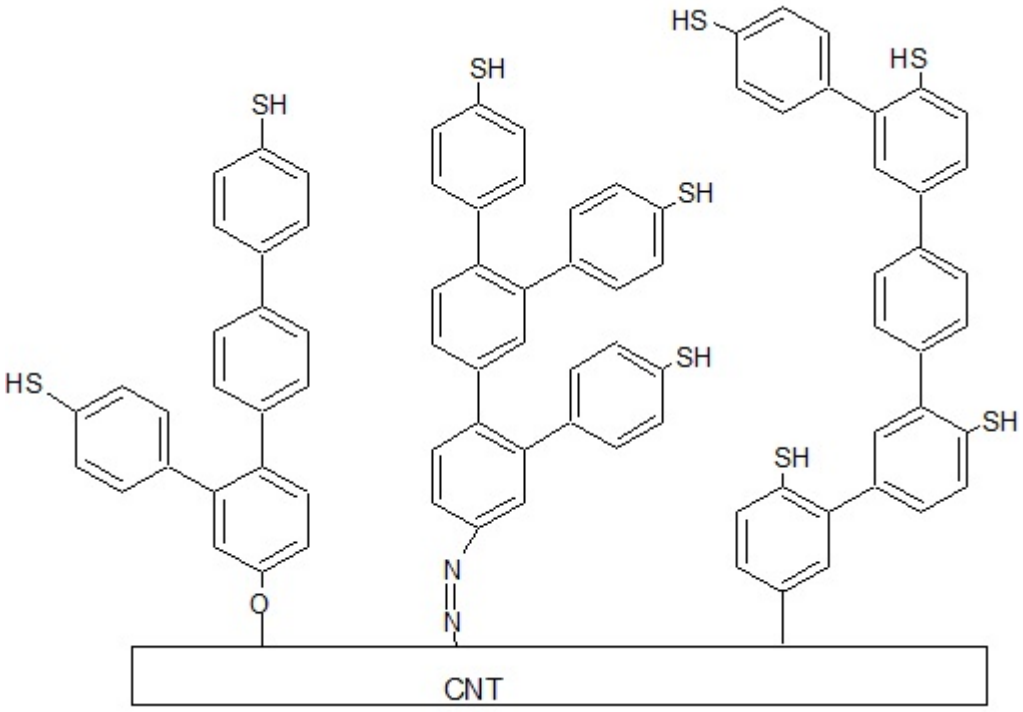

Fig. 47: possible real structure for CNT@diazo-SH compounds: aryl layers are probably oligomers

8.4.1 Synthesis

50 mg of MWNTs (1 equivalent) is put inside a two-necked Erlenmeyer bulb together with 1 g of 4-aminothiophenol (2 equivalent) and 1,12 ml of isoamylnitrite (2 equivalent). The bulb is deoxygenated by means of argon.

10 ml of acetonitrile is put inside another round bottom flask and the solution deoxygenated for 10 minutes; the acetonitrile is then transferred to the other flask because the first mixture is too viscous; thus the solution is heated at 60 °C for 3 hours.

The product is then purified by numerous washing, filtration and redispersion cycles: twice with DCM (dichloromethane), 4 times with acetonitrile (to take away the unreacted physically-adsorbed isoamylnitrite) and finally with acetone. It is called CNT@diazo-SH.

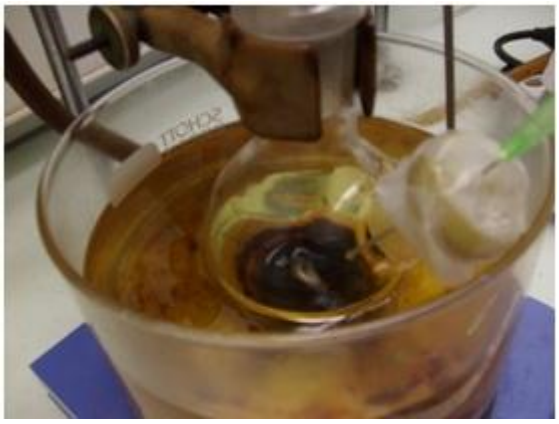

Fig . 48: functionalization of MWNTs with aminothiophenol

8.4.2 Results

From the analysis of XPS spectra first of all we can see that sulfur content is a bit greater compared to mercaptosilane-functionalized MWNTs: it reaches 7,2 % in atomic percentage. Nevertheless it is not all an R-SH bond but in part it is maybe oxidized in the SO_xH form. We can also hypothesize that part of the aminothiophenol reacts with CNTs through its thiol end, generating a S-C bond.

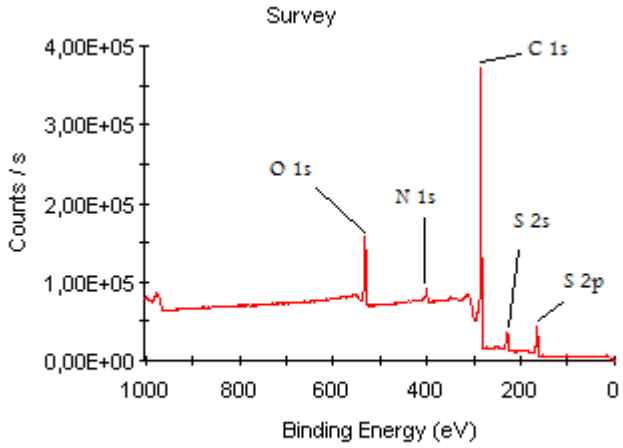

Fig. 49: XPS spectrum of CNT@diazo-SH

We have then to pay particular attention to the nitrogen spectrum: we can see more than one peak for it. In fact mainly two other kinds of bonds are expected to occur in the multilayer formation : after the formation of the initial monolayer thanks to the C-C covalent bonding between the CNT and the aromatic compound, the most probable reaction can occur between two phenyl rings: the diazonium cation in the solution can catch an electron thus releasing a N_2 molecule and generating an active radical which is able to attack the para-position of a phenyl already grafted to the surface of the CNT. CNTs could represent the source of electons which are supposed either to tunnel through the attached phenyl layer or to be conducted through the conjugated π-system.

Another possibility involves the azo-coupling of the diazonium cation with an attached ring. The diazonium cation attaches only electron-rich rings as the ones attached to the CNTs.

But in the sample that we have analyzed nitrogen content is too high (3,7 %) to be explained only by “diazonium interactions”.

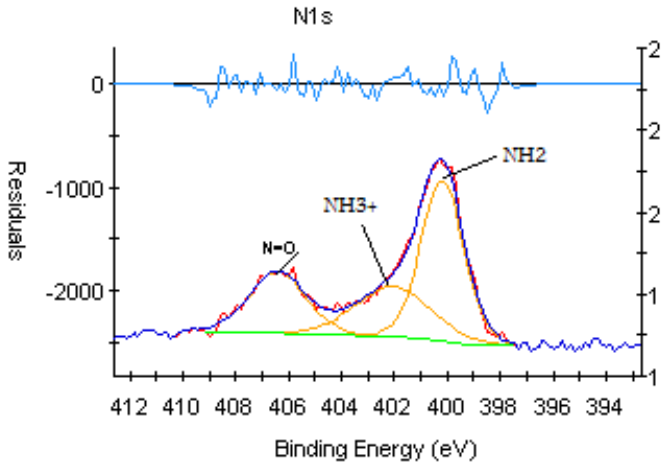

Fig. 50: XPS Nitrogen high resolution spectrum of CNT@diazo-SH

There is another peak for nitrogen (fig.50) that we could assign to a probable N=O bond; this could lead us to think about an isoamylnitrite content physically-adsorbed onto the CNT surface. The big amount of Oxigen (9,9 %, even if CNT are not oxidated) could confirm this hypothesis.

TEM analysis

This photos show us that the layers around CNTs are not as well defined as for mercaptosilane modified-CNTs and remarkable interactions remain among them. Probably onto CNTs we have the formation of multilayers of aromatic compounds.

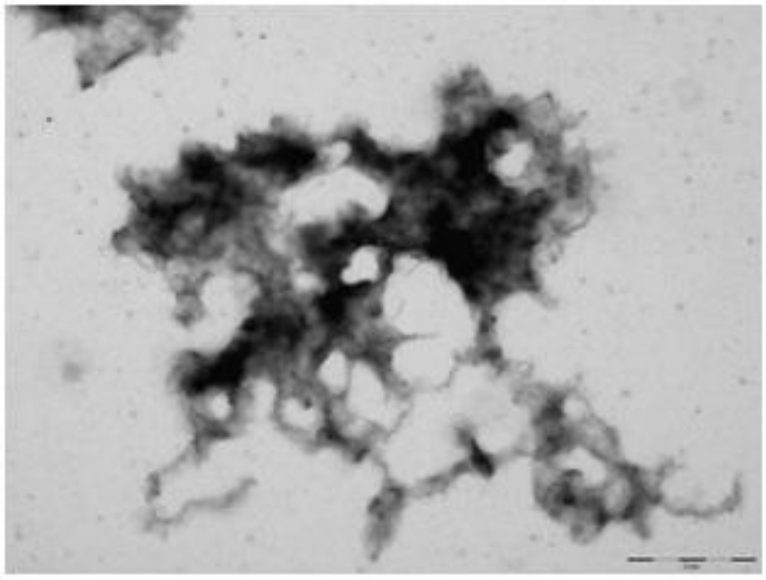

Fig. 51: CNT@diazo-SH: CNTs functionalized with aminothiophenol

On the other hand the concentration of the layer doesn't depend on the presence of carboxylic groups as for the mercaptosilane (that can attach only where it founds –COOH groups) and the aminothiophenol is instead equally distributed on all the wall.

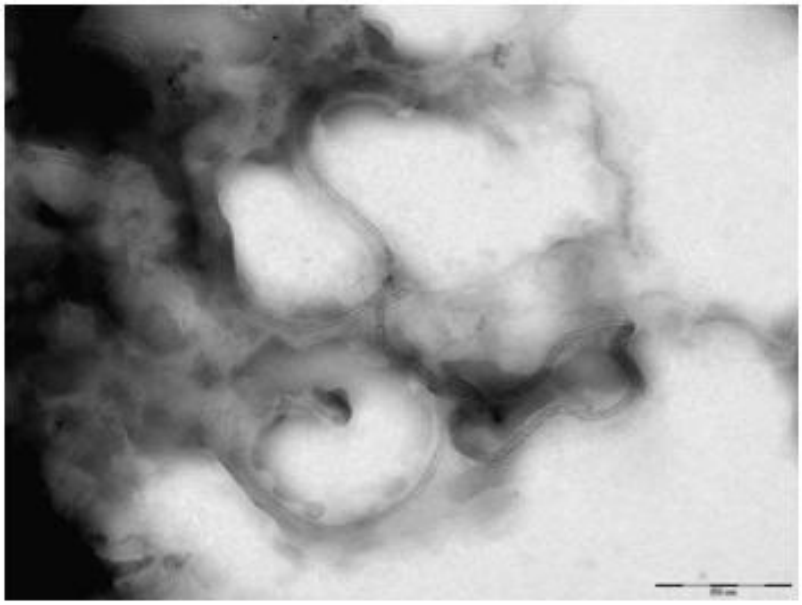

Fig. 52: CNT@diazo-SH: CNTs functionalized with aminothiophenol

Recapitulation

In the first part of our work we have functionalized some CNTs following different routes:

- some pristine CNTs have been first oxidized under various acid conditions and the as-produced samples have been functionalized with mercaptosilane molecules (MPTES)
- some pristine CNTs have been directly functionalized with a polyelectrolyte (poly-allylamine, Pah)
- some pristine CNTs have been directly functionalized with a diazonium compound (aminothiophenol)

Then the samples available for further modifications are the following

sample	Surface modification
CNT@mercaptosilane	CNT oxidized and functionalized with a mercaptosilane
CNT@Pah	CNT functionalized with an electrolyte (Pah)
CNT@diazo-SH	CNT functionalized with a diazonium compound (aminothiophenol)

9. Synthesis of quantum dots

To synthesize CdS quantum dots we follow the polyol method. Indeed an alcohol with polar and reductive characteristics is used as solvent. The most used polyols are some alpha-diols like ethylene glycol (EG) and some glycol ethers such as diethylene glycol (DEG). The diols are able to establish a lot of hydrogen bonds: this heightens their boiling temperature compared to alcohols with the same number of carbons (ethanol: T_b = 78 °C; EG: T_b = 198 °C) as well as their viscosity and water solubility.

For our purpose we use EG according to the method inspired to Fievet [(1)] and Feldmann's work. [(2)], [(3)] The advantage of this method resides in the possibility to lower the process temperatures and to exploit the ability of the polyol to be the solvent for metallic ions and the "environment" where NPs can grow up, the reducing agent, and sometimes a coupling agent.

We have tried to synthesize CdS NPs with different conditions taking advantage of the results developed by a trainee within another project. [(4)] The method is always the same, the differences consist in the kind of solvent, in the heating time, and presence of coupling agent.

The general procedure is the following: we start from reagents concentrations of $5*10^{-3}$ M in 120 ml of solvent (EG).

The reagents are:

Reagent	Molecular weight (g/mol)	n	Mass (mg)
Cadmium acetate **$Cd(OAc)_2$**	266,5	0,6 (1 equivalent)	159,9
Thiourea **$(NH_2)_2CS$**	386,5	0,7 (1,1 equiv)	50,2
TOPO	76,1	0,6 (1 equiv)	232,0

A four-necked Erlenmeyer bulb with cadmium acetate, TOPO and 100 ml of ethylene glycol is put under magnetic agitation. Temperature is increased to 180 °C with a 6 °C/min ramp. At about 140-150 °C thiourea, dissolved apart into the rest of EG (20 ml), is quickly added. As soon as the solution changes color (it becomes yellow) heating is stopped. The flask is then put inside cold water and thus the obtained solution centrifuged at 22.000 rpm for 10 minutes and washed with ethanol for 3 times. Finally the powder is dried at about 50 °C for some hours.

name	color	heating time (min)	Presence of TOPO	solvent	structure
LV16	dark orange	5	yes	EG	hexagonal
LV21	yellow	5	yes	DEG	cubic
LV23	yellow	0	no	EG	hexagonal
LV24	yellow	0	yes	EG	hexagonal

The influence of different parameters has been evaluated.

Heating time

Generally the solution with cadmium acetate and thiourea starts immediately changing color as soon as the second reagent is added. At the beginning it assumes a clear yellow color and darkens even more with passing time. Perhaps it is due to increasing dimensions of the nanoparticles which grow up. So heating times (we mean time after adding thiourea) have been decreased from 30 minutes, to 5 minutes and finally to 0 minutes.

Resulting analysis show that the shorter the heating time and the more little and less aggregated are the particles although polydispersity and a minor crystallization degree are observed.

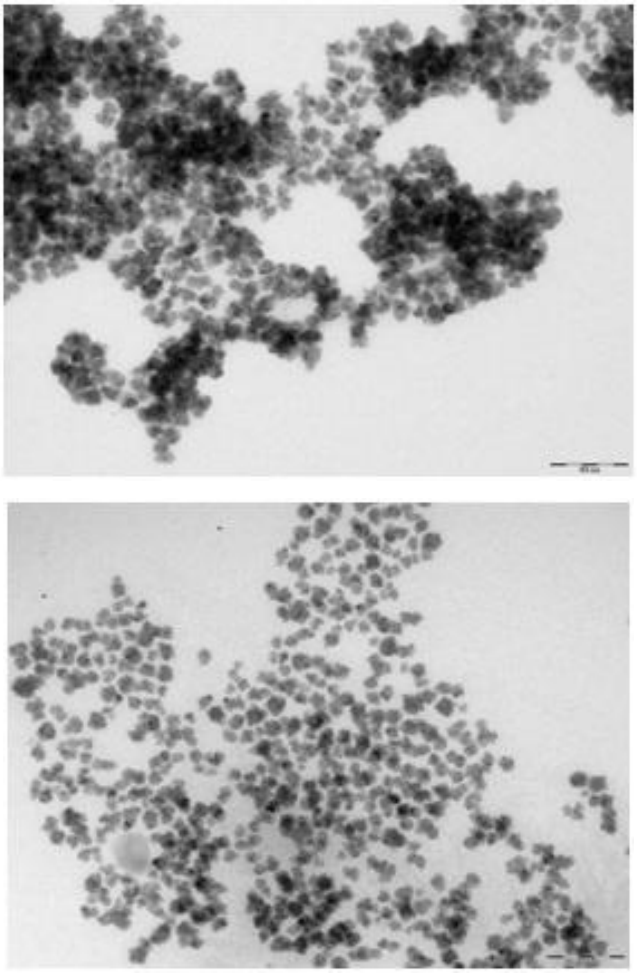

Fig. 53: LV16 (up) and LV24 (down): CdS NPs in ciclohexane

By looking at XRD spectra (fig.54) we can notice that peaks of LV-24 samples are not as well defined as LV-16: this means that NPs obtained with 0 minutes of heating time are less crystallized than the other ones.

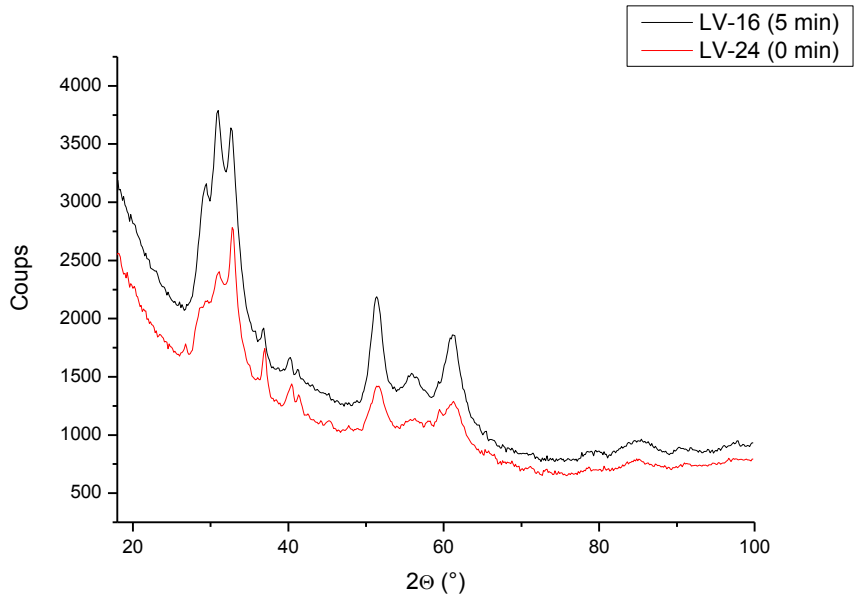

Fig. 54: XRD spectrum of LV-16 and LV-24

EDX analysis let us to attribute the lower S and the higher O content of the samples with a shorter heating time probably to a major quantity of defects.

Solvent

Synthesis performed inside EG yield yellow-orange NPs while in DEG they are of a rather light yellow. We could hazard that this corresponds to different crystallographic phases and particles dimensions: wurtzite (hexagonal crystal structure) for the former, with generally bigger dimensions (always more than 4 nm), and zincblende (cubic structure) for the latter, with diameters around 2-3 nm. In fact for example we see more defined peaks for LV-21 samples (fig.55) and larger peaks for LV-16 samples: this larger peaks, which could derive from different NPs dimensions, could correspond to more than one peak that we are only not able to separate.

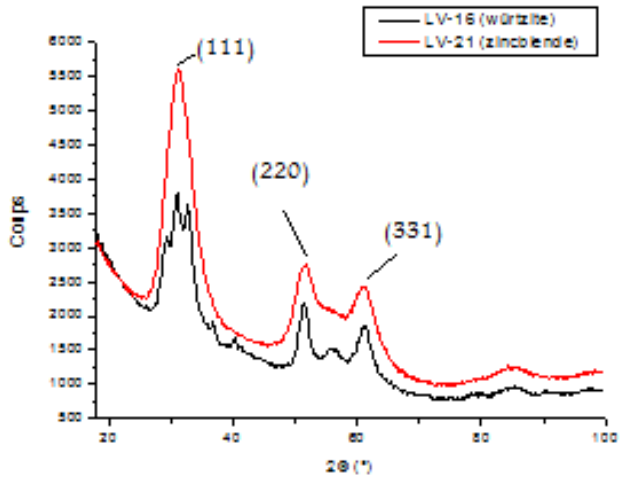

Fig. 55: XRD spectrum of LV16 and LV21

Coupling agent

The presence of TOPO in the mixture has an ambiguous effect that cannot be well interpreted. TOPO seems to play the part of "structuring agent", promoting monodispersity and crystallization.

However synthesis without TOPO produce particles with a dimension and aggregation conditions similar to the others with TOPO.

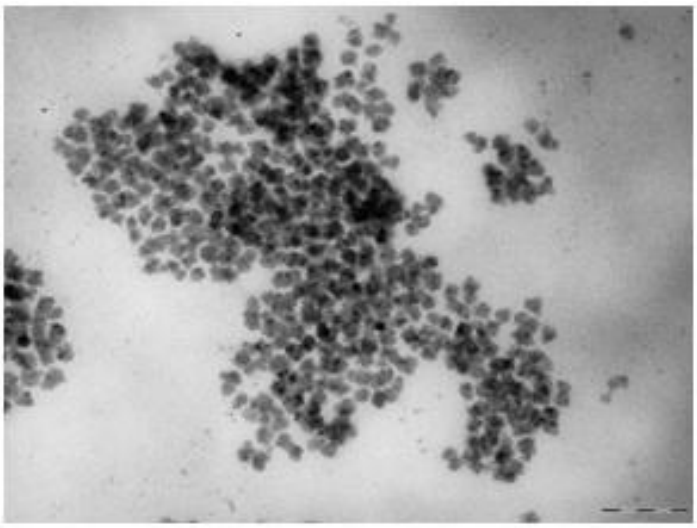

Fig. 56: LV23 without TOPO

Unlike our expectation EDX and XPS analysis indicate that TOPO is absent on the NPs surface: in fact the amount of phosphor detected is really weak. We can maybe hypothesize that TOPO has left the nanoparticles during the centrifugation cycles.

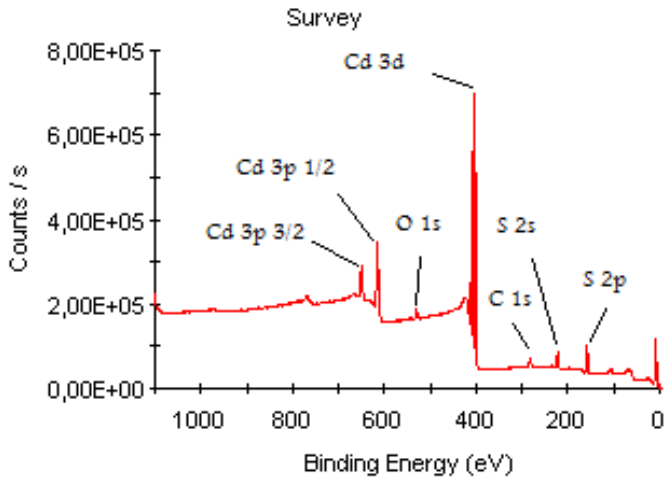

Fig. 57: XPS spectrum of CdS quantum dots

Despite all at the end NPs result in more or less large aggregates (10-15 nm) that can be annoying for further use of them (fig.58).

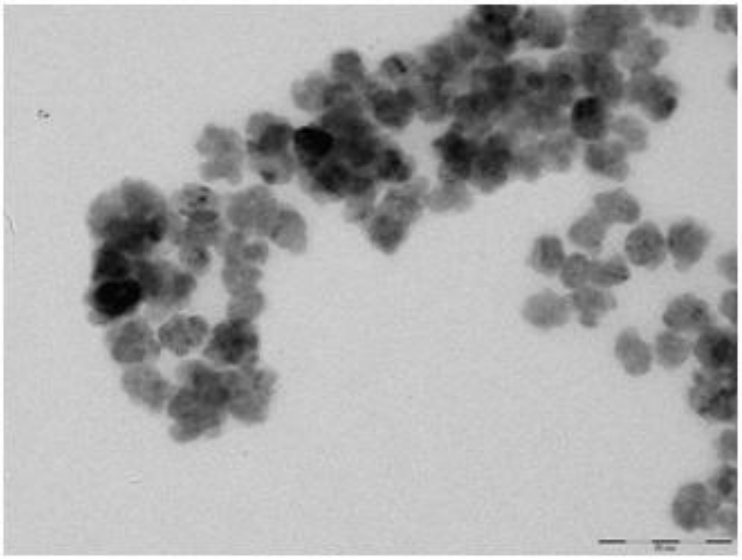

Fig. 58: LV16: presence of NPs aggregates

UV-VIS:

We have tried to get some information from UV-Vis spectra of CdS. (see chapter 11)

Recapitulation

We have synthesized CdS quantum dots in different conditions. Among all the samples we choose the NPs obtained in ethylene glycol with TOPO as capping agent (LV-16). These NPs will be subsequently mixed with the CNTs previously functionalized: CNT@mercaptosilane, CNT@Pah, CNT@diazo-SH.

10. Nanohybrids formation

10.1 Solubility

We generally find out that pristine CNTs cannot be dispersed in any organic/aqueous solvent even after sonication. For this reason they are usually functionalized by means of different molecules or simply by oxidation techniques to solubilize them in solvents of interest. According to the different compounds used to functionalize them they are able to be well-dispersed in some organic solvents such as toluene after some sonication process; however the suspensions are unstable because of competitive Van der Waals interaction between nanotubes. After assembling NPs the CNT@NPs hybrids can be well solubilized in most of common organic solvents such as toluene, THF, chloroform etc and the suspensions are stable. The enhanced stability of the nanohybrids in common organic solvents can be due to some combined effects: the NPs in fact can act as spatial blocking functions preventing the dispersed nanotubes from aggregating again and at the same time play an important role in solubilizing the hybrids as well as the functions grafted onto the CNTs' surfaces do.

10.2 CNTs and QDs Solubility tests

After lots of tests the best solvents for solubilizing purposes result the following ones

	CdS	MWNT@diazo-SH	MWNT@mercaptosilane	MWNT@PAH
ethanol	good	good (with sonication)	ok (after at least 1 h of sonication)	no
toluene	good	no	not so good	unknown
DMF	good	good (light yellow solution)	no	unknown
THF	good	good	no	unknown
H_20	quite good	unknown	unknown	Ok (after at least 2 h of sonication)

10.3 Mixing CNTs with QDs

As already said, our purpose is to graft quantum dots onto a modified CNT surface. To accomplish this we have taken advantage of the well-known interaction between thiols and metallic particles [(5), (6), (7)] and tried to extend this idea to the CdS quantum dots that we have produced.

According to the HSAB theory (the Pearson acid base concept), most of the transition metal semiconductor cations are soft acids; therefore it should be possible to well stabilize them with soft bases. Then, polymer blocks functionalized with N, S, or P ligands are generally applied. In our case Cd^{2+} present at the surface of QDs are soft acids and prefer to bond the mercapto-groups, which are soft Lewis bases, so forming a rather covalent bond (only soft acid-soft base bond is covalent). In the case of CdS/Zns core-shells maybe the bond is weaker because of the "borderline" characteristic of the Zn^{2+} ions (more acid than Cd^{2+}).

The covalent/ionic nature of the QD-ligand bond could be analysed through IR spectroscopy (to assess the possible disappearance of the S-H bond at 2560-2580 cm^{-1}).

So CNTs have been functionalized by means of some aryl/alkyl chains ending in thiol groups, i.e aminothiophenol and mercaptosilanes.

We would further investigate the bond strength of a dithiocarbamate by comparison with a single thiol. In fact the use of monothiol ligands makes QDs susceptible to oxidation. This drawback has been overcome by using dithiocarbamate moieties as ligands due to their strong chelate-type binding to metal atoms.

In literature some examples have been reported concerning the linkage between fullerenes and quantum dots [(8), (9)] and TiO_2 with CdSe/ZnS core-shells. [(10)]

Afterwards we have also tested the affinity between NH_2 groups and the same CdS quantum dots resting upon some literature advices [(11), (12), (13)].In the case of a primary amine maybe the QD/ligand bond is weaker than with mercaptans.

10.3.1 Experiments

Because of missing information in interactions between thiol modified CNTs and QDs we didn't know the maximum amount of nanoparticles that can be grafted onto the CNTs surface, so we just referred to some publications to try to put a right proportion of CdS nanoparticles. The synthesis procedure was the following:

25 mg of CdS (LV-16) is solubilized inside a tube with 15 ml of ethanol and sonicated for 2 hours; the same thing is done with 10 mg of MWNT@Diazo-SH, still in 15 ml of ethanol. Subsequently the two solutions are mixed together and sonicated for 30 minutes. The mixture is than left all the night and seems to be stable the following day.

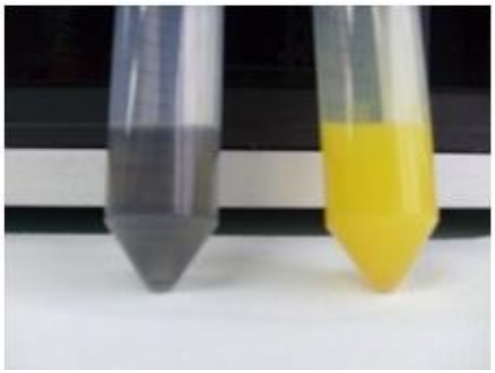

Fig. 59: two solutions: CNT@diazo-SH and CdS in ethanol

10 mg of CdS (LV-16) is solubilized inside 15 ml of ethanol and sonicated for 3 hours; 4 mg of MWNT@mercaptosilane is put inside 15 ml of ethanol and sonicated for 3 hours (solubilization of the mercaptosilane-functionalized CNTs is harder). Thus the two solutions are mixed, sonicated for 30 minutes and let stand for the night. Unlike the previous synthesis the mixture is not stable the following day: the CNT@CdS hybrids precipitate and deposit on the bottom of the tube. Perhaps this is due to a lower amount of QDs present around the tubes, which in theory prevent CNT bundles formation and then a more likely precipitation of the heavier aggregates.

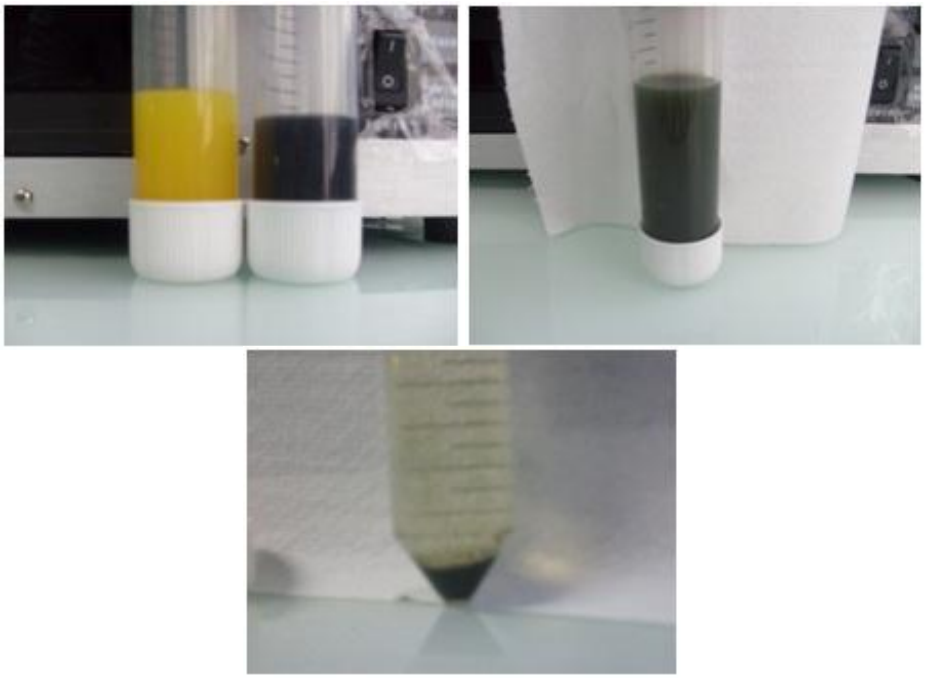

Fig. 60: two solutions: CdS and CNT@mercaptosilane (up left); two solutions mixed (up right); mixture after night (down)

Due to dispersion problems of CdS nanoparticles and to try to avoid their aggregation, another kind of synthesis has been performed:

CdS QDs have been prepared according to the already described polyol method with these particular conditions: 1 equivalent of $Cd(OAc)_2$ has been put into 120 ml of ethylene glycol, without TOPO. The solution is stirred and heated till 150 °C, thus thiourea (1,1 equivalent) is added and heating stopped as soon as it changes color, becoming yellow/orange.

Afterwards 5 mg of MWNT@diazo-SH has been sonicated for 2 hours inside 20 ml of ethanol. They have been thus added to 20 ml of the previous solution (it should correspond to about 14/15 mg of CdS). The mixture of nanoparticles and solvents (EtOH and EG are miscible, even if the mixture is initially made of two different phases) is put under ultrasounds for 1 hour. The solution is not so stable: after few hours we have a phase separation. The product is called ABQ1.

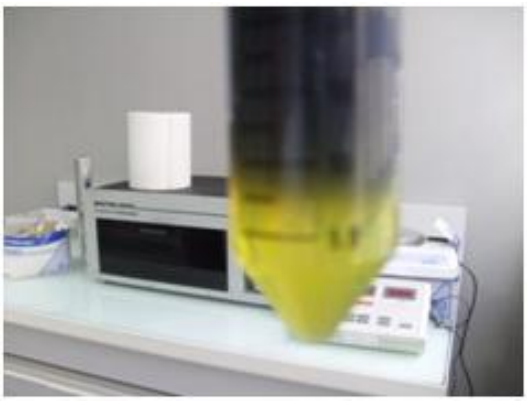

Fig. 61: mixture CNT@diazo-SH - ABQ1 before sonication

Fig. 62: CNT@diazo-SH@CdS, CNT@diazo-SH@ABQ1 and CNT@mercaptosilane@CdS just after sonication

Fig. 63: CNT@diazo-SH@CdS, CNT@diazo-SH@ABQ1 and CNT@mercaptosilane@CdS after 1 sedimentation week

10.3.2 Results

TEM analysis

TEM analysis show that the interaction between CNT functions and CdS nanoparticles works well for both the samples.

As MWNT@Diazo-SH is concerned, NPs distribution is quite uniform and involves all the CNT wall (fig.64).

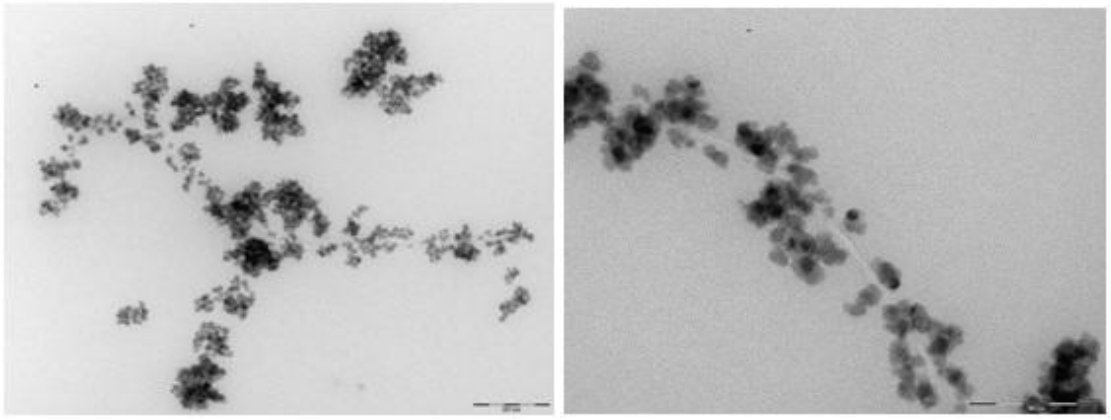

Fig. 64: CNT@diazo-SH@CdS

NPs grafted on MWNT@mercaptosilane are instead worse distributed along CNT wall: they are localized in certain regions (fig.65) and especially in correspondence of CNT ends, where CNTs result more modified, as we have stated before: in fact it's at the ends of CNTs and at defect

sites that CNTs are greater oxidized and then there will be a bigger functionalization degree in these zones.

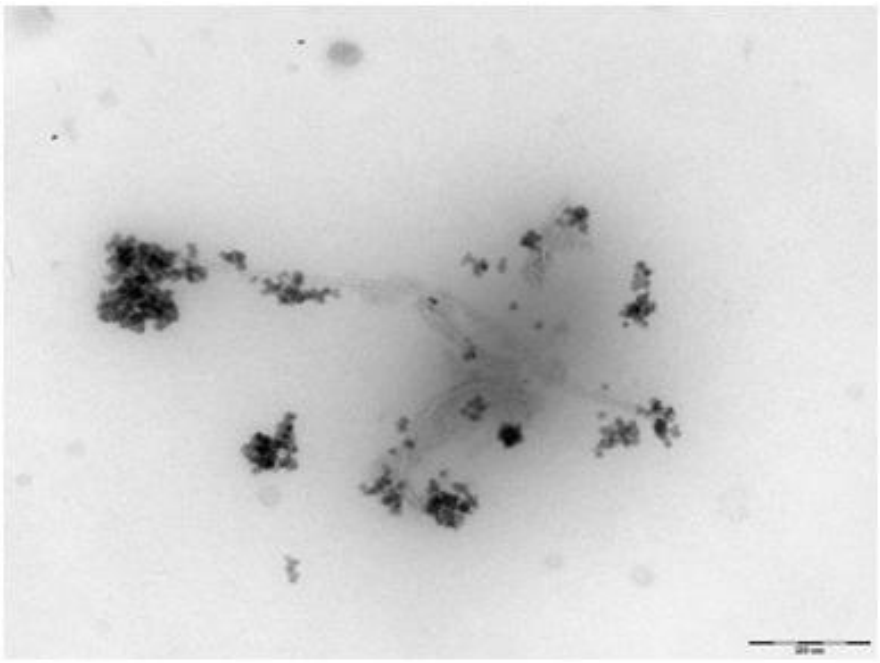

Fig. 65: CNT@mercaptosilane@CdS

From TEM analysis (fig.66) we have seen that the chosen amounts of NPs are too huge: too many QDs are present onto CNT surface (CdS aggregates simply deposited onto the surface).

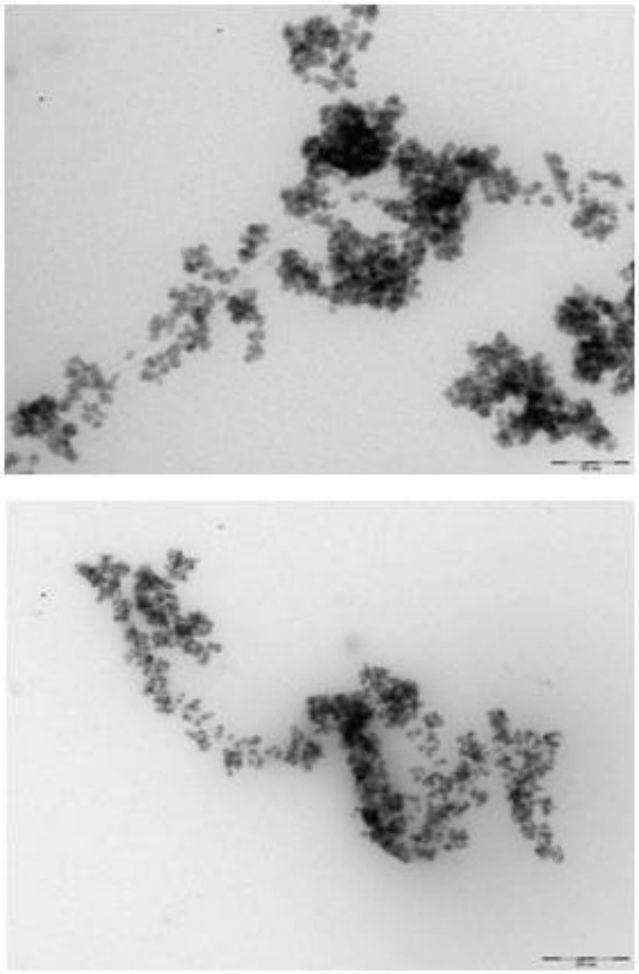

Fig. 66: CNT@diazo-SH@CdS before washing cycles

Two attempts could be made to focus our attention only to the NPs directly bound to the CNT through the *S-bond*: to lower the NPs quantity or better to try to take the excess particles away.

We have pursued the second route: the hybrids have been filtered by means of distilled water. TEM analysis confirm that this is not enough to take the particles away (fig.67 e 68). Perhaps we should try with more washing cycles, with a different solvent or by means of special filters [(14)] or by lowering the centrifugation rate, just to precipitate only the heavier hybrids and not the QDs that thus could remain in the supernatant [(15)]. We will focus on the latter point in our final experiment with core-shell QDs.

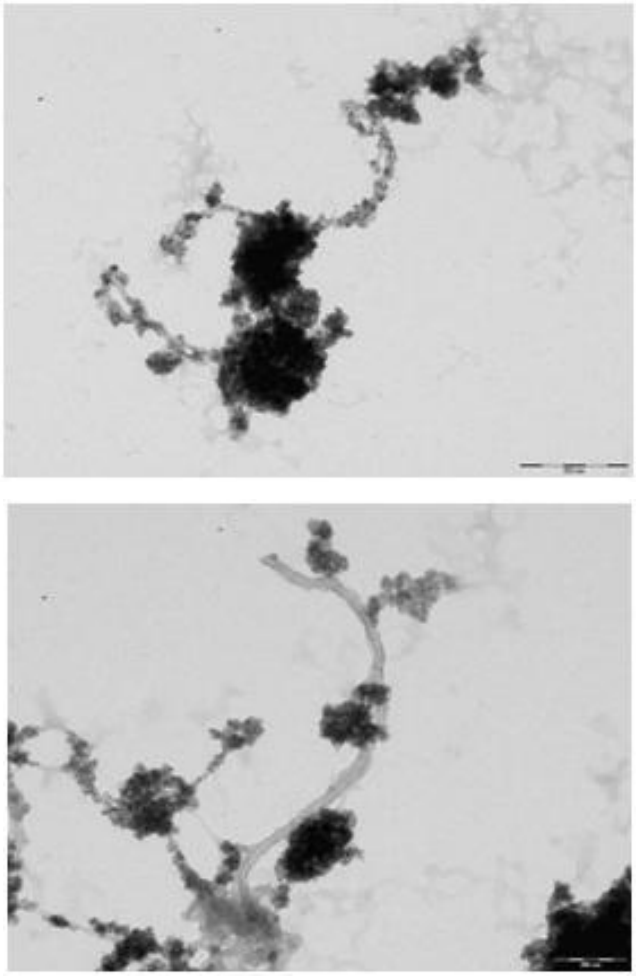

Fig. 67: CNT@mercaptosilane@CdS after washing cycles

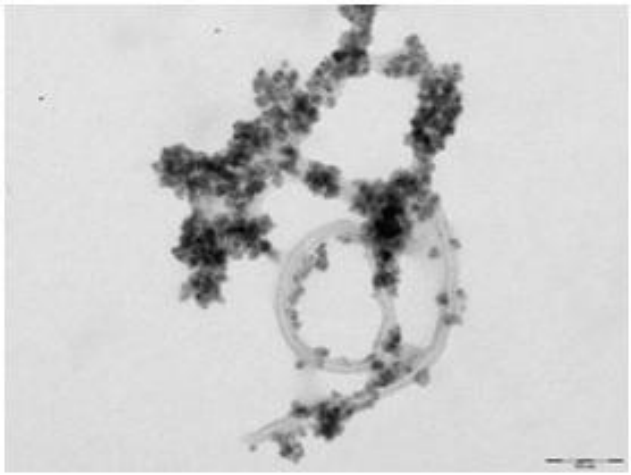

Fig. 68-A: CNT@diazo-SH@CdS after washing cycles

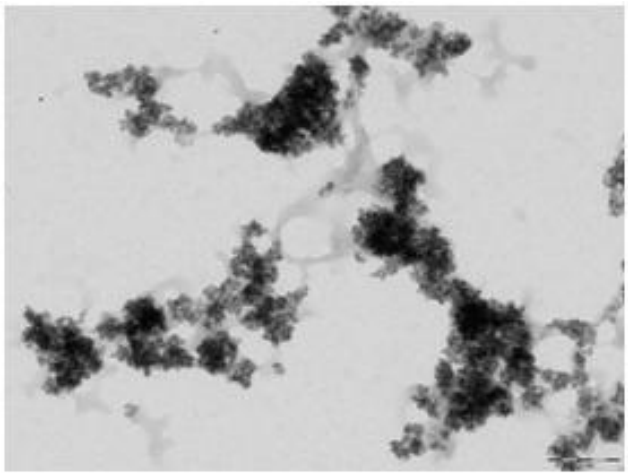

Fig. 68-B: CNT@diazo-SH@CdS after washing cycles

An equally valid route could be offered by the introduction of CNTs directly inside the non-centrifuged colloidal solution of QDs thus maybe encouraging a better dispersion of the NPs along the CNT. These kinds of nanohybrids should then be subjected to some appropriate low-rate centrifugation cycles.

This technique could also be used to finely control the amount of NPs we want to deposit on the CNTs: we could put into the initial solution just the right quantity of precursors to get the required amount of NPs and avoid a further centrifugation.

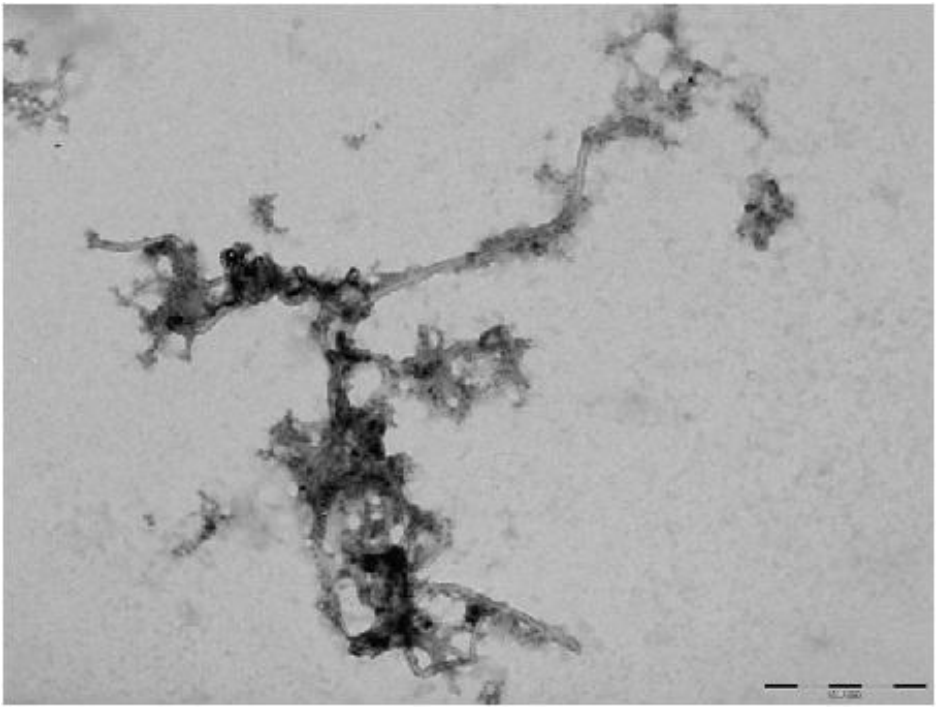

Fig. 69: CNT@diazo-SH@ABQ1: CNT inserted into the colloidal CdS solution (ABQ1)

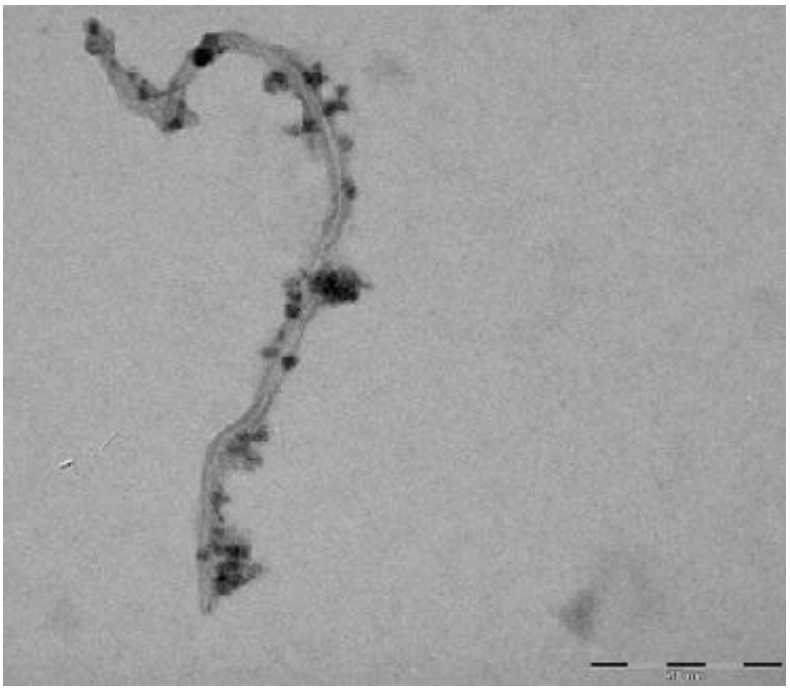

Fig. 70: CNT@diazo-SH@ABQ1

XPS analysis

From XPS spectra we can get some general information as for example the presence of CdS nanoparticles onto CNT surface.

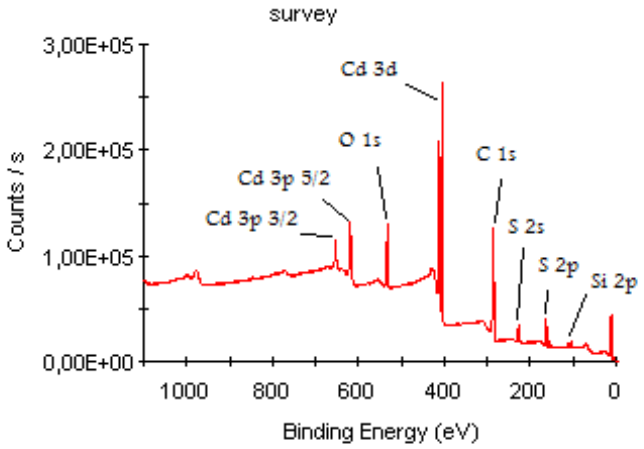

Fig. 71-A: XPS spectrum of CNT@mercaptosilane@CdS

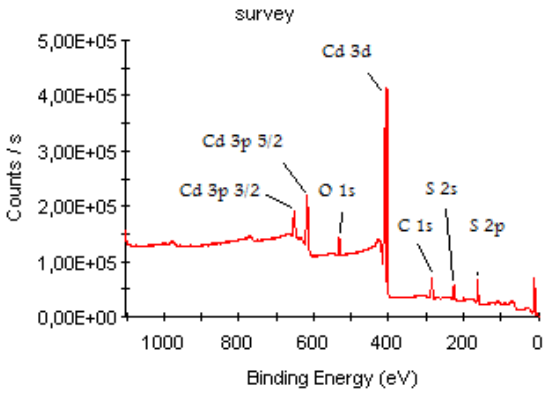

Fig. 71: XPS spectrum of CNT@diazo-SH@CdS

For MWNT@mercaptosilane we obtain an atomic percentage in Cd of 9,9 % and in S of 10,7 %: we cannot distinguish between S belonging to CdS NPs and that one of mercaptosilane but we can say for sure that a certain quantity of CdS is present (TEM analysis confirm this).

From the spectra we can clearly see the characteristic Cd doublet for 3d orbitals and that one of S for 2p orbitals (fig.72).

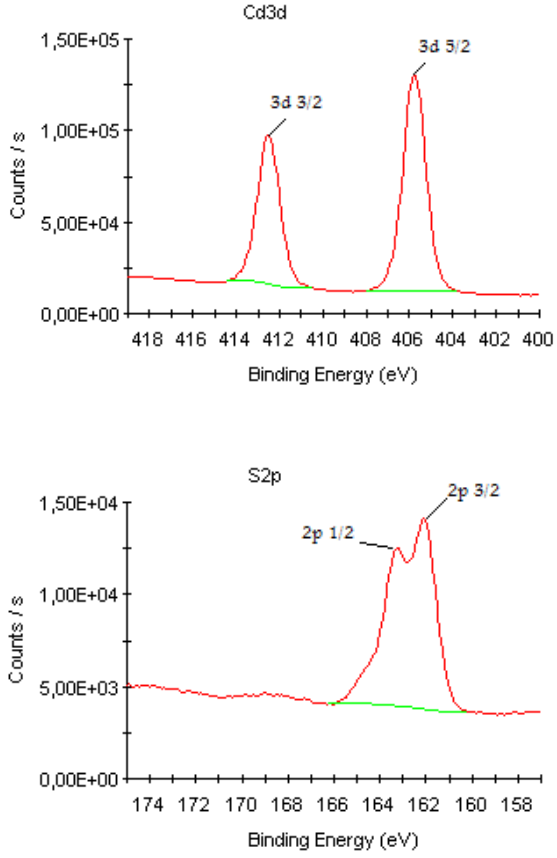

Fig. 72: XPS high resolution spectra of Cadmium and Sulfur of CNT@mercaptosilane@CdS

The atomic percentages for MWNT@Diazo-SH are rather different from the previous ones.

Cd percentage reaches 22,1 % and it can be compared with S percentage (24,8 %), considering that XPS measures are subjected to an error of 10 %.

In general data are less clear: for example the S peak doesn't display the characteristic doublet (fig.73), oxygen (16,12 %) is maybe too much (CNTs are not oxidized: it could be due to oxidized Cd or more probably to oxygen of isoamyltnitrite physically adsorbed onto CNT surface). We cannot assess nitrogen spectrum because of its superimposition with the Cd one.

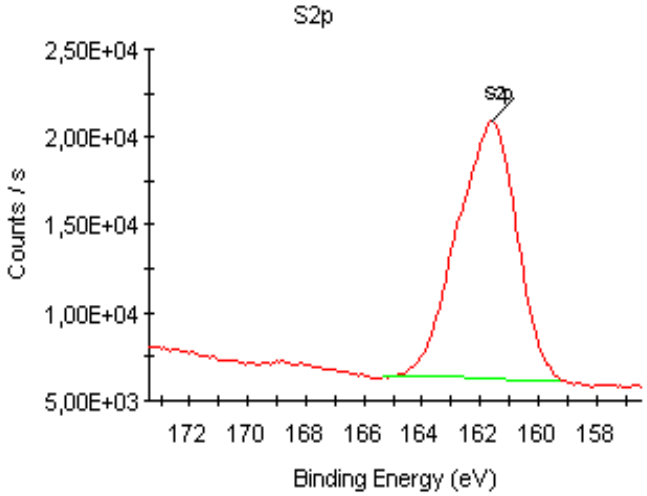

Fig. 73: XPS high resolution spectrum of CNT@diazo-SH@CdS

10.3.3 Other essays

To assess the binding between MWNTs and CdS we have also tried to create other types of mixtures, taking into account mainly the results obtained from other researchers in the field of in-situ generation of NPs onto CNT surfaces [(16)]. In fact in these publications NPs are supposed to grow up mostly where -COOH groups or CNT irregularities are present. According to these hints we have tried to make the following mixtures:

4,5 mg of pristine-MWNTs has been dispersed inside 15 ml of ethanol under ultrasounds for 3 hours; afterwards 11 ml (about 8 mg) of ABQ1 solution has been added and the mixture sonicated for 1 hour.

4,5 mg of acid-oxidized MWNTs has undergone the same treatment.

The last attempt involves the mixing of CdS with (NH_2)-modified-MWNTs. The nature of the NH_2-CdS bond has been inspired by solubility essays of quantum dots, [(11)] where these

nanoparticles were just modified by molecules with a double functionality to accomplish their dispersibility in different solvents.

Then 1,1 mg of MWNT@COOH@Pah has been dispersed in 15 ml of distilled water and sonicated for 2 hours. 2,3 mg of CdS has been sonicated into distilled water for the same time, and the two solutions have been mixed and further sonicated for 30 minutes.

We have to notice that MWNT@Pah requires long sonication times to be dispersed into water (into ethanol is impossible); besides CdS is much less soluble in water than in ethanol (there is neither the presence of OH groups nor a capping agent which can stabilize the NPs).

TEM analysis

In the TEM images (fig.74 and 75) concerning the mixture between MWNT@Pah and CdS (LV-16) quantum dots we can see that NPs seem anchored to the nanotubes but they are not well distributed throughout the CNT: maybe this is due to an unsuccessful functionalization of CNTs. Conversely NPs don't form too big aggregates as in other synthesis, but are somewhere present also in almost single units.

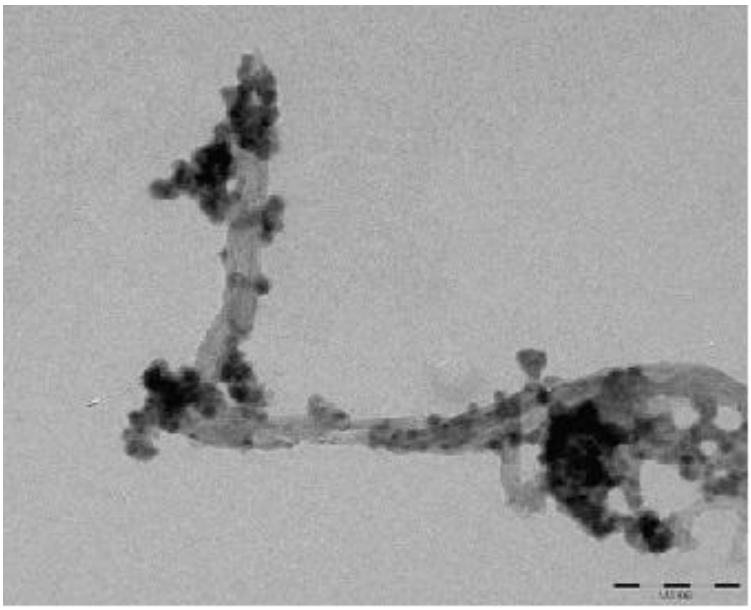

Fig. 74: CNT@Pah@CdS

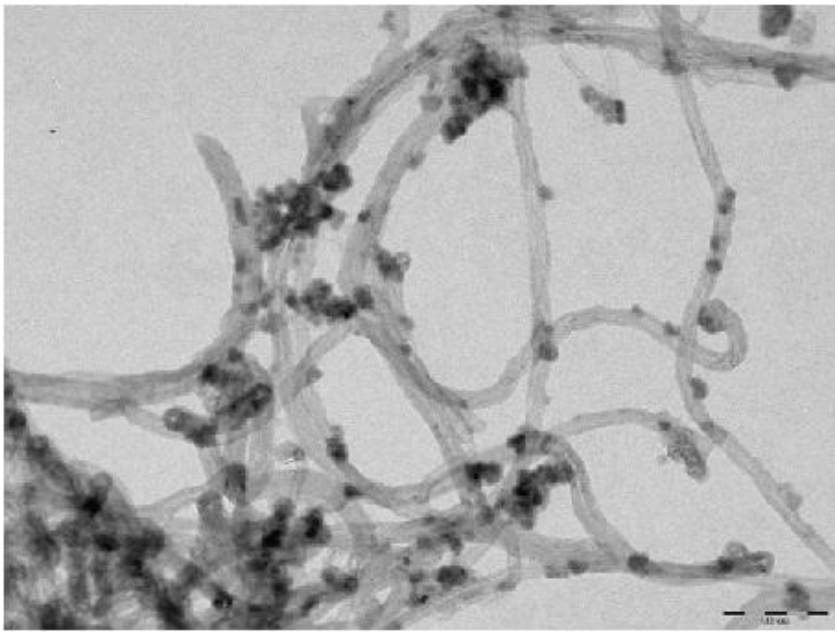

Fig. 75: CNT@Pah@CdS

In the case of MWNT@CdS hybrids (fig.76 and 77), we can perceive a not so deep interaction between the QDs and the CNTs: NPs seem to be collected in some chains or aggregates around certain points and not to have a real contact with the nanotubes.

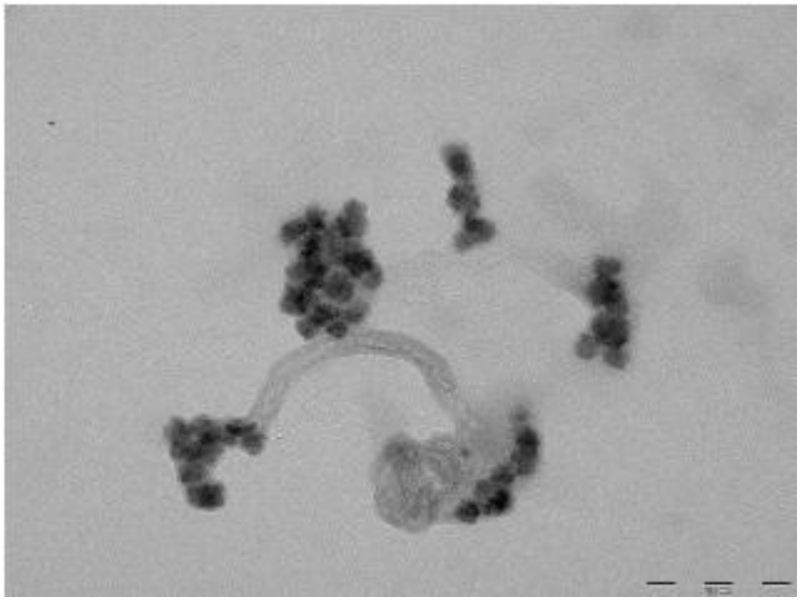

Fig. 76: CNT@CdS: pristine CNTs and CdS (ABQ1) quantum dots

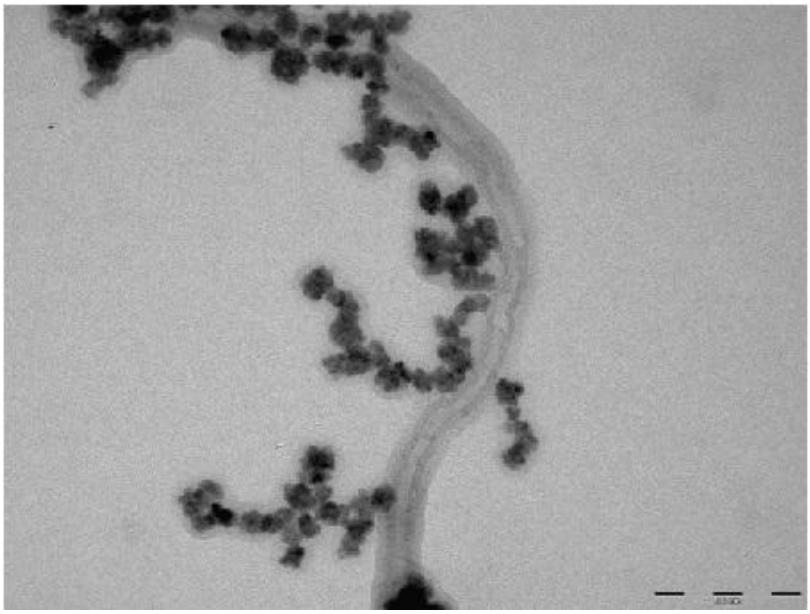

Fig. 77: CNT@CdS

Also in the oxidized-CNTs/CdS mixtures NPs are chiefly localized in certain points (fig.78), that are mainly CNTs ends, where maybe they are able to interact somehow with the carboxylic functions.

As explained in literature, oxidized-CNTs cannot hold NPs that have not been synthesized in-situ on nanotubes surface. The NPs aggregates can only stack up on the CNT and bundles surfaces (fig.79).

Some photoluminescence studies would be interesting just to exclude any sort of electronic communication.

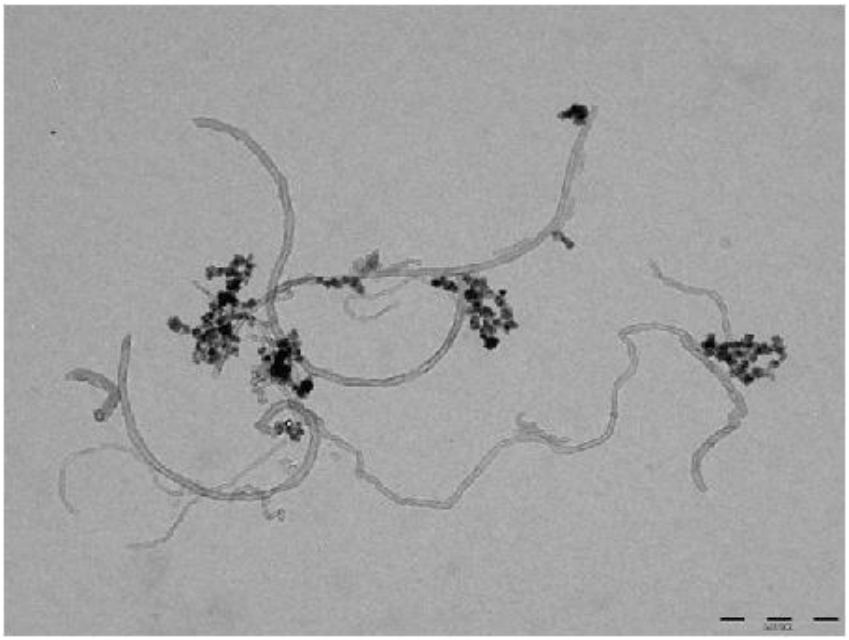

Fig. 78: CNT@COOH@CdS: oxidized CNTs and CdS (ABQ1) quantum dots

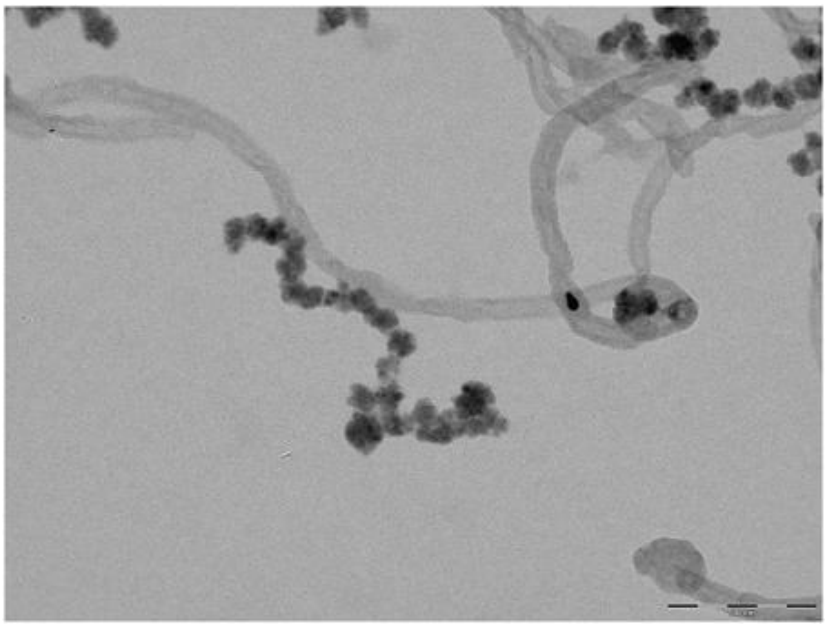

Fig. 79: CNT@COOH@CdS

Summary

At this point we can sum up the nanohybrids we have obtained in our experimental work

sample	Type of hybrid
CNT@mercaptosilane@CdS	CNT@mercaptosilane + CdS (LV-16)
CNT@Pah@CdS	CNT@Pah + CdS (LV-16)
CNT@diazo-SH@CdS	CNT@diazo-SH + CdS (LV-16)
CNT@diazo-SH@ABQ1	CNT@diazo-SH + CdS (ABQ1)
CNT@CdS	Pristine CNT + CdS (ABQ1)
CNT@COOH@CdS	Oxidized CNT + CdS (ABQ1)

We have seen that CNTs don't deposit onto the walls of pristine and oxidized CNTs. The synthesis with the polyelectrolyte (Pah) has to be improved but it is promising for a good nanotube coverage. At the same way the introduction of CNTs inside the non-centrifuged colloidal solution of the QDs could lead to a good CNT/QDs interaction maybe preventing NPs aggregation issues.

The more striking result involves the difference in CNT coverage when nanotubes are functionalized with a mercaptosilane or through diazonium chemistry. For the first case, NPs appear more localized in the zones of the nanotube where the functionalization degree is probably higher (which corresponds to the initial presence of more –COOH groups in the oxidized nanotubes), that is at the nanotube ends and near the defects of the pristine CNTs; in CNT@diazo-SH@CdS nanohybrids the NPs seem to be present along all the CNT wall. This fact could be differently exploited for various targets.

However we have just highlighted the presence of NPs on CNT walls. We haven't described their electronic interaction yet.

11. Uv-Vis and Photoluminescence analysis

We have probably reached the most interesting part of our work which could let us evaluate the effectiveness of the electronic interaction between the QDs and CNTs. In fact we have hypothesized the presence of CdS nanoparticles onto the surface of CNTs by means of XPS measurements, we have physically observed their presence through TEM analysis but we have never verified the real communication between the two main actors of our device. The final goal should be that of harvesting the sunlight, that is capturing it and allowing its "exploitation", thus converting it into ready-for-use electric energy. We have already acknowledged the light-catching properties of QDs and the electrical conducting ability of CNTs. So we have to focus our attention on the mechanism that lets the device pursue the light-electricity conversion, namely the CNTs/QDs communication skills. UV-Visible absorption and Photoluminescence analysis can provide some more information about it.

11.1 UV-VIS absorption analysis

After having assured that TOPO (maybe present onto QDs surfaces) doesn't absorb light between 300 and 800 nm, we have analyzed two CdS samples:

- CdS2: LV16 with ethanol as reference: 0,5 mg / 5 ml = 10^{-1} M
- CdS6: ABQ1 with EG : 0,125 mg / 5 ml = $2,5*10^{-2}$ M

Afterward UV-Vis analysis of the following samples have been performed:

- NTD1 : MWNT@diazo-SH in ethanol: 2 mg / 5 ml = $4*10^{-1}$ M
- NTM1 : MWNT@MPTES in ethanol: 2 mg / 5 ml = $4*10^{-1}$ M
- NTCdS3: we use the solution ABQ1* (made of two solvents: EG and ethanol, so the reference takes into account the presence of both of them): about 0,32 mg of MWNT@diazo-SH / 5 ml of EG = $6,4*10^{-2}$ M
- NTDCdS3: 0,4 mg of ABD162 / 5 ml of ethanol = $8*10^{-2}$ M
- NTMCdS2: 0,24 mg of ABME16-(washed) / 5 ml of ethanol = $4,8*10^{-2}$ M

All the solutions have been previously sonicated and not all of them reach a high solubility (some particles remain on the bottom of the cuvettes), so the quantities above mentioned are purely indicative. Because of the different concentrations among the samples, the spectra cannot be quantitatively compared, a more accurate analysis is worth being performed.

However, we can draw some useful conclusions from the spectra.

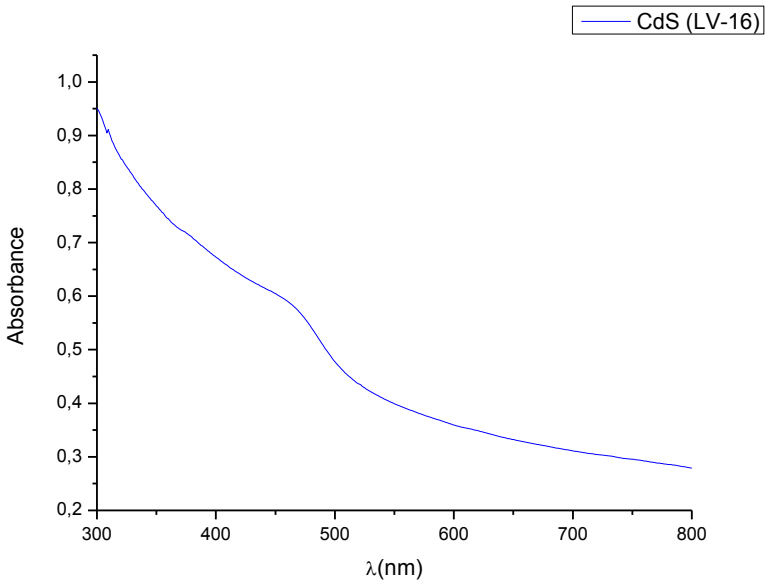

Fig. 80: "CdS2" (LV16) absorption spectrum

As far as the CdS (LV16) spectra are concerned (fig.80), we can highlight the presence of a shoulder at 467 nm that identifies the peak correspondent to the gap of the nanoparticles (1S(e)-1S transition). This peak is rather broadened and not too marked, moreover the absorption onset is not well defined, thus maybe involving the presence of a polydispersion of the NPs dimensions and some surface defects which allow absorption at wavelengths longer than the gap width.

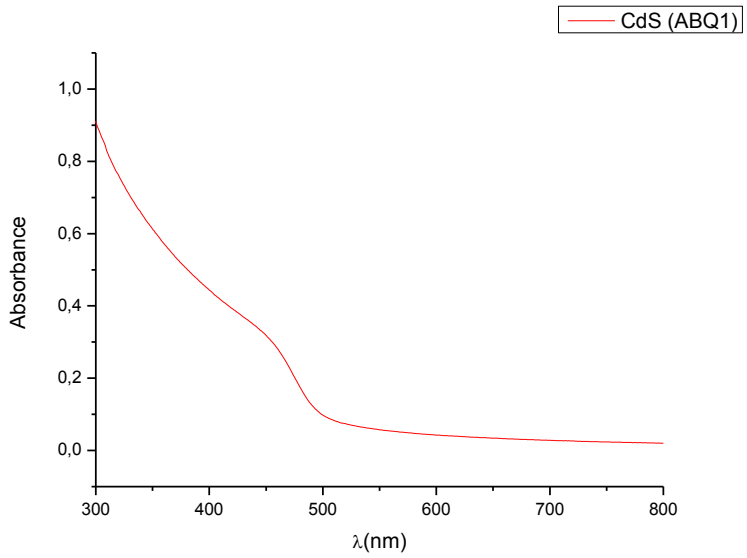

Fig. 81: "CdS6" (ABQ1) absorption spectrum

For the ABQ1 CdS samples (fig.81) the shoulder is more or less at the same position (about 460 nm), but the absorption onset is more defined. We have to say that this spectra belongs to the QDs still dispersed in the solutions, so not yet centrifuged and redispersed. So maybe NPs are subjected to some "alterations" after the centrifugation cycles: perhaps this is due to the loss of the capping agent.

Glancing at the spectra of the nanohybrids we can remark a substantial similarity to the spectra of the CdS quantum dots, and this is what we expected. By attentively observing it, it is possible to see the presence for the CNT@diazo-SH@CdS nanohybrids (fig.82) of the same exciton peak as CdS quantum dots alone, and a relative equality between the two spectra. The fact that the QD absorption edge can be distinguished can only be explained by a dense coating of relative monodisperse QDs onto the CNTs [(15)].

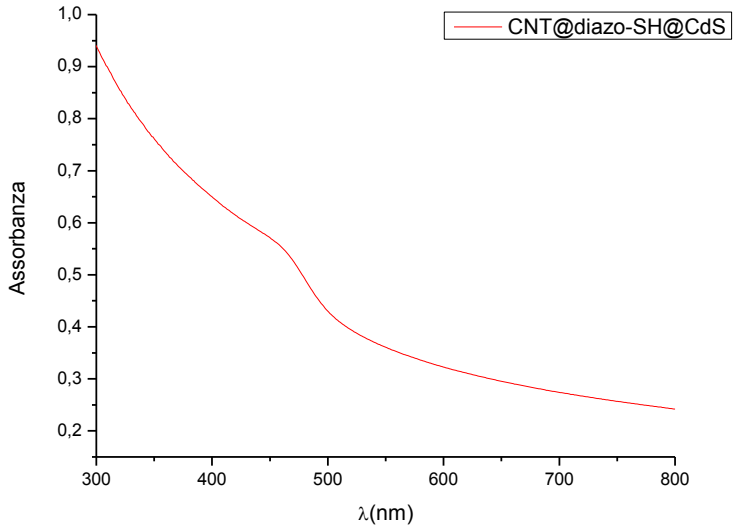

Fig. 82: Absorption spectrum of CNT@diazo-SH@CdS(LV16) nanohybrids

In the CNT@mercaptosilane@CdS (fig.83) we lose the presence of the band-edge peak but the rest of the spectrum is quite similar. Maybe this is due to the more feeble quantity of CdS quantum dots on the nanotubes.

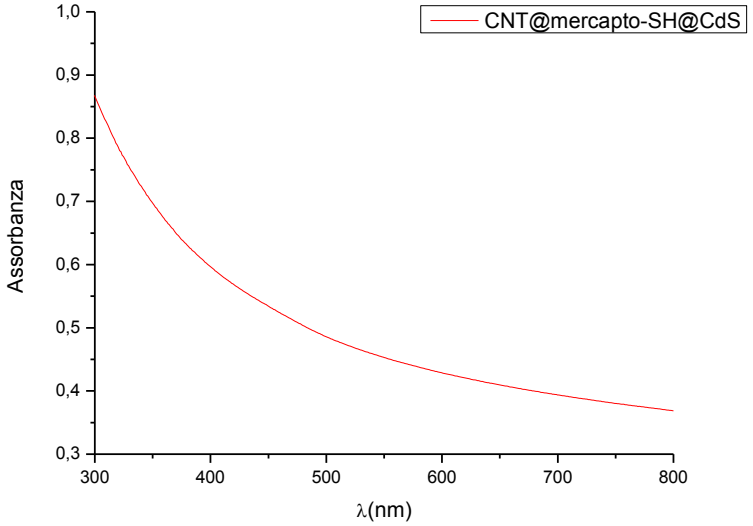

Fig. 83: Absorption spectrum of CNT@mercaptosilane@CdS(LV16) nanohybrids

Afterward if we compare the spectra of CdS quantum dots "ABQ1" with that of the CNT@diazo-SH mixed directly to the CdS solution (fig.84) we can still see the exciton peak at the same wavelength as well as a slightly different absorption profile at shorter wavelengths as well: another shoulder can be seen at about 360 nm, maybe corresponding to higher energies transitions (1P(e)-1P).

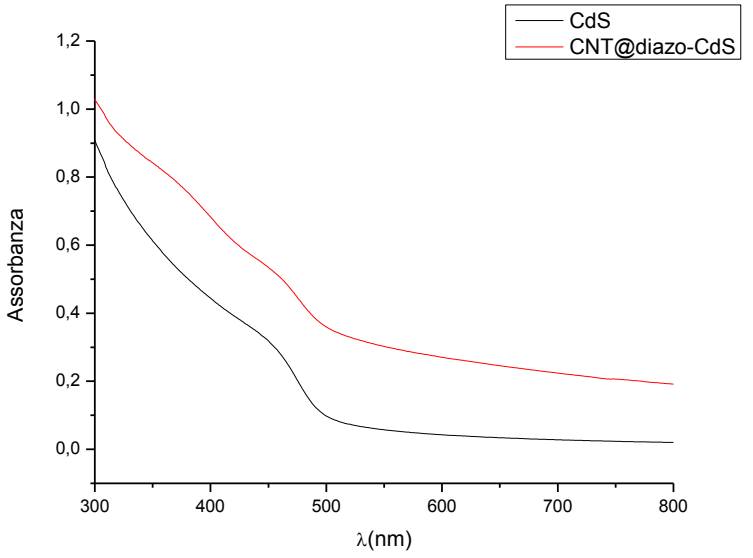

Fig. 84: Absorption spectrum of CdS (ABQ1) NPs and CNT@diazo-SH@CdS nanohybrids

In the end from the PL spectra of CdS quantum dots that we have synthesized we can notice the lack of luminescence. Then we have chosen to utilize some commercial quantum dots (see below) to evaluate the effectiveness of the CNT/QDs coupling. Their absorption spectrum is shown (fig.85): a shoulder is absent but of a more definite and less broadened peak is present at about 593 nm.

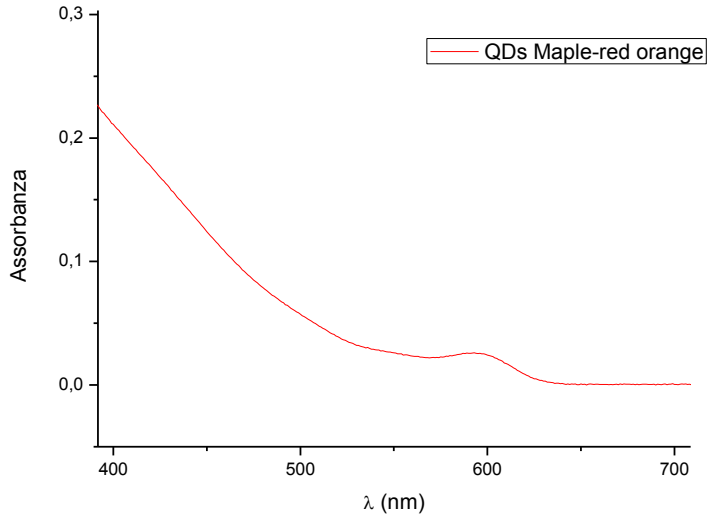

Fig. 85: Absorption spectrum of CdS/ZnS "Maple-red orange" commercial QDs

11.2 Photoluminescence

More than UV-Vis spectra, PL spectra can shed some light on the communication characteristics between QDs and CNTs.

Unfortunately some problems arose with the CdS NPs that we have synthesized and used in most of our nanohybrids. In fact from PL analysis we have seen that they are not luminescent; maybe this is due to aggregation issues, or to other non-radiative mechanisms that prevent a luminescent response.

So we have had to utilize something else to test our device: our availabilities consisted of some commercial core-shell quantum dots with a CdS core and a ZnS shell.

11.2.1 Experiments

For our synthesis we have used some commercial CdS/ZnS quantum dots: the Eudent Maple Red Orange. The only information we are provided is their structure: they are core-shell quantum dots with a nucleus of CdS and some outer layers of ZnS (we don't know the

thickness). They are dispersed in toluene in a concentration that should correspond to 19,5 mM.

Their characteristics are thus different from our homemade CdS quantum dots; however we have tried to insert them on our nanohybrids to study their optical properties.

First of all we had to test their solubility properties. We didn't know the original capping agent present on the nanoparticles, but we have realized that this quantum dots were not soluble in ethanol, yet since all our synthesis are performed in this solvent we needed to disperse them in it. Consequently we have tried to find the proper capping agent to reach this purpose. We have first tried to see if the particles could precipitate thanks to conjugation with the 6-mercapto-1-hexanol. From these essays one can infer that our QDs weren't capped with some thiol functionalities. Thereby we have switched to some amines: from the precipitation of the QDs by means of the 5-amino-1-penthanol in chloroform we have then hypothesized that the capping agent were an amine. We have then centrifuged our core-shells, washed them in chloroform to take all the previous capping agent out, and finally dispersed into ethanol thanks to the capping action of short chains of amino-penthanol: they resulted stable in solution. Eventually our NPs were ready to go on with the synthesis.

From TEM analysis (fig.86) we can see that our core-shells are composed of well dispersed NPs that don't present aggregation problems.

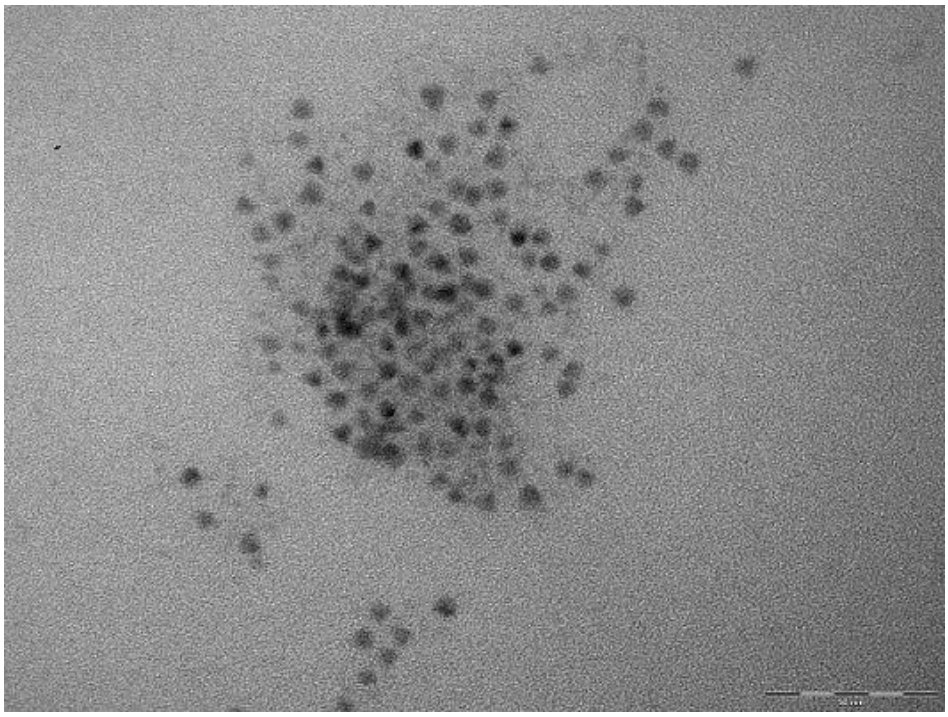

Fig. 86: CdS/ZnS core-shells in ethanol

Afterward we have chosen some standard amounts of CNTs and QDs in the attempting to evaluate the PL quenching behavior.

The initial core-shell solution has been diluted 10, 50 and 70 times for various purposes: the tenfold diluted solution will furnish an excess of NPs to the CNTs, the others are accomplished in order to graft a small quantity of NPs on the CNTs thus avoiding the problem to take all the excess particles out. The PL spectra have been recorded and they show that the QDs are rather luminescent.

Separately a small quantity of CNT@Diazo-SH and CNT@mercaptosilane (about 0,6 mg) has been dispersed in 10 ml of ethanol and sonicated for 3 hours. Then both the CNT solutions are independently mixed with a precise amount of the respectively fiftyfold and seventyfold diluted QDs in order to keep the same concentrations of NPs in ethanol (to appreciate a possible change in the PL peak respect to the bare core-shells) and PL measurements have been performed.

Aside the same amounts of CNT@Diazo-SH and CNT@mercaptosilane are mixed with the less diluted solution of core-shells (10 times) and the nanohybrids with an excess of NPs subjected to several centrifugation cycles at a low rate (3500 rpm).

Photoluminescence analysis

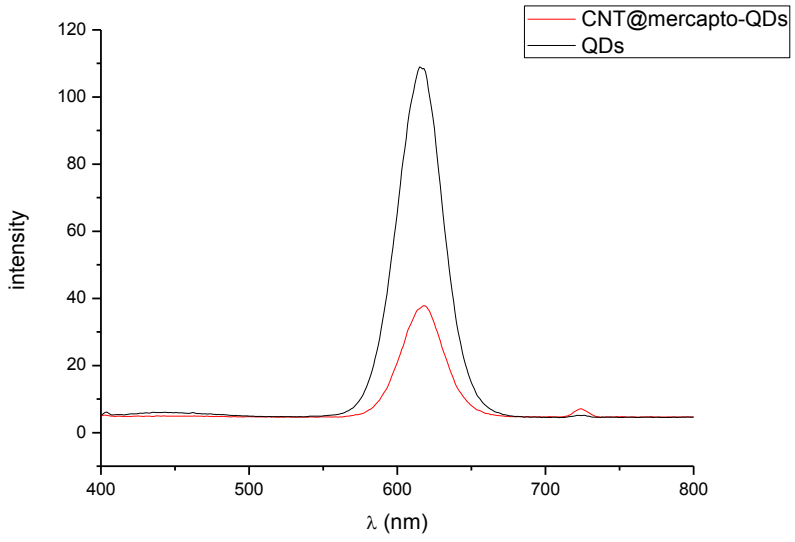

Fig. 87: CNT@mercaptosilane@QDs (QDs fiftyfold diluted, corresponding to about $3*10^{-3}$ M)

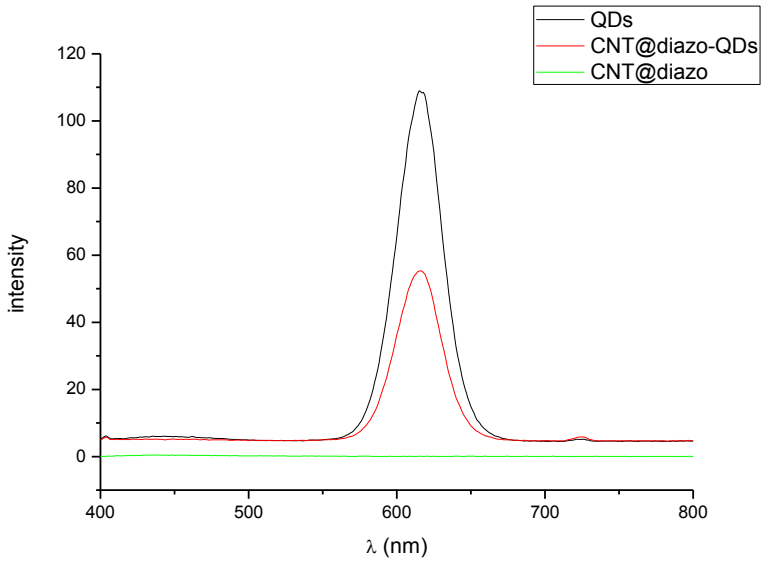

Fig. 88: CNT@diazo-SH@QDs (QDs fiftyfold diluted, corresponding to about $3*10^{-3}$ M)

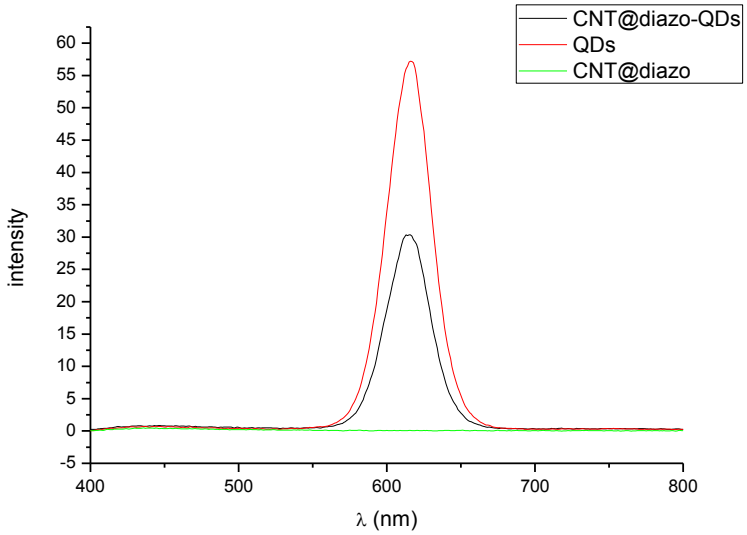

Fig. 89: CNT@diazo-SH@QDs (QDs seventyfold diluted, corresponding to about $2*10^{-3}$ M)

These spectra have been recorded just after the synthesis, however no significant changes occur after longer periods of time. The samples have been excited to 360 nm, with wavelength corresponding to the maximum of luminescence for the QDs.

We can basically notice that the quantum dots peak is well defined and corresponds to the band-edge emission: it is about 20 nm red-shifted compared to the corresponding absorption exciton peak. Besides the functionalized CNTs do not emit in the visible wavelength range.

So we can just make a few considerations: we can highlight that the peak decreases in all the spectra: as far as the CNT@diazo-SH mixed with QDs (with both the concentrations) is concerned (fig.88 and 89), we can notice that the peak halves; with the CNT@mercapto-QDs nanohybrids (fig.87) the reduction is more consistent (almost three times). We don't know if it is dependent on the concentration of the quantum dots on the nanotubes or if it is rather due to a more reliable transfer of charge between the QDs and the CNTs: in fact the mercaptosilane chains are shorter than the possible diazonium chains which could form on the nanotube so that the transfer for the first ones could be easier, despite the non-conductive nature of mercaptosilanes.

The obtained results are absolutely in agreement with literature's previous results [(14)] : because of the core-confinement of electrons by means of the ZnS shell the charge transfer between core-shell QDs and CNTs is dependent on the shell thickness and band-gap extension. In this case we excite at a wavelength sufficiently short to cross the gap of the CdS core but not that of the ZnS shell. So electrons create an exciton in the core region which can be partially spatially confined (it's a Type-I structure, thus both the carriers are confined in the core) and we can suppose a partial transfer of the photogenerated electrons, while the remainder of the electrons provides a reduced emission by the electron-hole recombination process. From this we can hypothesize the presence of a thin shell-layer around the CdS cores so that electrons are not well confined inside the NP and can pass through the particle thanks to an electro-tunneling mechanism.

Another aspect that may be considered is the slight shift in the PL peak after the hybrids conjugation: for the CNT@mercapto-QDs the peak shifts to longer wavelengths (from 615 nm for the QDs to 618 nm for the nanohybrids), for the CNT@diazo-QDs hybrids the shift is less remarkable (about 1 nm). Maybe this can be a synonymous of interaction between the functionalized CNTs and the QDs.

TEM analysis

From TEM images we can evaluate the CNTs coverage degree. By utilizing a more concentrated solution of core-shells we perceive that also after several slow rate centrifugation cycles an excess of NPs surrounds the CNT (fig.90), and probably just a part of them is effectively linked to the nanotubes.

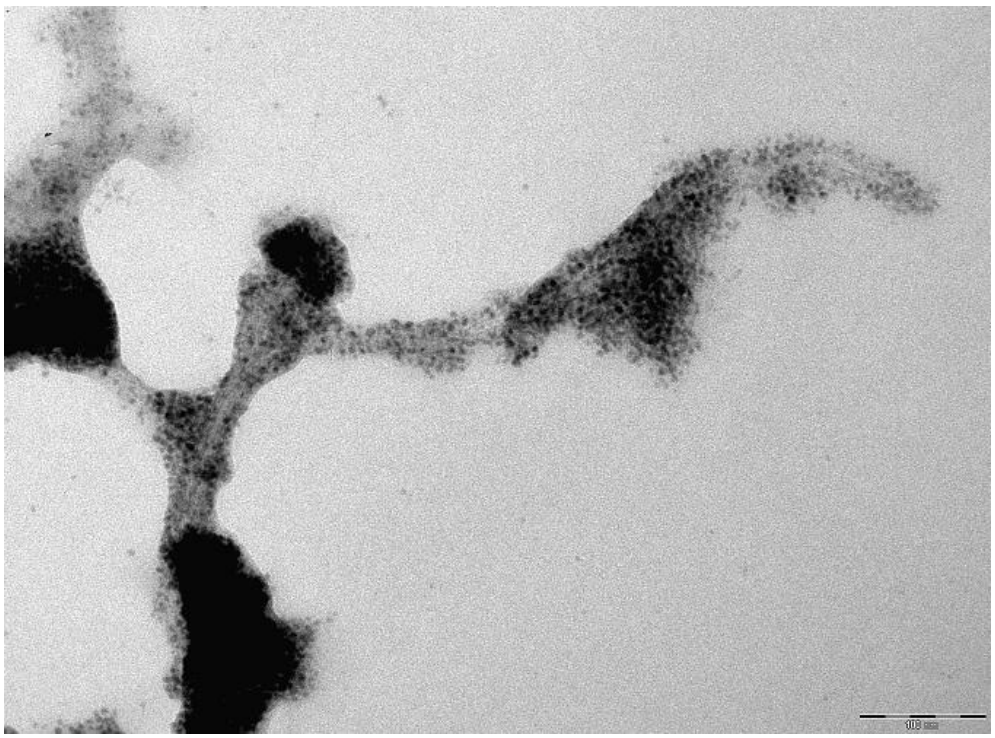

Fig. 90: CdS/ZnS core-shells onto CNT@diazo-SH after several centrifugation cycles

Instead when the NP concentration is consistently decreased NPs result well disposed on the CNT walls. The situation is better defined in CNT functionalized with diazonium compounds (fig.91), where it seems that all the NPs in solution are attached to the nanotubes (the samples didn't undergo centrifugation); it is a bit more confused in CNTs functionalized with the mercaptosilane (fig.92) where somewhere we notice some NPs aggregations, perhaps in correspondence of the CNT ends, and we don't know if it stands for a too high NPs concentration or to a weaker CNT-NPs interaction but because of the more reliable photoluminescence response we are inclined to the first hypothesis. Even XPS should confirm our assumptions, in fact the percentage of sulfur on the CNT@mercaptosilane wall is lower than for the CNT@diazo-SH, thereby the NPs concentration (the same as for diazonium compounds) is maybe still too high.

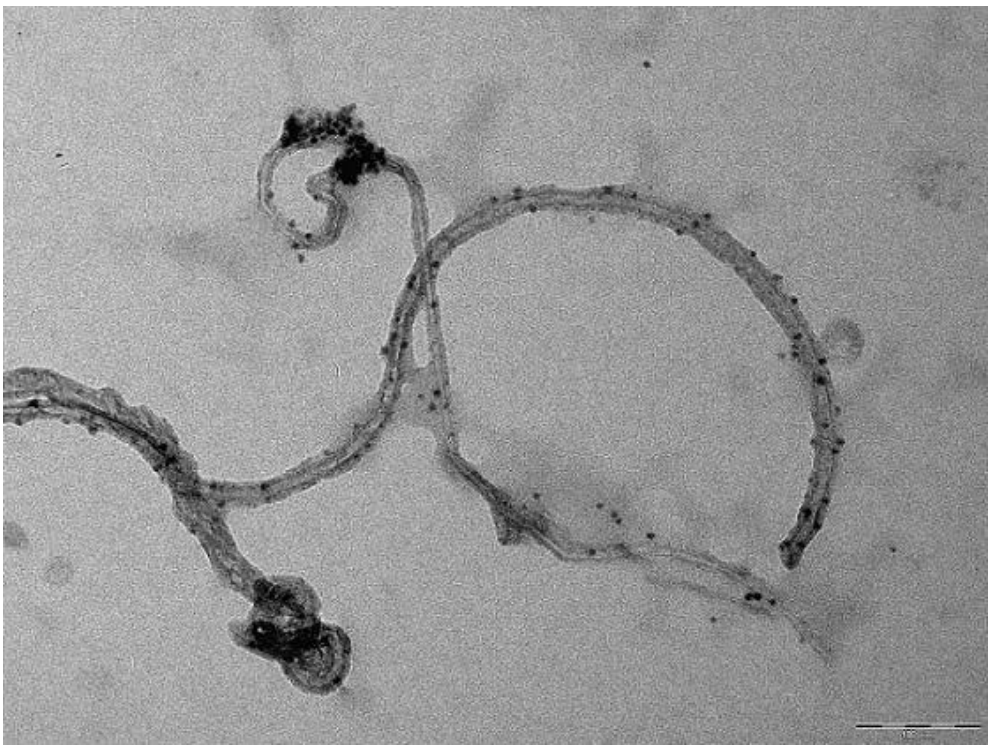

Fig. 91: more diluted solution of CdS/ZnS core-shells onto CNT@diazo-SH

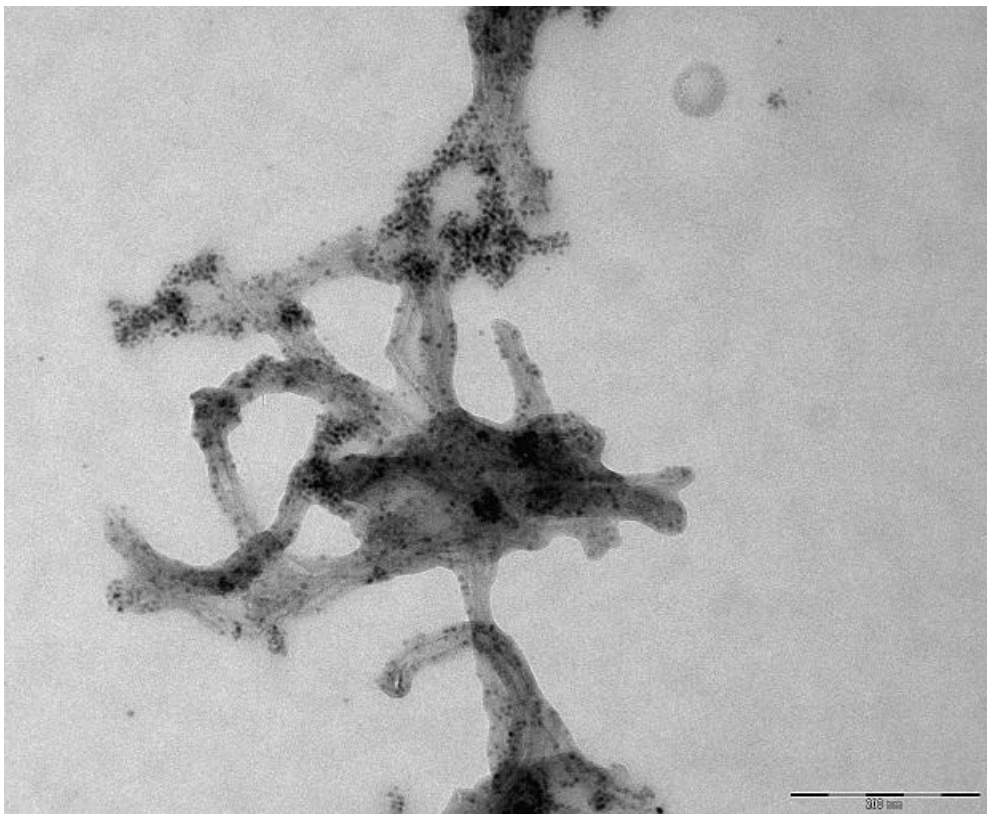

Fig. 92: more diluted solution of CdS/ZnS core-shells onto CNT@mercaptosilane

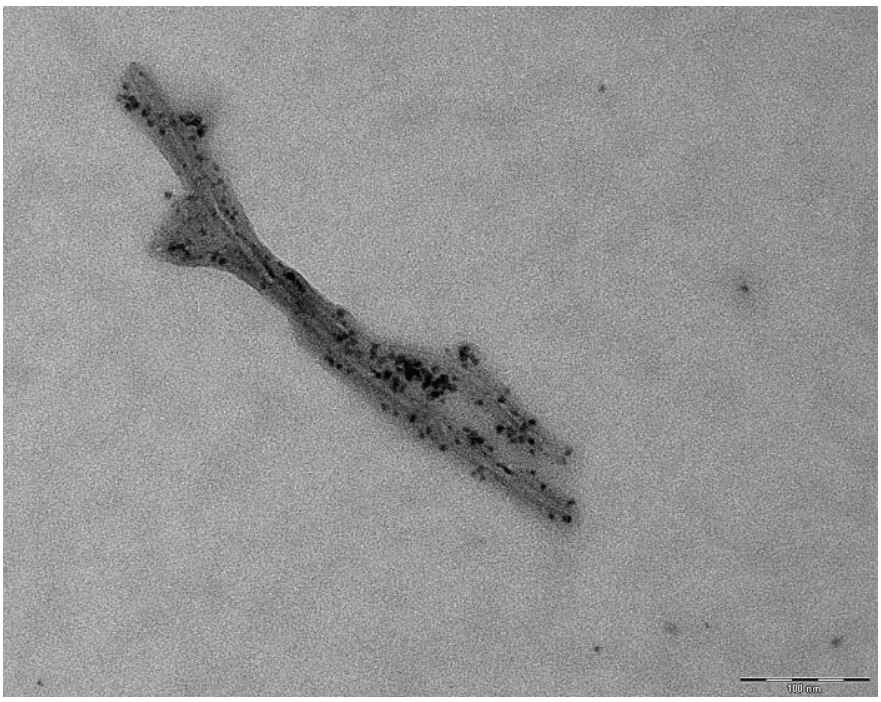

Fig. 93: more diluted solution of CdS/ZnS core-shells onto CNT@mercaptosilane

Centrifugation cycles

As for the previous synthesis also this time we have used some excess of QDs when mixed with CNTs. However the mixtures have undergone some low speed centrifugation cycles in order to let only to heavier CNTs deposit on the tubes bottom with the aim of removing the excess particles present in the supernatant.

TEM images of the gathered hybrids show still a big amount of NPs all around the CNTs which probably aren't all linked to the surface but just leant to each other (fig. 94 and 95).

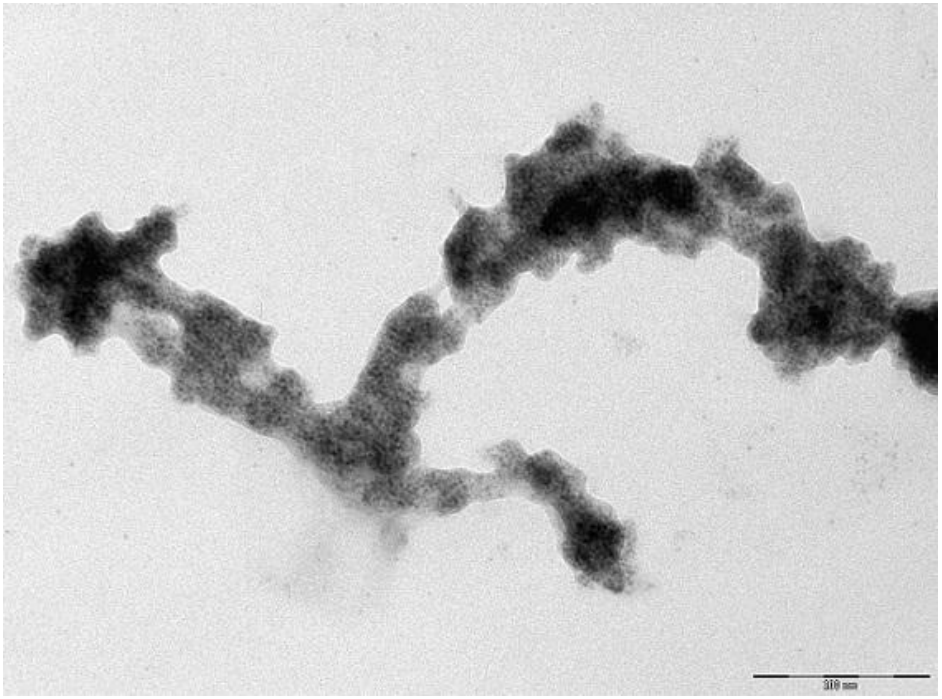

Fig. 94: CdS/ZnS core-shells onto CNT@diazo-SH after centrifugation

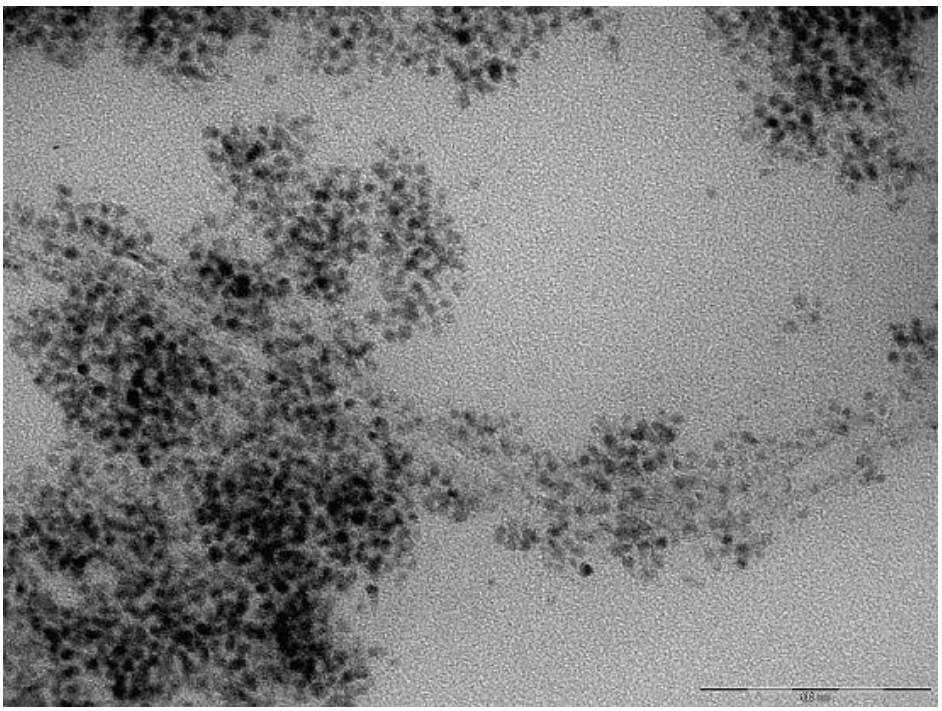

Fig. 95: CdS/ZnS core-shells onto CNT@diazo-SH after centrifugation

On the other hand, from TEM analysis of the supernatant we can notice the presence of a great deal of NPs and only few isolated CNTs: this could mean that the adopted technique holds good. Perhaps the centrifugation rate can still be lowered.

12. Conclusion and future work

Our experimental work aimed at synthesizing two kinds of CNT/QDs nanohybrids.

On the one hand pristine CNTs have been oxidized and further functionalized with a mercaptosilane, on the other hand, pristine CNTs have undergone a non-covalent functionalization by means of diazonium compounds.

Functionalization with mercaptosilane has been accomplished on oxidized CNTs, thus it involved principally the end parts of CNTs and the ones with defects. Diazonium salts allow to better functionalize all the CNT walls. Despite this, it was difficult to create just a monolayer of the aromatic compound and this could be penalizing for use in photovoltaic applications where a direct contact between NP and CNT is more desirable.

However XPS and TEM measurements have confirmed the clear and fundamental presence of thiol functions in anchoring NPs to CNT surface in both the obtained samples. In fact other attempts have revealed a missing interaction between pristine and oxidized CNTs and the nanoparticles.

The amount of NPs anchored to CNTs has to be optimized. We can follow two routes: either functionalized CNTs can be directly dispersed into a colloidal solution of nanoparticles or an imprecise quantity of quantum dots can be mixed to nanotubes and the hybrid centrifuged to low rates in order to take the excess NPs out.

Photoluminescence spectroscopy has suggested CNT/QDs communication skills. In all samples analyzed a decrease in the PL peak has been observed: it roughly halves in CNT@diazo-SH@QDs nanohybrids and reaches almost one third of the original height in CNT@mercaptosilane@QDs. This highlights an interaction between the semiconductors and the nanotubes but it is impossible to determine whether the incomplete PL quenching is effectively due to the core confinement of electrons in the type-I structures which hampers the transfer of charge or to the type of CNT functionalization. Substitution with type-II core-shells in the nanohybrids is stimulated.

As far as the CNT functionalization with a polyelectrolyte is concerned some promising results have been obtained: that pushes to optimize the synthesis procedure and test the amine function-QDs interaction with photoluminescence measurements.

Moreover it will be interesting to compare the electric communication in our nanohybrids with other hybrids functionalized with some dithiol functions to see if their anchoring and transfer of charge ability is higher.

The particular conformation of CNT@mercaptosilane hybrids suggests to exploit the functionalization with organosilanes in CNT forests directly grown up on the electrodes. In fact the simple deposition on single functionalized-CNTs on the surface of the electrodes or in other matrices prevents obtaining high efficiencies in the respective devices because of charge dispersion.

Substitution of CNTs with TiO2 nanotubes could be another practicable route that could be exploited in DSSCs. Generally Grätzel cells make use of TiO_2 nanoparticles and because of the porous structure the transport of charge is not optimal; an electron acceptor tubular structure could facilitate the electrons mobility.

13. Bibliography

1. F. Fievet, J.P. Lagier et al, *Solid State Ionics*, (1989)
2. C.Feldmann, *Advance Functional Materials*, 13, (2003), No.2, 101
3. C.Feldmann, C.Metzmacher, *Journal of Material Chemistry*, (2001), 11, 2603
4. Lydie Vivet, Incorporation d'ions Gd3+ dans des nanoparticules de semi-conducteurs pour l'élaboration de sondes bimodales pour l'imagerie médicale, Rapport de stage, (2010)
5. Jin Shi, Zhe Wang, Hu-lin Li, *Journal of Nanoparticlen Research*, (2006), 8, 743
6. Jui-Ming Yeh, Kuan-Yeh Huang et al, *Journal of Nanotechnology*, (2009)
7. Jin Shi, Yu-Qi Hu, Yi-Xin Hua, *Electroanalysis* 20, (2008), 13, 1483
8. Dongfang Liu, Wei Wu, Shihe Yang, *J. of Physics and Chemistry of Solids* 70, (2009), 694
9. Dongfang Liu, Wei Wu et al, *Journal of Physical Chemistry C*, (2007), 111, 17713
10. Jun Wang, Jun Xu et al, *Journal of Materials Chemistry*, (2008), 18, 3270
11. M.Olek, T.Busgen et al, *J. Phys. Chem. B*, (2006), 110, 12901
12. Yunlong Zeng, Chunran Tang et al, *Spectrochimica Acta Part* 70, (2008), 966
13. X. Li, Yi Jia, A. Cao, *AcsNano*, vol.4, (2010), 1, 506
14. S.Jeong, H.C.Shim et al, *AcsNano*, vol.4, (2010), 324
15. H.Y.Si, C.H.Liu et al, *Nanoscale Res Lett*, (2009), 4, 1146
16. F.Li, S.H.Cho et al, *Applied Physics Letters*, (2009), 94, 111906
17. Miao Feng, R.Sun et al, *Carbon 48*, (2010), 1177
18. Z.Zhu, R.Yang et al, *Anal Bioanal Chem*, (2010), 396, 73
19. G.Mountrichas, A.S.D. Sandanayaka et al, *J.Mater.Chem*., (2009), 19, 8990
20. B.Farrow, P.V.Kamat, *J.Am.Chem.Soc*., (2009), 131, 11124
21. I.Robel, B.A.Bunker, P.V.Kamat., *Adv. Mater*. (2005) 17 2458
22. T.C.W.Mak, K.S.Jasim, C.Chieh, *Can. J. Chem.,* 62 (1984), 808
23. L.A.Ramos, E.T.G.Cavalheiro, G.O.Chierice, *Journal of Thermal Analysis and Calorimetry*, vol. 79, (2005), 349
24. Synthesis of new dithiocarbamates. Hu, Zhenshan et al. 1986.

25. S.Goubert-Renaudin, R.Schneider, A.Walcarius, *Tetrahedron letters* 48, (2007), 2113

26. V.K.Tiwari, A.Singh et al, *Monatshefte fur Chemie*, 138, (2007), 653

27. L.Sheeney-Haj-Ichia, et al, *Angew. Chem. Int. Ed*. (2005) 44, 78

28. C.A.Dyke, M.P.Stewart et al, Diazonium-based functionalization of Carbon Nanotubes. XPS and GC-MS analysis and mechanistic implications, (2003)

29. P.R.Marcoux, P.Hapiot,P.Batail and J.Pinson, *New. J. Chem*, (2004), 28, 302

30. R.L.McCreery, B.L.Hurley and, *Journal of the electrochemical society*, (2004), 151(5), B252

31 L.Sheeney-Haj-Ichia, et al, *Angew. Chem. Int. Ed.* (2005) 44, 78

32 . D.Yu.Parashchuk, A.I.Kokorin, *Russian Journal of General Chemistry* (2009) 11 2543

33. P.Brown,K.Takechi, V.Kamat, *J. Phys. Chem. C* (2008) 112 4776

34. Chuan-Yu Yen, Yu-Feng Lin et al, *Nanotechnology* (2008) 19 375305

35. T.Y. Lee, P.S.Alegaonkar, Ji-Beom Yoo, *Thin solid films* (2006) 5131

36. I. Mora-Sero',S.Giménez et al, *Accounts of chemical research* (2009)

37. D.M. Shewchuk, M.T. McDermott, *Langmuir Article*, (2009), 25(8), 4556

38. J.L Delgado, M.A. Herranz, N. Martin, *Journal of Material Chemistry* (2008) 18 1417.

39. D. Tasis, N. Tagmatarchis, et al, *Chem. Rev.* (2006) 106 1105.

40. Y. Xing, *J. Phys. Chem. B* (2004) 108 19255.

41. P.R. Marcoux, P. Hapiot et al, *J. New J. Chem.* 28 (2005) 302

42. W. Wu, N.V. Tsarevsky, et al, *Small* (2007) 3 1803.

43. M. Grzelczak, A. Correa-Duarte, L.M. Liz-Marzan, *Small* (2006) 2 1174

44. A.M. Gilmore, *Nanophotonics*, Proc. of Spie, Vol. 6195, (2006), 61950M-1

45. A. Hartschuh, H.N. Pedrosa et al, *ChemPhysChem*, (2005), 6, 1

46. S. Baskoutas, A.F. Terzis, *J. Appl. Phys*., (2006), 99, 013708

47. A.M.Smith, S. Nie, *Accounts of chemical research*, (2009)

48. O. Ovits, R. Tel-Vered et al, *J. Mater. Chem.,* (2009), 19, 7650

Ringraziamenti

In ordine assolutamente sparso tengo a ringraziare

La prof.ssa Giovanna Brusatin, per avermi spedito in Francia con il rapido dell'11 marzo 2010

La prof.ssa Fayna Mammeri, per avermi accolto all'arrivo del rapido dell'11 marzo, nel laboratorio multietnico che ha cominciato a farmi amare Parigi, dimenticando quella sana e riconosciuta antipatia che accomuna i nostri due popoli

Marion Giraud, per aver sostenuto il mio lavoro, e per avere una casa a Parigi, che potrebbe fare presto la mia conoscenza.

Il quarto, quinto, sesto, ottavo piano dell'Itodys, mi è mancato solo il settimo, ma mai dire mai.

Luciano, per essere italiano, ed anche per essersi sorbito le mie richieste assieme a Guillaume

M.Chehimi, Samia, Chantal, il China-team & dintorni e tutti quelli che in un modo o nell'altro sono stati presenti durante il mio lavoro

Torniamo in Italia.. grazie ai miei compagni di corso, per essere tutti diversi l'uno dall'altro, e scampare un po' al prototipo di ingegnere "sfigato"

Grazie alla mia famiglia, perché è la mia famiglia

Grazie ad amici di oggi e di allora, perché mi sono sempre intorno

Grazie a chi non è incluso in questa lista, perché sarà incluso in un'altra, più approfondita, mai stampata!